ELASTIC BUCKLING BEHAVIOR OF PLATE AND TUBULAR STRUCTURES

by

ARKA PRABHA CHATTOPADHYAY

B. Tech., Jawaharlal Nehru Technological University, 2008

A THESIS

submitted in partial fulfillment of the requirements for the degree

MASTER OF SCIENCE

Department of Mechanical and Nuclear Engineering
College of Engineering

KANSAS STATE UNIVERSITY
Manhattan, Kansas

2011

Approved by:

Co-Major Professor
Kevin B. Lease

Approved by:

Co-Major Professor
Jack Xin

Copyright

Abstract

The study of buckling behavior of tubular and cellular structures has been an intriguing area of research in the field of solid mechanics. Unlike the global Euler buckling of slender structures under compressive loads, tubular and cellular structures deform with their walls buckling as individual supported plates. The aspect ratio and the dimensional characteristics of the tube define the buckling behavior of any tube structure. In this thesis, a thorough study on the buckling of polygon tubular structures with different cross sections is discussed.

In the first study, the theoretical buckling formulation of a square tube using the energy method is reviewed from existing solutions in literature. The elastic critical load of a square tube derived from the theoretical solution is then compared with results of finite element elastic buckling simulations. The formation of lobes along the height of the walls at different aspect ratios of the tube is investigated and compared to theory. Also, the buckling behavior of multi-wall structures is studied and the relationship between these structures and a rectangular simply supported plate is established. A brief study on the buckling behavior of rhombic tubes is also performed. The results of the simulation match closely with the theoretical predictions.

The study is then extended to quadrilateral tubes with cross-sections in the shape of square, rectangle, rhombus and parallelogram. The theory of buckling of these tubes is explicitly defined using classical plate mechanics based on the previous works presented in literature. Also, the possibility of global Euler buckling in the tubular structures after a certain critical height is discussed. The prediction from the theory is validated using extensive finite element elastic buckling simulations and experimental tests on square and rhombic tube specimens. The results of the simulations and experiments are observed to be consistent with the theory.

Using the formulation of plate buckling under different boundary conditions, the buckling behavior of triangular tubes is also determined. A theoretical formulation for calculating the critical load of triangular tubes is derived. The theoretical critical loads for a range of aspect ratios are compared with corresponding finite element simulation results. The comparisons reveal high degree of similarity of the theoretical predictions with the simulations.

Table of Contents

List of Figures vii
List of Tables xi
Acknowledgements xii
Dedication xiii
Chapter 1 - Introduction 1
1.1 Thesis Format 1
1.2 Overview of the Thesis 1
1.3 References 3
Chapter 2 - Effects of aspect ratios and side constraints on elastic buckling of multi-wall structures and tubes 4
2.1 Abstract 4
2.2 Introduction 4
2.3 A brief review of buckling theory of simply supported plates and square tubes 6
2.3.1 Buckling of plates 6
2.3.2 Transition of number of half waves in plate buckling 9
2.3.3 Buckling of square tubes 9
2.4 Computational model of single plate, multi-wall structures, square tubes and rhombic tubes 10
2.4.1 Buckling of a simply supported plate 11
2.4.2 Buckling of multi-wall structures 13
2.4.3 Buckling of square tubes 15
2.5 Results and discussion 16
2.5.1Comparisons of critical loads of single plate, multi-wall structures and square tubes . 16
2.5.2 Effects of wall angle in multi-wall structures 19
2.5.3 Effects of wall angle of rhombic tubes 21
2.6 Implications for structural properties of honeycomb 22
2.7 Summary and conclusions 22
2.8 References 23

Chapter 3 - Elastic Buckling Characteristics of Quadrilateral Tubes under Uni-Axial Compressive Loads 25
3.1 Abstract 25
3.2 Introduction 25
3.3 Elastic Buckling of Quadrilateral Tubes 28
3.3.1 Buckling Condition of Buckling Walls Based on the Theory of Supported Rectangular Plates 29
3.3.2 Bending equation of the restraining walls 32
3.3.3 Transition of Number of Half-Waves in Plate Buckling 35
3.3.4 Buckling of square tubes 36
3.3.5 Buckling of Rectangular Tubes 37
3.3.6 Buckling of Rhombic and Parallelogram Tubes 39
3.3.6 Euler Buckling of Rhombic and Parallelogram Tubes 40
3.4 Finite Element Buckling Simulations of Plate and Tubular Geometries 44
3.4.1 Elastic Buckling Simulations of a Square Tube 45
3.4.2 Finite Element Elastic Buckling Simulations of Rectangular Tubes 47
3.4.3 Finite Element Simulations of Rhombic and Parallelogram Tubes 50
3.5. Buckling experiments in ABS plastic tube specimens 53
3.6 Results 55
3.6.1 Comparison of results for square tubes 55
3.6.2 Comparison of Results for Rectangular Tubes 56
3.6.3 Comparison of results of Rhombic and Parallelogram tubes 57
3.7 Conclusions 60
3.8 References 60
Chapter 4 - Elastic Buckling Characteristics of Triangular Tubes under Uni-Axial Loading 62
4.1 Abstract 62
4.2 Introduction 62
4.2.1 Buckling of plate structures 62
4.2.2 Buckling of square and rectangular tubes 63
4.2.3 Buckling behavior of circular tubes 64
4.2.4 Buckling of triangular tubes 64

4.3 Theoretical Buckling phenomenon of Triangular Tubes 65
4.4 Critical Load of Buckling of an Angle Section 69
4.4.1 Equation of Deflection of the Main Wall 69
4.4.2 Calculation of Restraint Coefficient using the Deflection Equation of the Restraining Wall 75
4.5 Critical Load Derivation of an Isosceles Tube 81
4.6 Finite Element Simulation of Buckling of Different Triangular Tubes 84
4.6.1 Finite Element Simulations of an Equilateral Tube and Corresponding Angle Section 84
4.6.3 Simulation Results of the Angle Section of an Equilateral Tube 86
4.6.3 Simulations on Angle Section of Short-Sided Isosceles Tubes 89
4.7 Discussion of Results 91
4.8 Conclusion 92
4.9 References 92
Chapter 5 - Conclusions and Scope of Future work 95
Appendix A - Deflection Equation of the Restraining Walls of a Rectangular Tube 97
Appendix B - Minimum Moment of Inertia of a Parallelogram Tube Cross-Section 99
Appendix C - General Deflection Equation of the Main Wall of a Triangular Tube 101
Appendix D - Buckling Condition of the Main Wall of a Triangular Tube 103
Appendix E - Out-of-plane Deflection Equation of the Restraining Wall of an Angle Section. 104

List of Figures

Figure 2.1: The rectangular plate (a) with the coordinate axis and dimensions, (b) as a model with restraints and load, and (c) deformed model of the plate from simulation result 7
Figure 2.2: Variation of k with the change in aspect ratio of a simply supported rectangular tube under uni-axial loading 8
Figure 2.3: The meshed model of a single rectangular plate with aspect ratio two with the simply supported boundary conditions and loads on it..... 12
Figure 2.4: Buckling of a single plate with aspect ratio of (a) 1.2, (b) 1.4, (c) 1.41, (d) 1.414, (e) 1.417 and (f) 1.45 13
Figure 2.5: The finite element models of (a) two joint walls and (b) three joint walls 14
Figure 2.6: The model of the geometry in Figure 2.5(a) with applied boundary conditions and loads 14
Figure 2.7: (a) The buckled profiles of a square tube with the simply supported conditions applied to the top and bottom edges, (b) four individual plates with simply supported conditions applied to all their edges put together in the shape of square tube and (c) buckled profile of Figure 2.7(b) exhibiting outward or inwards folds independent of adjacent plates 16
Figure 2.8: Plot of critical loads against the aspect ratios for the various geometries..... 18
Figure 2.9: The buckled shapes of two joint plate geometry with the angle of (a) 175 (b) 135 (c) 90 (d) 45 and (e) 10 degrees between the plates 20
Figure 2.10: The rhombic tubes with the acute angle between the walls as (a) 10, (b) 45 and (c) 90 degrees showing the buckled shapes after simulation 21
Figure 3.1 The rectangular plate (a) with the coordinate axis and dimensions, (b) as a model with restraints and load, and (c) deformed model of the plate from simulation result 29
Figure 3.2 Plot of μ versus ζ for $m/\phi = 1$ 31
Figure 3.3 Schematic representation of one of the restraining walls of the tube with coordinate system and dimensions 33
Figure 3.4 The plots of k for a wall with l_r/l ratio 0.5 35
Figure 3.5 Plot of the values of k with varying aspect ratios of the walls of a square tube..... 37

Figure 3.6 Plots of k of different rectangular tubes varying with aspect ratio 38
Figure 3.7 Minimum values of k for different l_r/l ratios 39
Figure 3.8 The representation of the cross-section of a general rhombic tube of each wall of width l, wall thickness of t and acute angle of rhombus as θ 41
Figure 3.9 The critical load of a rhombic tube with $l = 2$ *in*, $\theta = 60^{o}$ *in* and $t = 0.08$ *in* 42
Figure 3.10 The representation of the cross-section of a general parallelogram tube with longer walls of length l, shorter walls of length l_r, wall thickness of t and angle of θ 43
Figure 3.11 The critical load plot with different aspect ratios of a parallelogram tube with $l = 2$ *in*, $l_r = 1$ *in*, $\theta = 60^{o}$ and $t = 0.08$ *in* 44
Figure 3.12 Finite element model of a square tube with sides of length 2 *in* and aspect ratio of 1, with exaggerated deformation 46
Figure 3.13 Front view of the buckled profile of finite element model of the tube at an aspect ratio of (a) 1.4, (b) 1.41, (c) 1.414, (d) 1.417 and (e) 1.45 47
Figure 3.14 Isometric view of the buckled shape from the simulation of the rectangular tube model ($l = 2$ in, $l_r = 1$ in) of aspect ratio 1 with boundary conditions, applied forces, in an exaggerated scale 48
Figure 3.15 The exaggerated buckled shapes from the elastic buckling simulations at aspect ratios of (a) 1.18, (b) 1.19, (c) 1.2, (d) 1.21 and (e) 1.3 49
Figure 3.16 Exaggerated buckled shapes from the finite element simulation of (a) a rhombic tube of aspect ratio 1 with $\theta = 45°$ and $l = 2$ in and (b) a parallelogram tube of aspect ratio of longer walls equal to 1 with $\theta = 60°$, $l = 2$ and $l_r/l = 0.5$ 50
Figure 3.17 Initiation of Euler buckling in a (a) rhombic tube with $l = 2$ *in*, $t = 0.08$ *in* and $\theta = 60^{o}$ at $h = 23.5$ *in* and (b) parallelogram tube with $l = 2$ *in*, $l_r = 1$ *in*, $t = 0.08$ *in* and $\theta = 45^{o}$ at $h = 9.5$ *in* 52
Figure 3.18 The buckled profile of the ABS square tubes with aspect ratios (a) 1, (b) 2, (c) 3, (d) 1.41 and (e) 2.44 54
Figure 3.19 Buckled shape of a rhombic tube with aspect ratio of 1 and angle of 45^{o} with the cross section dimensions similar to that of the square tubes presented in Figure 3.18(a) 55
Figure 3.20 Comparison of theoretical, computational and experimental critical load variance with aspect ratio of a square tube with $l = 2$ *in* and $t = 0.08$ *in* 56

Figure 3.21 The comparison of theoretical expectations and simulation results of the buckling critical loads of a rectangular tube with $l = 2$ *in*, $l_r = 1$ *in* and $t = 0.08$ *in*, over different aspect ratios 57
Figure 3.22. The critical load behavior of a rhombic tube with angle 60^o with the consideration of Euler buckling after the critical height of the tube 59
Figure 3.23 The critical load behavior of the parallelogram tube with the consideration of Euler buckling after the critical height of the tube 59
Figure 4.1 The schematic representation showing the formation of single lobe in all the walls violating the initial angle between the walls of the tube 66
Figure 4.2 Schematic representation of the top views of possible lowest critical load buckling patterns of an equilateral triangular tube. The dotted lines represent the original shape and solid lines represent the assumed buckled shape (for the present theoretical study, shape (a) was considered) 67
Figure 4.3 Division of the triangular tube into two half triangular tube sections called as angle sections 68
Figure 4.4 Schematic representation of the angle section with illustration of main wall and restraining wall 69
Figure 4.5. Representation of the main wall with coordinate axes and dimensions, showing the simply supported condition along one vertical edge and elastically restrained condition along the other vertical edge 70
Figure 4.6 Variation of μ^2 with ζ when m/ϕ is 1 73
Figure 4.7 Geometry of the restraining wall with a diagrammatic representation of bending moment acting along the common edge due to buckling of main wall 75
Figure 4.8 Plot showing the variation of coefficient ζ with the change of ratio m/ϕ for $l_r/l = 0.5$ 78
Figure 4.9 Plot showing the curves of k for different number of half sine waves varying with the values of aspect ratios 80
Figure 4.10 Simulation result of buckling of a long-sided isosceles tube showing the buckling of the walls at an exaggerated scale 81
Figure 4.11 Plots of k curves for various l_r/l ratios varying with aspect ratio ϕ 82
Figure 4.12 Curve showing the minimum values of buckling factor k of the main wall of an angle section for different length ratios l_r/l 83

Figure 4.13 Finite element simulation results showing top views of the buckled shapes of (a) a triangular tube, (b) corresponding angle section and (c) trimetric view of the angle section at an exaggerated scale..... 85
Figure 4.14 (a) Top view and (b) trimetric view of the deformed model of a two legged angle section with aspect ratio of 1, at an exaggerated scale after buckling simulation 86
Figure 4.15 Comparison of the *k* curves obtained from theoretical and computational results over different aspect ratios..... 88
Figure 4.16 Exaggerated scale simulation results of the angle section of an equilateral tube at aspect ratio of (a) 1.23, (b) 1.24, (c) 1.25, (d) 1.26 and (e) 1.29..... 89
Figure 4.17 An exaggerated scale deformed shape of angle sections with l_r/l ratios as (a) 0.01, (b) 0.1 and (c) 0.3 after buckling simulation at aspect ratio of 1..... 90

List of Tables

Table 2.1 Critical load comparison of a square tube and four independent simply supported plates put together in the form of a tube 16

Table 2.2: The critical load data for the series of simulations performed on multi-walled structures for various aspect ratios..... 17

Table 2.3: The critical load per wall data of a simply supported hexagonal tube and the corresponding 5-wall open section 19

Table 2.4: The critical loads of the two-wall structure geometry with different wall angles and a single plate from simulation..... 21

Table 2.5: The critical loads of the rhombic tubes with different acute angles between the walls and a square tube from the results of simulation 22

Table 3.1. The critical load data of a rhombic tube with $l = 2$ *in*, $t = 0.08$ *in* and $\theta = 45^{o}$, from theoretical, computational and simulation methods..... 58

Table 4.1 Theoretical calculation of the values of k for different values aspect ratios for m=1 ... 79

Table 4.2 Critical loads of the two sections from the result of FEM simulations 85

Table 4.3 Theoretical and simulation results of k of the angle section of equilateral tube, with main wall of length 3.175 *mm* and restraining wall of length 1.5875 *mm*..... 87

Table 4.4 Simulation results of the buckling analysis on the sections shown in Figure 4.17..... 91

Acknowledgements

The last two years of my master's study in the Mechanical and Nuclear Engineering Department of Kansas State University has been a very eventful and knowledgeable time. Today, as I come to the end of this journey, I would like to take the opportunity to thank the people without whom I could not have finished my master's studies.

First, I would like to thank my major professors Dr. Kevin Lease and Dr. Jack Xin for supporting and encouraging me on every step. I am grateful to them and appreciate their patience with me. I could not have finished my graduate studies without their guidance and support. I would like to thank Dr. Sameer Madanshetty for agreeing to be a part of my thesis committee and guiding me with suggestions. I would also like to thank Dr. Gurpreet Singh for his knowledgeable advices in the course of my studies.

I would like to thank Elizabeth Frink for being a wonderful research partner who has helped me with different parts of my research in numerous occasions. I also thank Andrew Dickson for helping with the experimental studies of this research. I also extend my gratitude to all of the people in the Mechanical and Nuclear Engineering Department of Kansas State University for their support.

In the journey of my master's, I have made many good friends in the university. I would like to express my gratitude to all the friends, especially Sohini Roy Chowdhury, Parangiri Nivas, Siddharth Deshmukh and Viet Nguyen for encouraging me at numerous occasions. I also thank all my colleagues from the graduate office and the MTEL laboratory. Without them, the time I have spent in the University would not have been the same.

Dedication

I would like to dedicate this thesis to my parents, who have been the constant source of encouragement and inspiration in all my academic endeavors.

Chapter 1 - Introduction

1.1 Thesis Format

In this Thesis, the technical work is presented in three chapters following this introductory chapter. The following chapters are in the form of accepted publications or manuscripts of publications to be submitted in Scientific Journals. Chapter 2 is the draft of an accepted article which is to be published in the proceedings of ASME Manufacturing Science and Engineering Conference 2011. Chapters 3 and 4 are the manuscript versions of journal articles which are in the process of being submitted to Elsevier-Thin wall Structures. In this thesis, each chapter is included with a separate abstract, literature review and conclusions. The overall conclusions and the scope of future work are discussed in the final chapter of the thesis.

1.2 Overview of the Thesis

Buckling of plates and shells has been an important area of research in the area of solid mechanics. The major fields of applications of supported plates and tubular structures as structural members include aeronautical, marine and civil engineering. In this study, the buckling characteristics of plates and polygon tubular structures are investigated using theoretical methods and compared with computational simulation and experimental results.

In the second chapter of this thesis, the buckling properties of plates, multi-wall structures and square tubes are discussed. Also, the buckling behavior of rhombic tubes is briefly looked into using finite element simulation results. Study of the critical load of buckling of plates and tubes under uni-axial loading using energy method is reviewed from the existing study presented by Timoshenko and Gere [1]. These theories are used to predict the buckling characteristics of multi-wall structures with simply supported boundary conditions along the open edges. Also, a series of finite element simulations are performed on different plate, multi-wall and tube geometries to compare it with the theory. It is observed from the simulation results that the critical load of a multi-wall structure is equal to the critical load of a single simply supported rectangular plate times the number of walls in the multi-wall structure. It the case of a polygon tube, the critical load of the tube is observed to be equal to the number of sides of the polygon times the critical load of each wall of the tube. This agrees with the theory suggested by

Timoshonko and Gere [1] for the case of square tubes. It is also observed that the critical load of buckling of the multi-wall structures does not depend on the angle between the adjacent walls of the structures. Similarly, it is observed that the critical load of a rhombic tube is equal to the critical load of the corresponding square tube. Based on these theoretical and simulation results, it is inferred that the critical load of a square cell honeycomb structure can be calculated by calculating the critical load of individual cell walls behaving as simply supported rectangular plates.

The study on the square and rhombic tubes presented in the second chapter is then extended to quadrilateral tubes with cross sections in the shapes of rectangular and parallelogram tubes. This study is presented in Chapter 3 of this thesis. The theoretical buckling critical loads of all the tubes are derived from the buckling behavior of each wall of the tube. General equation of buckling of a rectangular plate elastically restrained along the vertical edges is derived explicitly using classical mechanics. The derivation process is based on plate and tube buckling theories presented in literature [1-3]. Also, the possibility of Euler buckling of the tubes is investigated and the expression for the Euler buckling critical height of a rhombic or parallelogram tube with a certain angle is derived. A tube of height greater than the critical height under uni-axial load is predicted to buckle in global Euler mode. The proposed theories are compared with extensive finite element simulations. The critical aspects of buckling, including the formation of lobes (half waves) along the height of the tube are closely examined. The results of simulations exhibit good consistency with the theoretical predictions. Also, experiments to observe the behavior of square and rhombic tubes under compressive loading are carried out on tube specimens. The specimens are made of Acrylonitrile Butadiene Styrene (ABS) plastic. The results from the experiments are observed to be in agreement with the theoretical and simulation results.

The following chapter presents the study of the buckling behavior of triangular tubes. The study involves the theoretical derivation of the critical loads of triangular tubes as a function of dimension and aspect ratio of the tube. The theory is derived by the assumption of the behavior of walls of an isosceles triangle under buckling loads. The buckling expression of the critical wall of the tube is derived using a process similar to the derivation process of the walls of a rectangular tube. The results predicted from the theoretical procedure are compared with an

extensive finite element study on models of triangular tubes. The comparison reveals good agreement of the results of simulations with the theory.

Extensive literature review and elaborate introduction to each study is presented in the respective chapters of this thesis. This chapter was intended to provide a brief overview of the work accomplished in this thesis.

1.3 References

[1] Timoshenko S. P, Gere J. M, (1961), *Theory of elastic stability*, New York, McGraw-Hill, 1969

[2] Bulson P. S., (1969), *Stability of Flat Plates.* American Elsevier Publication Company, New York, pp. 27, 295.

[3] Bleich F., (1952), *Buckling Strength of Metal Structures.* McGraw-Hill New York, pp. 302

Chapter 2 - Effects of aspect ratios and side constraints on elastic buckling of multi-wall structures and tubes

2.1 Abstract

Buckling of plates and tubes plays an important role in structural safety and energy absorption. Although buckling of plates and tubes has been studied theoretically and experimentally in the past, the effects of aspect ratio and side constraint on buckling of multi-wall structures and tubes has not been investigated systematically. In this work, finite element simulations have been carried out to investigate the buckling behavior of multi-wall structures and tubes. A series of one- to three-panel walls and square tubes with various aspect ratios were simulated. The critical aspect ratios causing buckling mode transition were obtained and compared with theoretical predictions available in the literature. Effects of wall angle and side constraint on buckling behavior were investigated. The relevance of research findings to honeycomb-like structures was discussed.

2.2 Introduction

The study of buckling of tubes and plates has been an important area of research for researchers for a long time because of their extensive use in various fields like marine applications, aeronautics, automobiles, etc. Structures like supported plates with stiffeners, tubes and honeycombs offer high strength-to-weight ratios. Plate structures are widely used in the design of ship hulls, aeronautical structures and other structural members, whereas tubes under compression play a major role in the design of energy absorbing structures [1–3]. Soden *et al* [4] and Johnson *et al* [5] studied the energy absorbing capacity of circular tubes by the formation of traveling plastic hinges. Apart from circular tubes, square and rectangular tubes also play a major role in energy absorbing structures. Work in [1–3, 6, and 7] investigated the crashworthiness of square and rectangular sections under static and impact loading and their effectiveness in vehicular safety designs.

Elastic buckling of plates with varying edge conditions with extension to the buckling of square tubes was carried out by Timoshenko and Gere [8]. Their work established that when a simply supported plate buckles elastically under a uniform compressive in-plane load, the out-of-

plane displacement profile forms sinusoidal waves along the length and width of the plate. Subsequent research on the elastic buckling and post buckling of plates were carried out by different researchers [9–12] for various boundary conditions of non-loading edges such as fixed along both edges, fixed along one edge and elastically restrained along other edge, simply supported along both edges, and elastically restrained about one edge and free on other end. Von Karman *et al* [9] extended the theory of buckling of a plate with simply supported conditions to post buckling analysis. Bradford and Azhari [13] studied the buckling behavior of plates using finite strip method for various end conditions of the non-loading edges. The buckling characteristics of plates were investigated using the finite element method in [14–16]. Swartz and O'Neill [14] developed a finite element code to find the lowest critical load of a plate under various end conditions with combined loading conditions. Elgaaly [17] presented a non-linear finite element analysis on the post-buckling behavior of plates with simply supported edges and stiffened edges.

It was postulated in [8] that a square tube behaves as four simply supported independent plates joined together and a uniformly applied load acting on it is equally shared by all of the plates. All plates buckle simultaneously while the angles between adjacent walls remain unchanged before and after buckling. Based on this postulation, the study of various square and rectangular tubes in elastic and post buckling has been conducted by researchers [10, 11, 18–22]. The values of buckling factor 'k' for rectangular tubes with simply supported end conditions were calculated by Lundquist [18] and Bulson [10]. Kandil and Calladine [23] suggested more realistic values of buckling factors for rectangular tubes.

When a simply supported plate undergoes elastic buckling, the critical load and mode of buckling depend on the aspect ratio of the plate. The aspect ratio of the plate determines the number of folds or lobes formed at buckling. For simply supported plates, the number of half sine waves is equal to the aspect ratio if the ratio is an integer. This phenomenon was confirmed experimentally on a steel plate by Rasmussen *et al* [24]. Meng *et al* [25] performed buckling experiments on polyvinylchloride tubes of different aspect ratios. The formation of elastic folds or lobes was clearly visible in their experiments. Along with experimental studies, finite element analysis of elastic and post buckling study of plates and tubes under different boundary conditions has also been performed [26, 27].

In this paper, a systematic study of the elastic buckling of plates and tubes using finite element analysis has been carried out. The buckling characteristics and critical loads for different kinds of thin wall structures including single plate, multi-wall structures, and square and rhombic tubes were investigated. A series of simulations for a single, simply supported wall with various aspect ratios was carried out and compared with theoretical predictions from literature. The transition of number of waves formed was clearly observed in the buckled profile. The simulations were then extended to multi-wall structures and the relation between the buckling characteristics of single plate and multi-wall structures were investigated. The buckling characteristics of rhombic tubes were investigated and compared with those of square tubes, and the effect of wall angle on critical loads was studied.

2.3 A brief review of buckling theory of simply supported plates and square tubes

2.3.1 *Buckling of plates*

Theory of plate buckling is well established in literature [8, 10, 11, and 15]. According to the theory, a plate acted upon by a vertical in-plane buckling load results in the formation of lobes along the height and width of the plate. These lobes are in the form of sinusoidal waves and are generally called half sine waves because each lobe looks like a sine wave in the period of 0 to π. This phenomenon is illustrated in Figure 2.1.

In this section, the theoretical formulation of the buckling of a plate simply supported or hinged along all the edges is reviewed in brief.

Figure 2.1(a) shows an example of a simply supported plate of width '*l*', height '*h*', and thickness '*t*'. Figure 2.1(b) and 2.1(c) show, respectively, the finite element model of the plate with loads and restraints and the buckled profile of the plate with two half sine waves.

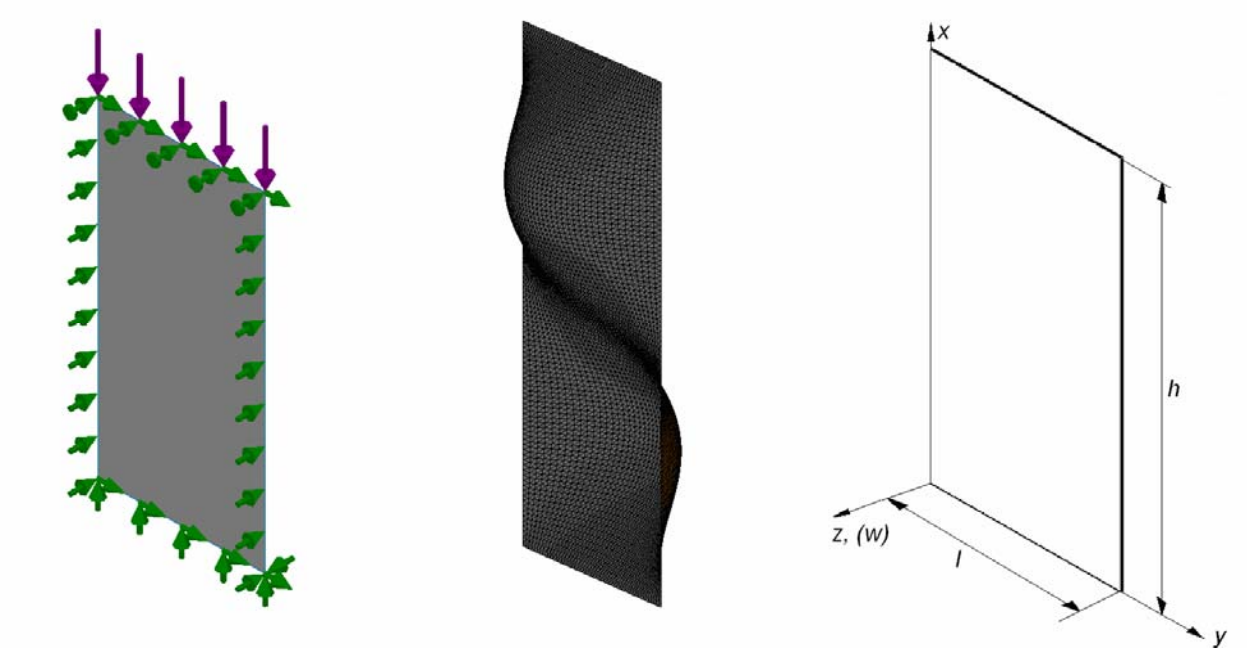

(a) **(b)** **(c)**

Figure 2.1: The rectangular plate (a) with the coordinate axis and dimensions, (b) as a model with restraints and load, and (c) deformed model of the plate from simulation result

Using a coordinate system as defined in Figure 2.1(a), the out-of-plane displacement '*w*' of a rectangular plate can be expressed in a double trigonometric series as [8]

$$w = \sum_{m=1}^{\infty} \sum_{n=1}^{\infty} a_{mn} \sin \frac{m\pi x}{h} \sin \frac{n\pi y}{l} \tag{2.1}$$

where, m and n are the number of half waves in x and y directions respectively, for the m-n buckling mode. The critical load is obtained by equating the work done by the compressive load and the strain energy of the plate at buckling as, [8]

$$F_x = \frac{\pi^2 h^2 D \sum_{m=1}^{\infty} \sum_{n=1}^{\infty} a_{mn}^2 \left(\frac{m^2}{h^2} + \frac{n^2}{l^2} \right)^2}{\sum_{m=1}^{\infty} \sum_{n=1}^{\infty} m^2 a_{mn}^2} \tag{2.2}$$

where, F_x is the critical value of compressive load per unit width of the plate and D is the flexural stiffness of the plate. It can be shown that for F_x to be minimum in Eqn. (2.2), all the values of coefficient a_{mn}, except one, are equal to zero [8]. For the lowest value of critical load, number of half waves along the width of the plate n is one, while the number of half waves formed along the height of the plate is governed by the aspect ratio of the plate. This leads to,

$$F_x = \frac{\pi^2 h^2 D}{m^2}\left(\frac{m^2}{h^2}+\frac{1}{l^2}\right)^2 \tag{2.3}$$

From this expression of the critical load per unit width of the plate, the total critical load of the plate of width l is equal to l times F_x and is expressed as,

$$P_{cr} = \frac{k\pi^2 E}{12(1-\nu^2)}\left(\frac{t^3}{l}\right) \tag{2.4}$$

where, E is the Young's modulus and v is the Poisson's ratio of the material, t is the thickness of the plate, and k is known as the buckling factor of the plate defined as,

$$k = \left(\frac{m}{\phi}+\frac{\phi}{m}\right)^2 \tag{2.5}$$

where $\phi = h/l$ is the aspect ratio. The value of k depends on the number of half waves m and the aspect ratio ϕ, as graphed in Figure 2.2.

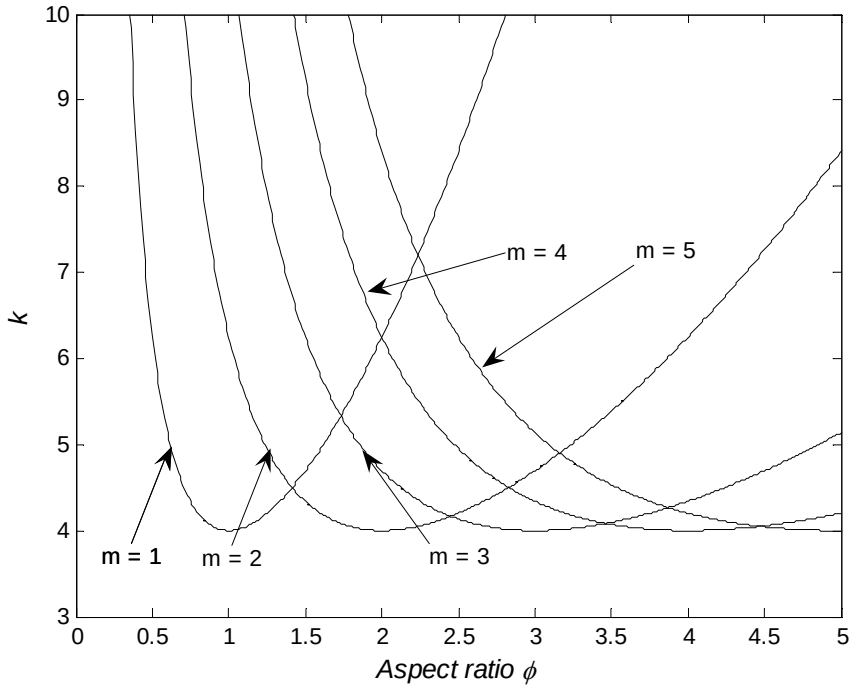

Figure 2.2: Variation of k with the change in aspect ratio of a simply supported rectangular tube under uni-axial loading

The value of k is minimal at the integer values of aspect ratio for which the number of half waves is equal to the aspect ratio as seen in Figure 2.2. This condition is theoretically

derived from the expression of k. The value of $(m/\phi + \phi/m)^2$ is minimum and equal to 4 when $\phi = m$. For example, a square plate ($\phi = 1$) will have lowest critical load when only one half wave is formed along the height direction. At the aspect ratio of the plate more than the transitional value of ϕ for $m = 1$ to $m = 2$, the number of half waves formed will change to 2 to maintain the lowest value of k. Derivation of the values of transitional aspect ratios is discussed in the following section.

2.3.2 Transition of number of half waves in plate buckling

According to Eqn. (2.4), at the lowest critical load or the least energy mode of buckling, the value of k should be minimal. Using Figure 2.2, the transitional aspect ratios at which the k-curve for m number of half waves and the k-curve for $m+1$ number of half waves intersect is determined by:

$$\left(\frac{m}{\phi_t}+\frac{\phi_t}{m}\right)^2 = \left(\frac{m+1}{\phi_t}+\frac{\phi_t}{m+1}\right)^2 \tag{2.6}$$

where ϕ_t, the transitional aspect ratio, is equal to

$$\phi_t = \sqrt{m(m+1)} \tag{2.7}$$

From Eqn. (2.7), the transitional aspect ratios is $\sqrt{2}$ for $m = 1$ to $m = 2$, $\sqrt{6}$ for $m = 2$ to $m = 3$, $\sqrt{12}$ for $m = 3$ to $m = 4$ and so on.

The critical load predicted by Eqn. (2.4) is only accurate when the buckled mode is a pure sine wave with m extrema. Such a pure sine wave mode occurs at the minima of the k-ϕ curves shown in Figure 2.2. Near m to m+1 wave transition, however, the buckled mode is no longer a pure sine wave, and more than one non-zero a_{mn} exist in Eqn. (2.2). Therefore, prediction by Eqn. (2.4) becomes approximate. However, FEM simulations, as presented in the later sections of this work, show that errors caused by the pure sine wave assumption are negligible and predictions from Eqn. (2.4) and Eqn. (2.7) agree very well with FEM results.

2.3.3 Buckling of square tubes

The buckling characteristics of a square tube or any even sided equilateral polygon tube is the simplest case of polygon tube buckling where each wall behaves as a simply supported plate. For a square tube under an axial compressive force with the top and bottom edges hinged or simply supported, the load is equally distributed on all of the plates. As all the walls are

identical in geometry and load, each plate has the same individual critical load, and therefore each wall reaches instability simultaneously. The waves on adjacent walls are formed in such a way that the common edges do not buckle, both walls rotate the same amount and in the same direction about the common edge, and therefore the wall angle remains unchanged before and after buckling [11]. This results in zero restraining moments at the common edges for the walls and the tube behaves as four independent simply supported plates put together with common edges. The critical load of the tube is therefore four times the critical load of the single plate [8], i.e.,

$$P_{cr} = 4 \times \frac{k\pi^2 E}{12\left(1-\nu^2\right)}\left(\frac{t^3}{l}\right) \tag{2.8}$$

The value of k is decided by the aspect ratio of the tube and the number of half sine waves formed, as described in the preceding section for the single plate. The theoretical buckling load is minimal for the tube when the aspect ratio of the tube has integer values for which the factor k is minimal.

Until the point of elastic buckling of a supported plate, multi-wall or a tubular structure, the buckling occurs with the buckling of the walls only. In the elastic-plastic buckling regime, the walls lose the load carrying capacity and the load is carried by the vertical edges of the structure. In a supported plate structure, part of the plate near the vertical edges acts as the load carrier whereas, in tubular and multi wall structures, the common vertical edges start to buckle in the post buckling range thus providing post-buckling strength to the structure. A review on the elastic-plastic buckling and post buckling analysis of plate and tube structures is presented in [21].

2.4 Computational model of single plate, multi-wall structures, square tubes and rhombic tubes

In this section, finite element modeling and simulations of a simply supported plate, multi-wall structures, square tubes and rhombic tubes are presented. For the finite element simulations, a commercial software package, SolidWorks Simulation (http://solidworks.com/), was used. SolidWorks uses linearized Eigenvalue method to solve the elastic buckling problem.

2.4.1 Buckling of a simply supported plate

A plate simply supported about all of its edges was simulated for buckling using SolidWorks Simulation. The plate dimensions were l = 3.175 mm, t = 0.025 mm, and the height of the plate was varied to obtain the required aspect ratio from 0.25 to 4. For the thin wall structures simulated in this work, the height to thickness ratio of the plates had a range of 30 to 1000, and shell mesh was used for meshing the geometries. The present study was performed with a future goal of investigating the behavior of cells of a square cell honeycomb structure. Hence, the dimensions of the walls of all geometries used in this study were selected as that of the wall dimensions of each cell of the honeycomb.

Triangular shell elements with three vertex nodes and three mid-edge nodes per element were used. Every node of the elements had six degrees of freedom. Figure 2.3 shows a typical meshed model of the single plate with an aspect ratio of two under simply supported conditions along all edges. The mesh had a total of 4920 triangular elements with 10,055 nodes. The material has E = 100 GPa and ν = 0.3. The material properties used in the simulation study represents a titanium alloy. Type of simulation was purely elastic buckling and thus, value of yield strength was not required in the simulation.

Bottom edge of the plate was restrained as hinged, that is, translational degrees of freedom for all nodes along the edge were blocked but rotation about the edge was allowed. The top edge was free to move only in the vertically downward direction and was free to rotate about the edge. The non-loading vertical edges were restrained from moving in the direction perpendicular to the plate. In Figure 2.3, a short, green arrow indicates that the degree of freedom in the arrow direction is restrained. The force was applied on the top edge in vertically downward direction, represented by long, purple arrows in the figure.

Critical buckling loads for all the simulations were recorded and plotted against the aspect ratios. These are shown in following sections.

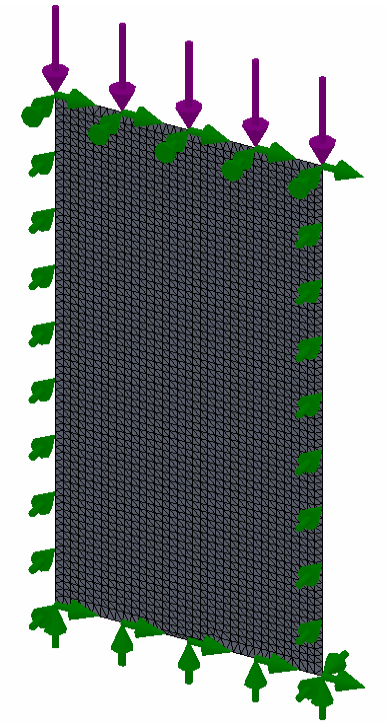

Figure 2.3: The meshed model of a single rectangular plate with aspect ratio two with the simply supported boundary conditions and loads on it

According to the plate buckling theory, the transitions of number of half waves take place at certain values of aspect ratios to maintain the lowest value of buckling factor k, as expressed by Eqn. (2.7). From the equation, the transition of number of half waves from $m = 1$ to $m = 2$ takes place at an aspect ratio of $\sqrt{2}$. To observe this phenomenon, a plate was simulated under buckling load with a series of aspect ratios around $\sqrt{2}$ at small intervals. From the results of the simulation, the transition of the number of half waves was clearly observed. Figure 2.4 shows the transition of number of half waves m from 1 to 2.

The figure shows that the transition of number of half waves from 1 to 2 took place at an aspect ratio of 1.414 (or $\approx\sqrt{2}$) which agrees with the theoretical expectation. Further transitions of number of half waves to 3, 4 and 5 were observed in the simulation at aspect ratios of 2.449 ($\approx\sqrt{6}$), 3.464 ($\approx\sqrt{12}$) and 4.47 ($\approx\sqrt{20}$) respectively, in agreement with plate buckling theory.

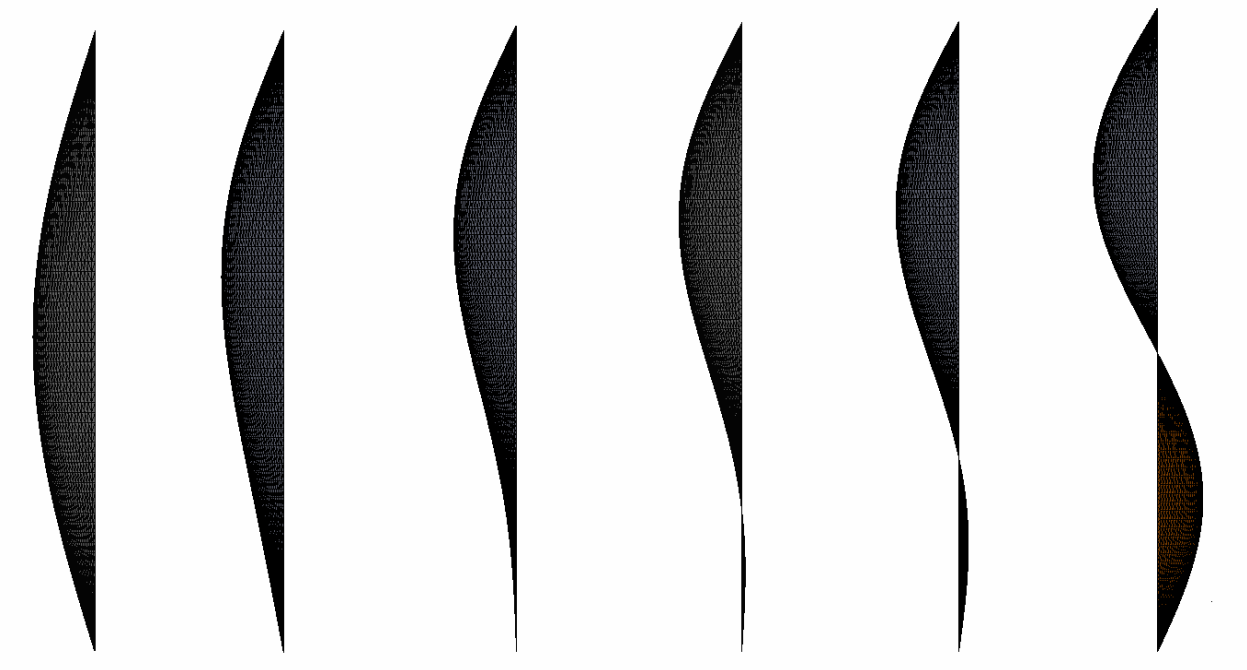

(a) **(b)** **(c)** **(d)** **(e)** **(f)**

Figure 2.4: Buckling of a single plate with aspect ratio of (a) 1.2, (b) 1.4, (c) 1.41, (d) 1.414, (e) 1.417 and (f) 1.45

2.4.2 Buckling of multi-wall structures

Finite element simulations were also performed for multi-wall structures including joint walls with a wall angle of 90 degrees and three joint walls (U-section) also having 90 degrees angle between the adjacent walls. The walls had following dimensions: l = 3.175 mm and t = 0.025 mm. Figure 2.5 shows the models of these structures. Similar element type and material properties were used for these models as were used for the single plate. The open vertical edges were constrained from moving in their respective out-of-plane direction and the top and bottom edges were restrained as hinged. Hinged condition of the top edges allowed motion of the edge only in vertically downward direction and rotation about the edge. Figure 2.6 shows the boundary conditions applied to the edges of two joint plates shown in Figure 2.5(a).

Aspect ratios of the thin wall structures were varied, similar to the single plate, and the lowest critical buckling loads were noted. The transition of number of half waves took place in the expected manner as was observed in the case of single plate. The results are discussed in the Results and Discussion section where they are compared with the critical loads for a single plate

and for other thin wall structures. These results confirm that the multiple plate structure behaves as a set of individual simply supported plates.

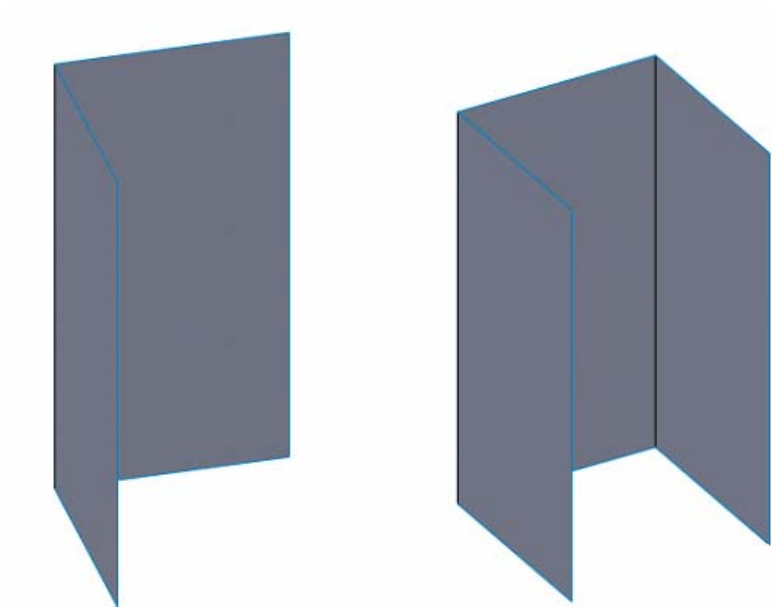

(a) **(b)**

Figure 2.5: The finite element models of (a) two joint walls and (b) three joint walls

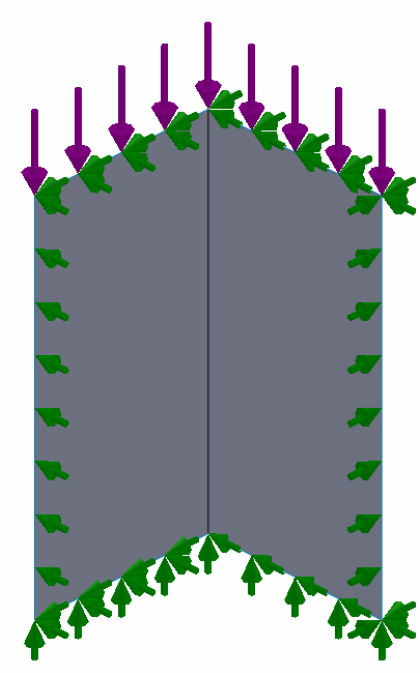

Figure 2.6: The model of the geometry in Figure 2.5(a) with applied boundary conditions and loads

2.4.3 Buckling of square tubes

It was postulated in [8] that a square tube under a uniformly distributed buckling load behaves as four individual simply supported plates. Critical load of the tube is thus four times the critical load of a simply supported plate. To confirm this postulation, critical load and buckling behavior of simply supported tubes were compared with the total critical buckling load of four separate simply supported single plates. Figure 2.7 shows the buckling simulation results of the square tube and four single rectangular plates simply supported about all its edges. Walls of the square tube and the multi-wall sections were modeled with a width of 3.175 *mm* and a height of 6.35 *mm*, similar to that of the model of the simply supported plate. Each wall and plate had a uniform thickness of 0.025 *mm*. The four plates in Figure 2.7(b) were placed together in the form of a square tube. Each plate was independent of its adjacent plates. The material used in this simulation had a Young's modulus of 100 GPa and Poisson's ratio of 0.3. Triangular shell elements with six nodes were used to model the square tube as well as the four separate plates. Total number of elements in the square tube was 5,184 in the square tube with each element of size 0.18 mm.

Critical loads of the two different structures were found to match very well, as shown in Table 2.1. Square tubes obey the condition that after buckling, the buckled profile maintains the initial wall corner angle of 90 degrees between adjacent plates. This is evident by the deformation profile which shows alternate inward and outward folds in adjacent plates as shown in Figure 2.7(a). However, when the four independent rectangular plates are placed in the form of square tube (Figure 2.7(b)), the adjacent plates have no relation with each other. The buckled profile exhibits outward or inwards folds independent of adjacent plates (Figure 2.7(c)). Subsequent FEM simulations were performed on square tubes of the same width and thickness of walls by gradually varying the height starting from an aspect ratio of 0.25 to 4.4. The results of these simulations are discussed in the Results and Discussion section where the critical loads of the square tubes are compared with those of other structures.

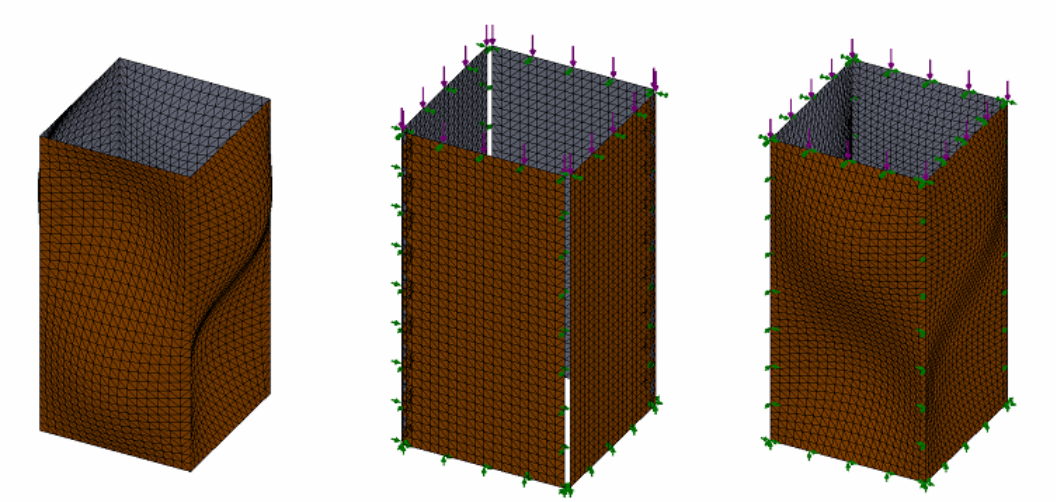

(a) **(b)** **(c)**

Figure 2.7: (a) The buckled profiles of a square tube with the simply supported conditions applied to the top and bottom edges, (b) four individual plates with simply supported conditions applied to all their edges put together in the shape of square tube and (c) buckled profile of Figure 2.7(b) exhibiting outward or inwards folds independent of adjacent plates

Table 2.1 Critical load comparison of a square tube and four independent simply supported plates put together in the form of a tube

Geometry	Critical load [N]	Critical load per plate [N]
Square tube	6.953	1.738
Four independent simply supported plates	6.954	1.739

2.5 Results and discussion

2.5.1Comparisons of critical loads of single plate, multi-wall structures and square tubes

The results of a series of simulations performed on the multi-wall structures starting from the single plate were recorded and the critical loads per plate were compared for some aspect ratios. Table 2.2 lists the critical loads for a single plate, two walls, three walls and a square tube for certain aspect ratios. The critical load per wall of each structure was compared at respective

values of aspect ratios. Critical load per wall was determined by dividing the total critical load of the structure by the total number of walls or plates present in the structure,

$$P_{cr} / wall = \frac{P_{cr}}{N} \tag{2.9}$$

where *'N'* is the number of walls of the geometry.

The results in this table reveal that the critical loads reach a local maximum at the transition aspect ratios on the k versus ϕ curve as predicted by Eqn. (2.7). It is also observed that the critical loads reach a minimum at the integer aspect ratios and then increase monotonically till the transitional aspect ratio. At transition, the change of number of half waves takes place and the critical load decreases with increasing aspect ratio until the next integer aspect ratio. This cycle continues with increasing aspect ratio.

The data in Table 2.2 is plotted in Figure 2.8 which shows the variation of the critical load per wall of the different structures with the change of aspect ratio. Theory suggests that a multi-wall structure under buckling loads behaves as multiple simply supported plates and that the critical load of the structure is number of walls times the critical load of each wall (considered as a simply supported plate). This was verified as the results of critical load per wall for all simulated structures were virtually indistinguishable. The theoretical values of critical loads were also plotted in the figure using the values of k from Eqn. (2.5) and the critical load values using Eqn. (2.4). The aspect ratio at which transition of number of half waves takes place is in good agreement with theoretical prediction. It was found that the critical loads from the simulations of all structures investigated had a maximum discrepancy of 5% with the theoretical result.

Table 2.2: The critical load data for the series of simulations performed on multi-walled structures for various aspect ratios

Aspect ratio	Critical load per wall (P_{cr}/Number of Plates) [N]			
	One plate	Two plates	Three plates	Square tube
0.25	7.838	7.840	7.842	7.845
0.75	1.825	1.825	1.825	1.825
1	1.699	1.699	1.699	1.699
1.4	1.931	1.931	1.931	1.930
1.41	1.936	1.936	1.936	1.936
1.414 (≈√2)	1.936	1.936	1.936	1.936

1.417	1.935	1.935	1.935	1.935
1.42	1.934	1.933	1.933	1.933
1.8	1.754	1.754	1.754	1.754
2	1.739	1.739	1.738	1.738
2.2	1.758	1.758	1.758	1.758
2.445	1.815	1.815	1.815	1.815
2.449 (≈√6)	1.815	1.815	1.815	1.815
2.45	1.815	1.815	1.815	1.815
2.455	1.815	1.814	1.814	1.815
2.8	1.758	1.758	1.758	1.758
3	1.751	1.751	1.751	1.751
3.2	1.760	1.760	1.760	1.760
3.45	1.787	1.787	1.787	1.787
3.464 (≈√12)	1.788	1.788	1.788	1.788
3.47	1.788	1.788	1.788	1.788
3.48	1.787	1.787	1.787	1.787
3.8	1.761	1.761	1.761	1.761
4	1.757	1.757	1.757	1.757
4.4	1.774	1.774	1.774	1.774

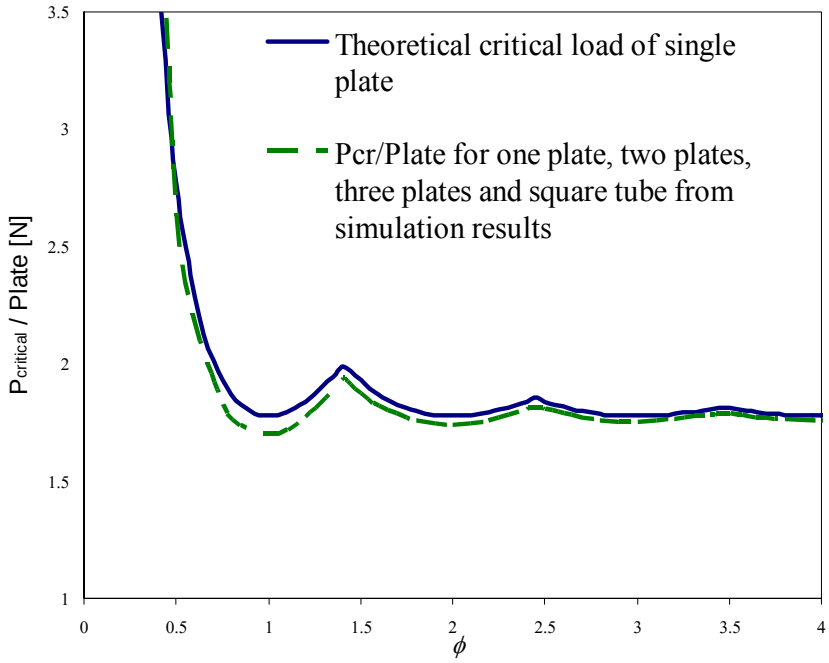

Figure 2.8: Plot of critical loads against the aspect ratios for the various geometries

Based on simulation results from this work, it was inferred that the critical load of open wall structures with any number of walls with simply supported open edges and closed tube structures with even number of walls is equal to the critical load of a single simply supported plate multiplied by the number of walls in the structure. For regular closed wall structures or tubes, the statement holds true only for tubes with even number of sides. For regular tubes with odd number of walls, the buckling mode tends to form double half waves in the non-loading direction to maintain same wall angles before and after buckling. To test this inference, a few simulations were performed on a hexagonal tube and a five wall open section with simply supported open edges (l = 3.175 mm, t = 0.025 mm, and at some selected aspect ratios). Table 2.3 shows the results of critical loads per wall for these simulations. It was observed that the critical load pattern and the change of number of half waves were the same as the behavior of the single simply supported plate.

Table 2.3: The critical load per wall data of a simply supported hexagonal tube and the corresponding 5-wall open section

Aspect ratio	Critical load per wall P_{cr}/wall	
	Hexagonal tube	5-wall open section
1	1.699	1.699
1.414 (≈√2)	1.936	1.936
2	1.738	1.7385
2.449 (≈√6)	1.822	1.815
3	1.751	1.751

2.5.2 Effects of wall angle in multi-wall structures

The elastic buckling theory of plates postulates that a square tube is essentially four simply supported plates put together. From the simulation results in the previous sections, it was seen that the two-, three- and four-wall structures have the critical loads of twice, thrice and four times the critical load of a simply supported single plate respectively. This implies that each wall of a square tube behaves as an independent plate under the action of a critical buckling load. The only relation obeyed by the adjacent walls of a multi-wall structure is that the walls rotate by the same amount about the common edge and the wall angle remains same before and after buckling. Work in [8, 28] have proposed theoretically that the elastic buckling critical load of a rhombic

tube and a square tube will be the same. From this postulates, it is therefore proposed in this work that the value of the wall angle should not have any effect on the critical load of the geometry as long as the open edges are subjected to the simply supported condition and the angle between the plates is maintained before and after buckling.

To verify the above proposal, simulations were performed on some two-plate geometries and rhombic tubes having dimensions similar to the previous geometries with l = 3.175 mm, t = 0.025 mm and h = 6.35 mm to keep the aspect ratio of 2. The wall angle was varied and critical loads in each case were noted. Figure 2.9 shows the deflected profiles of different wall angles. Except for the case in which the angle between the two plates was 180 degrees (which means the two plates are in fact a single plate of twice the width), all the plates had almost the same critical load value. Table 2.4 summarizes the values of wall angle used in the simulation and their corresponding critical loads.

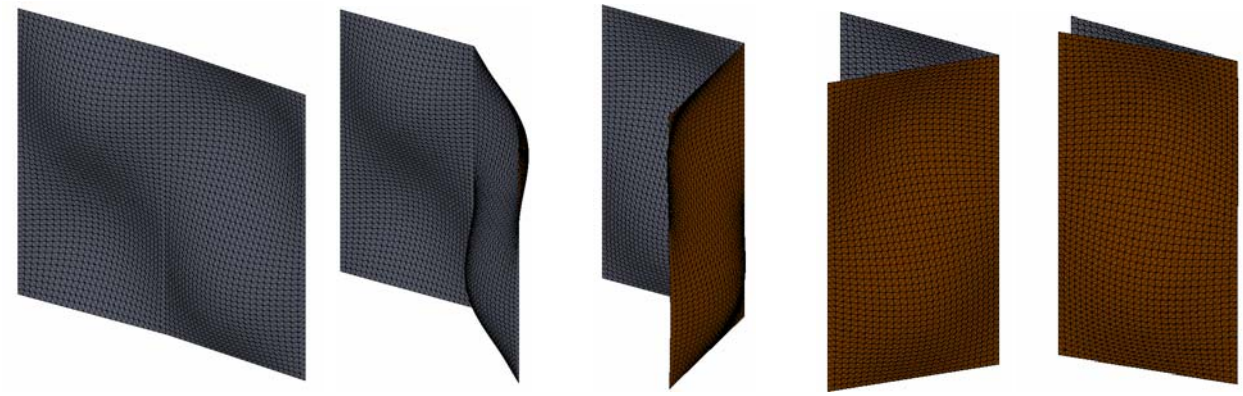

(a) **(b)** **(c)** **(d)** **(e)**

Figure 2.9: The buckled shapes of two joint plate geometry with the angle of (a) 175 (b) 135 (c) 90 (d) 45 and (e) 10 degrees between the plates

Table 2.4: The critical loads of the two-wall structure geometry with different wall angles and a single plate from simulation

Wall Angle [degrees]	Critical load P_{cr} [N]	Critical load per plate P_{cr}/plate [N]	Critical load of a single plate [N]
175	3.4661	1.7330	
135	3.4769	1.7384	
90	3.4770	1.7385	1.7387
45	3.4749	1.7374	
10	3.4254	1.7127	

The results in the table reveal that the critical load of the two-wall structure is practically independent of the wall angle and the value of critical load of a two wall structure with any wall angle is the same as that of the wall angle of 90^o.

2.5.3 Effects of wall angle of rhombic tubes

The previous subsection establishes that the wall angle of a two-wall structure does not affect the critical load of the structure. It follows logically that the critical loads of rhombic tubes with different wall angles should be the same. To verify this inference, FEM simulations were performed on different rhombic tubes. Figure 2.10 shows the buckled geometry of different rhombic tubes. The tubes used here had wall angles of 10, 45 and 90 degrees. Table 2.5 shows the critical load data obtained from the simulation results.

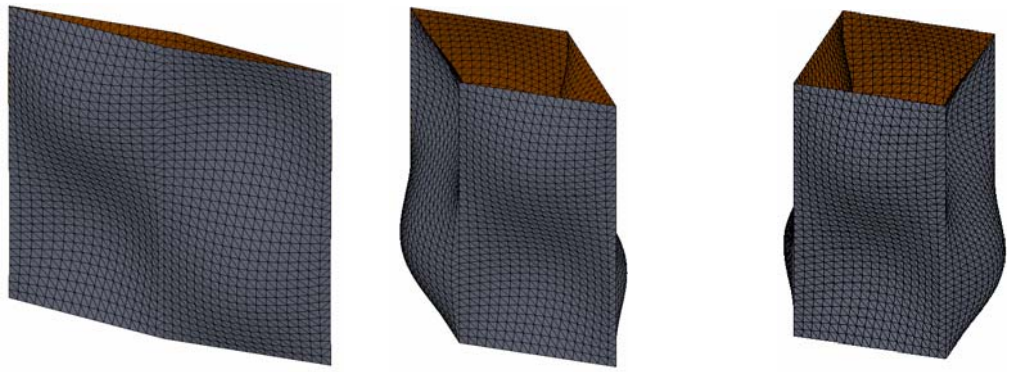

(a) **(b)** **(c)**

Figure 2.10: The rhombic tubes with the acute angle between the walls as (a) 10, (b) 45 and (c) 90 degrees showing the buckled shapes after simulation

The simulation results in Table 2.5 reveal that the critical buckling load of a rhombic tube is practically independent of wall angle. This implies that a tube with a wall angle of 10^o has the same elastic buckling critical load as that of a square tube. However, it is noted that for very small wall angles ($<10^o$) and above a certain height of the tube, the Euler buckling mode prevails in which the tube buckles as a uniform column instead of four related buckling plates, resulting in a lower critical load than the total critical load of four walls. Euler buckling of rectangular and square tubes in plastic phase was observed experimentally in [29].

Table 2.5: The critical loads of the rhombic tubes with different acute angles between the walls and a square tube from the results of simulation

Acute angle between the plates in degrees	Critical load P_{cr} for the structure [N]
10	6.8484
45	6.9496
90 (Square tube)	6.9528

2.6 Implications for structural properties of honeycomb

Theory of buckling of plate and tubes can be applied to the study of elastic buckling of honeycomb structures. Structures of honeycombs are in the form of square or hexagonal cells. For each of these cells, represented as a square or hexagonal tube, the critical load can be represented as

$$P_{cr} = N \times \frac{k\pi^2 E}{12\left(1-\nu^2\right)}\left(\frac{t^3}{l}\right) \tag{2.10}$$

Here, N is the number of walls in each cell which depends on the shape of the honeycomb cells. Estimation of critical load of a square cell honeycomb based on this approach has been presented in [30].

2.7 Summary and conclusions

Elastic buckling of thin plates, multi-walls, and tubes was studied theoretically and computationally using the finite element analysis. The theoretical predictions were compared with finite element simulation results, and the agreement was excellent. The postulation in [8] that each wall of a square tube under uniform buckling load behaves as a simply supported plate

was confirmed by the finite element simulations. It was shown that the critical load of buckling of a square tube is equal to four times the critical load of an individual simply supported plate. The occurrence of transition of number of half waves was observed in the simulation results at the values of transitional aspect ratios defined by the theory. The effect of wall angle of a multi-wall structure or a rhombic tube on the critical buckling load was investigated. It was found that the critical load of a multi-wall structure or rhombic tube is independent of the wall angle unless the wall angle is very small ($<10^{o}$), and that the elastic buckling critical load of a rhombic tube of any angle will be equal to the critical load of a square tube of the same wall geometry. The extension of theory of buckling of plates and tubes to honeycombs was discussed.

2.8 References

[1] Wierzbicki T. and Abramowicz W., (1983), "On The Crushing Mechanics of Thin Walled Structures", *Journal of Applied Mechanics*, Vol: 50 No. 4 pp. 727–734

[2] Mahmood H. F. and Paluszny A., (1981), "Design of Thin Walled Columns for Crush Energy Management – Their Strength and Mode of Collapse", *Proc. Of 4th Int. Conf. of Vehic. Struct. Mech.*, SAE, pp. 7–18

[3] Zhang X., Cheng G., You Z. and Zhang H., (2007), "Energy Absorption of Axially Compressed Thin Walled Square Tubes With Patterns", *Thin–Walled Structures*, Vol: 45, Issue: 9, pp. 737–746

[4] Soden P. D., Al-Hassani S. T. S. and W. Johnson, (1974), "The Crumpling of Polyvinylchloride Tubes Under Static and Axial Dynamic Loads". *Conference on Mechanical Properties at High Rates of Strain., Inst. of Physics (London)*, Conf. Series No. 21, pp. 327–338

[5] Johnson W., Soden P. D. and Al-Hassani S. T. S. , (1977), "Inextensional Collapse of Thin-Walled Tubes Under Axial Compression". *Journal of Strain Analysis*, Vol: 12 No. 4, pp. 317–330

[6] Lowe W. T., Al-Hassani S. T. S., Johnson W., (1972), "Impact Behavior of Small Scale Model Motor Coaches", *Proceedings – Institution of Mechanical Engineers*, Vol: 186, pp. 409–419

[7] Wierzbicki T., Akertstrom T., (1977), "Dynamic Crushing of Strain Rate Sensitive Box Columns", *International Conference on Vehical Structural Mechanics – Proceedings*, Month – April, pp. 19–31

[8] Timoshenko S. P. and Gere J. M, (1961), *Theory of Elastic Stability.* McGraw-Hill New York pp. 351

[9] Von Karman T., Sechler E. E. and Donnell L. H., (1932), "The Strength of Thin Plate in Compression", *Transaction of ASME*, Vol: 54, pp. 53–57

[10] Bulson P. S., (1969), *Stability of Flat Plates.* American Elsevier Publication company, New York, pp. 27, 295.

[11] Bleich F., (1952), *Buckling Strength of Metal Structures.* McGraw-Hill New York, pp. 302

[12] Winter G., (1947), "Strength of Thin Steel Compression Flanges", *Transactions of the ASCE*, Vol: 112, pp. 527–576

[13] Bradford M. A. and Azhari M., (1995), "Buckling of Plates with Different End Conditions Using the Finite Strip Method", *Computers and Structures*, Vol: 56, No. 1, pp. 75–83

[14] Swartz S. E. and O'Neill R. J., (1995), "Linear Elastic Buckling of Plates Subjected to Combined Loads", *Thin–Walled Structures*, Vol: 21 Issue: 1, pp. 1– 15.

[15] Paik J. K. and Thayamballi A. K., (2000), "Buckling Strength of Steel Plating with Elastically Restrained Edges". *Thin-Walled Structures*, Vol. 37: Issue: 1, pp. 27–55.

[16] Byklum E. and Amdahl J., (2002), "A Simplified Method for Elastic Large Deflection Analysis of Plates and Stiffened Panels Due to Local Buckling". *Thin-Walled Structures*, Vol: 40 Issue: 11, pp. 925–953.

[17] Elgaaly M., (2000), "Post-buckling Behavior of Thin Steel Plates Using Computational Models". *Advances in Engineering Software*, Vol: 31 Issue: 8, pp. 511–517.

[18] Lundquist E. E., (1939), "Local Instability of Symmetrical Rectangular Tubes Under Axial Compression*". Nat. Advisory Comm. Aeronaut. Tech. Note* No. 686,

[19] Li S. and Reid S. R., (1990), "Relationship Between the Elastic Buckling of Square Tubes and Rectangular Plates", *Journal of Applied Mechanics*, Vol: 57 No: 4, pp. 969–973.

[20] Hui D., (1986), "Design of Beneficial Geometric Imperfections for Elastic Collapse of Thin Walled-Box Columns", *International Journal of Mechanical Sciences*, Vol: 28 Issue: 3, pp. 163–172.

[21] Rhodes J., (2002), "Buckling of Thin Plates and Members – and Early Work on Rectangular Tubes". *Thin-Walled Structures*, Vol: 40 Issue: 2, pp. 87–108.

[22] Li S. and Reid S. R., (1992), "The Plastic Buckling of Axially Compressed Square Tubes", *Journal of Applied Mechanics*, Vol: 59, No. 2, pp. 276–282

[23] Kandil K. S. and Calladine C. R., (1986), "Classical, Local Buckling of Tubes having Rectangular Cross-Sections". *International Journal of Mechanical Sciences*, Vol: 28 Issue: 11, pp. 789–797.

[24] Rasmussen K., Burns T., Bezkoravainy P. and Bambach M., (2003), "Numerical Modeling of Stainless Steel Plates in Compression", *Journal of Constructional Steel Research*. Vol: 59, Issue: 11, pp. 1345–1362

[25] Meng Q., Al-Hassani S. T. S. and Soden P. D., (1983), "Axial Crushing of Square Tubes", *International Journal of Mechanical Sciences*, Vol: 25 Issue: 9, pp. 747–773.

[26] Fillipov S. B., Haseganu E. M. and Smirnov A. L., (2000), "Buckling Analysis of Axially Compressed Square Elastic Tubes with Weakly Supported Edges", *Technische Mechanik*, Vol: 20 Issue: 1, pp. 13–20.

[27] Karagiozova D. and Jones N., (2004), "Dynamic Buckling of Elastic-Plastic Square Tubes Under Axial Impact–II: Structural Response"*, International Journal of Impact Engineering*, Vol: 30 Issue: 2, pp. 167–192.

[28] Wittrick W. H, Curzon P. L. V., (1968), "Local Buckling of Long Polygon Tubes in Combined Compression and Torsion". *International Journal of Mechanical Sciences*. Vol 10, No. 10, pp. 849–857.

[29] Reid S. R., Reddy T. Y. and Gray M. D., (1986), "Static and Dynamic Axial Crushing of Foam-Filled Sheet Metal Tubes". *International Journal of Mechanical Sciences*. Vol: 28 No. 5, pp. 295–322.

[30] Cote F., Deshpande V. S., Fleck N. A. and Evans A. G., (2004), "The Out-of-Plane Compressive Behavior of Metallic Honeycombs". Materials Science and Engineering A. Vol: 380, pp. 272–280.

Chapter 3 - Elastic Buckling Characteristics of Quadrilateral Tubes under Uni-Axial Compressive Loads

3.1 Abstract

Plate and tubular structures constitute of an important segment in the design of various structural members in automobile, aeronautical and civil applications. Properties of these structures in elastic buckling and post-buckling are well established in various studies existing in literature. In this study, the theoretical formulation of the critical load calculations of quadrilateral tubes was explicitly reviewed and some important aspects of buckling of rhombic and parallelogram tubes were introduced. Also, the possibility of Euler buckling of tubular structures after certain aspect ratio was investigated for any generalized rhombic and parallelogram tube. Following the theoretical study, a systematic process of analyzing the elastic buckling characteristics of tubes having square, rectangular, rhombic and parallelogram cross-sections was approached using finite element simulation. The simulation results were compared with the expected predictions from the theory of buckling of plates and tubes. Also, some experimental tests were carried out on some square and rhombic tubes of certain aspect ratios. The goal of these experiments was to validate the theoretical and computational results of the buckling critical load and buckling mode shape of the square and rhombic tubes.

3.2 Introduction

Elastic buckling behavior of simply supported plates was first studied theoretically by Bryan [1] in 1891. Since then, the investigation of buckling behavior of supported plate structures and polygon tubular structures has emerged as one of the important fields of research of structural mechanics. Supported plates and tubular structures have evolved to be widely applied in various applications in aeronautical, marine and civil applications. The plate, tube and cellular structures have an excellent strength-to-weight ratio. These are also widely used as crash-safety structures in various impact scenarios because of their energy absorbing properties in post-buckling. In this study, the elastic buckling properties of square and rectangular tubes are revisited with the use of theoretical, computational and experimental studies. Also, a study on

rhombic and parallelogram tubes was carried out with the use of theory of buckling of plates and finite element method (FEM) studies.

Early studies on buckling behavior of polygon tubes by Timoshenko and Gere [2] postulated that the buckling behavior of any polygon tubular structure depends on the behavior of walls of the tube. According to this theory, the simplest case of tube buckling is a case of a regular polygon tube with even number of walls. In this case, all the walls start buckling as simply supported plates in wall buckling mode at a same load with the formation of lobes in the shape of sine waves along the height of the walls. Thus, the critical load of a square tube is derived as four times the critical load of each wall in simply supported condition. In the case of rectangular tubes however, the critical load of the longer walls is lower compared to the critical load of the shorter walls. This makes the shorter walls restrain the longer walls from buckling thus pushing the critical load to a higher value. This study was first performed by Lundquist in [3] and later presented in [4-6]. Some of the recent theoretical works discussing on stability of plates are presented in [7- 9]. Following the theoretical work, numerous studies have presented computational and experimental studies to investigate the buckling characteristics of plate structures and square and rectangular tube structures. Some of the works on computational and experimental studies of buckling of plates and tubes are presented in [10-12].

Also, an extensive research on the post-buckling of polygon tubular structures following the buckling behavior has been performed in the past. The post-buckling behavior of tubular structures is an important field of research due to the extensive use of polygon tubes, along with circular tubes in the crash safety structures in automobiles. The post-buckling strength of supported plates and polygon tubes depend on the history of elastic buckling behavior of the tube and the load carrying capacity of the vertical edges of the structure in post-buckling. After the first elastic buckling point, the walls lose the load carrying capacity. At this state, the un-deformed vertical edges act as the load carrying members of the structure. Works on the post-buckling strength of a supported plate has been illustrated in [13-15]. Relating to the buckling and post-buckling properties of plates and their behavior in the quadrilateral tube structure, the energy absorbing characteristics of square and rectangular tubes has been discussed by many researchers. Some of the work on these studies is presented in [16-18]. Apart from the theoretical work, considerable amount of experimental and computational work has been presented in many articles. Some of the important works are shown in [16, 19-22]. A review on the theoretical

works on the buckling and post buckling of plate and quadrilateral tubular structures has been presented in [23].

In the present study, the first section discusses the elastic buckling properties of square and rectangular tubes. The discussion presented in this study is based on the previous works presented in various studies on the tube buckling properties. The buckling of supported plates was reviewed and explicitly discussed by elaborating the method used in [4]. The buckling behavior of square and rectangular tubes of various length ratios was derived by considering different cases of the supported plate structures representing walls of the tube. A plot of values of the buckling factor *k* with varying aspect ratios of different tubes is presented with the use of this theory. Also, studies on the behavior of rhombic and parallelogram tubes under buckling loads were carried out. Theory of multi walled structures postulates from [2] states that the angle between the walls of a structure buckling in wall buckling mode does not affect the overall critical load of the structure. This implies that the behavior of rhombic and parallelogram tubes is expected to be similar to the behavior of corresponding square and rectangular tube respectively. This theory was verified in [24] for the case of rhombic tubes, using finite element simulation results. In the present study, the possibility of Euler buckling was also considered for tubes and an equation to derive the critical height of the tube was formulated. The equation calculates the critical height after which the tube buckles in Euler mode instead of the walls buckling in plate buckling mode. The study of Euler buckling of square tubes was previously discussed in [16,25]. Abramowicz *et al* [25] derived the equation of critical aspect ratio of the square tube considering the top and bottom faces of the tube as fixed faces. The present study presents a more realistic case for both rhombic and parallelogram tubes by considering the Euler buckling of the tubes along the minimum inertia axis. The top and bottom faces of the tubes were considered as hinged along the minimum inertia axis and the equation was derived for a hinged condition which is more practical in a real scenario. With these considerations, a MATLAB program was coded to calculate the critical load at any given height of a tube by considering both the wall buckling mode and Euler buckling mode. The program was coded to decide the buckling mode by comparing the critical load in each mode of buckling.

Following the theoretical studies, an extensive finite element simulation study was performed on each of the tube geometries discussed theoretically. The phenomenon of transition of number of half-waves formed along the height of the tube was observed in the simulation

results of all the tubes. This was examined by critically studying the tube behavior at the transition aspect ratios. Also, the Euler buckling of the rhombic and parallelogram tubes were studied using finite element models of the tubes with angles of 45^0 and 60^0 respectively. The next section discusses the procedure of the experimental method performed on some of the tubes made of Acrylonitrile Butadiene Styrene (ABS) plastic. A total of twelve tubes were tested, out of which, two tubes were made of rhombic cross-section with an angle of 45^o and an aspect ratio of 1. The remaining ten tubes had a square cross section and were made of heights corresponding to the aspect ratios of first three minima of the buckling factor and first two transitional aspect ratios. The tubes were tested under uniform compressive loads and the elastic buckling critical loads were calculated from the test data.

Finally, the theoretical predictions were compared to simulation and experimental results to validate the studies. Good accuracies were observed with agreement of the three results. The critical load data comparisons of the respective tubes are presented in graphical forms.

3.3 Elastic Buckling of Quadrilateral Tubes

Elastic buckling principles of a quadrilateral tube (with each wall of the tube buckling individually) depends on the buckling characteristics of each wall. For the critical load formulation of tubes, the walls of a tube are assumed to behave as independent supported plates under the action of uni-axial load along the top and bottom edges and the non-loading edges subjected to different boundary conditions. The boundary conditions of the walls depend on the geometry of the walls of the tube. The simplest case of quadrilateral tube buckling is a case of a square tube under uniform uni-axial loading and the most complicated case is of an irregular quadrilateral cross-section. In the case of a square tube, all of the individual walls have the same value of critical load in the lowest energy buckling mode. This results in the simultaneous buckling of all of the walls of the square tube with the value of critical load equal to four times the critical load of each wall. In the case of a rectangular tube, however, the critical load of the longer walls (hereafter referred to as buckling walls) is lower than the shorter walls (hereafter referred to as restraining walls). This causes the buckling walls to reach their instability point before the restraining walls under the application of a uniform load. As a result of this, a restraining moment provided by the restraining walls acts on the buckling walls, which tries to restrain the bending of buckling walls. Based on this explanation and earlier studies [3,4], the

buckling theory of square and rectangular tubes is reviewed and discussed elaborately in the following sub-sections. A generalized condition of buckling of the buckling wall is discussed and the dependency of the critical load on the dimensions of restraining walls is derived. This theory is then extended to rhombic and parallelogram tubes and the transition from wall buckling to global Euler buckling of the tubes is investigated.

3.3.1 Buckling Condition of Buckling Walls Based on the Theory of Supported Rectangular Plates

The theory of plate buckling is well established in numerous works in the past. Some of the works illustrating the theory of elastic buckling of plates are presented in [2, 4, 5]. According to this theory, a plate acted upon by a vertical in-plane buckling load results in the formation of lobes along the height and width of the plate. These lobes are in the form of sinusoidal waves and are generally called half-sine waves or half-waves because each lobe resembles a sine wave in the period of 0 to π. This phenomenon, as exhibited in a plate simply supported along all the edges is illustrated in Figure 3.1. Figure 3.1(a) shows an example of a supported plate of width 'l', height 'h', and thickness 't'. Figure 3.1(b) and 3.1(c) show the finite element model of the plate with loads and restraints and the exaggerated buckled profile of the plate with two half-waves, respectively.

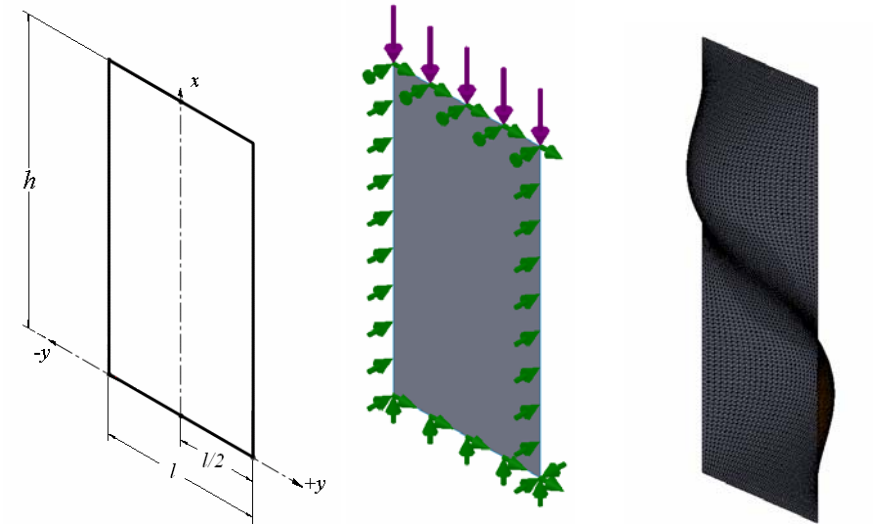

(a) **(b)** **(c)**

Figure 3.1 The rectangular plate (a) with the coordinate axis and dimensions, (b) as a model with restraints and load, and (c) deformed model of the plate from simulation result

In the buckling phenomenon of a rectangular tube, as discussed earlier, the buckling wall behaves as a plate torsionally or elastically restrained along the vertical edges. In this sub-section, the general theoretical condition of the buckling of a plate equally elastically supported along both of the vertical edges is discussed. The work presented in this section is a discussion of rectangular tube buckling, based on the derivation of the elastic buckling of a rectangular plate elastically restrained along the edges, presented in [4]

In the derivation process, the buckling walls of a rectangular tube are considered as supported plates under the action of uni-axial in-plane force acting parallel to the tube axis. The general equation of bending for such a plate with the dimension notations as in Figure 3.1(a) is represented as, [4]

$$D\left(\frac{\partial^4 w}{\partial x^4}+2\frac{\partial^4 w}{\partial x^2\partial y^2}+\frac{\partial^4 w}{\partial y^4}\right)+t\left(\sigma_x\frac{\partial^2 w}{\partial x^2}\right)=0 \tag{3.1}$$

where, w is the out-of-plane displacement of the plate, σ_x is the stress in the plate due to the force in x direction and D is the flexural stiffness of the plate , which is expressed as,

$$D=\frac{Et^3}{12\left(1-\nu^2\right)} \tag{3.2}$$

where, E is the Young's Modulus and ν is the Poisson's ratio of the material of the plate. Using a coordinate system as defined in Figure 3.1(a), the boundary conditions for the present equation are represented as,

at $x = 0$ and $x = h$,

$$w=0 \tag{3.3}$$

$$M_x=0 \tag{3.4}$$

and, at $y = \pm l/2$,

$$w=0 \tag{3.5}$$

$$M_y=-\bar{\zeta}\times\bar{\theta}=M \tag{3.6}$$

where, M_x and M_y are the moments along the edges about the x and y directions respectively.

The moment acting along the vertical edges is assumed to be proportional to the angle of deflection of the shorter restraining walls and $\bar{\zeta}$ is the proportionality constant representing the stiffness of the system. A term ζ, referred to as the restraint coefficient and corresponding to the compliance of the common edge is introduced into the derivation and is represented as,

$$\zeta = \frac{2}{l}\frac{D}{\bar{\zeta}} \tag{3.7}$$

With the use of boundary conditions from Eqns. (3.3), (3.4), (3.5) and (3.6) and the introduction of restraint coefficient from Eqn. (3.7), the buckling condition of the buckling wall is derived as,

$$\sqrt{\mu+1}\tanh\left(\frac{\pi}{2}\sqrt{\mu+1}\frac{m}{\phi}\right)+\sqrt{\mu-1}\tan\left(\frac{\pi}{2}\sqrt{\mu-1}\frac{m}{\phi}\right)+\zeta\pi\mu\frac{m}{\phi}=0 \tag{3.8}$$

where, m is the number of half-waves formed along the height of the wall, ϕ is the aspect ratio of the wall represented by $\phi = h/l$, and μ is a term defining the critical load of the buckling wall and is defined as,

$$\mu^2 = \frac{\sigma_c t}{D}\left(\frac{h}{m\pi}\right)^2 \tag{3.9}$$

where σ_c represents the buckling critical stress of the buckling wall. Eqn. (3.8) represents the condition of buckling of any general rectangular plate equally restrained along the vertical edges. Using this condition, the values of μ were plotted against various values of ζ for different values of the m/ϕ ratio. An example of this plot at $m/\phi = 1$ is shown in Figure 3.2.

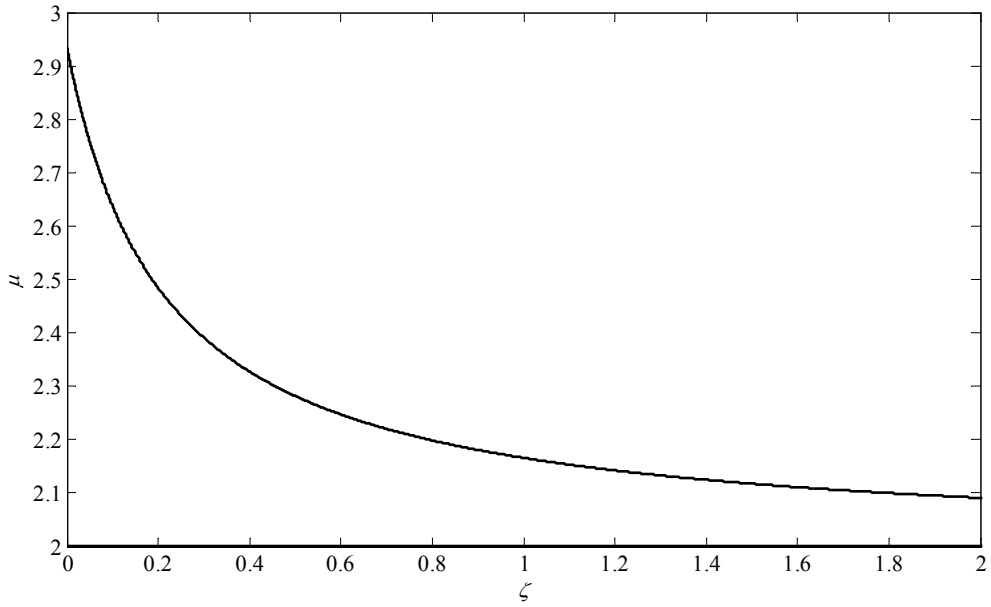

Figure 3.2 Plot of μ versus ζ for $m/\phi = 1$

In the case of a rectangular tube, the buckling behavior of the buckling wall is defined by the condition from Eqn. (3.8) and the relation of the buckling wall with the restraining walls is

established by the term ζ. Calculation of the restraint coefficient is executed by studying the bending of the restraining walls of the tube. This is presented in the following sub-section in this study.

A specific case of Eqn. (3.8) is the condition corresponding to the condition $\zeta = \infty$, which represents the condition of buckling a plate simply supported along the vertical edges. Substitution of this condition in Eqn. (3.8) yields the result

$$\sigma_c = \frac{k\pi^2 E}{12\left(1-\nu^2\right)}\left(\frac{t}{l}\right)^2 \tag{3.10}$$

where k is the buckling factor of the plate and is expressed as,

$$k = \left(\frac{m}{\phi}+\frac{\phi}{m}\right)^2 \tag{3.11}$$

This result of the critical load of the plate is considered over the unit width of the plate. Thus, the critical load of the whole plate is,

$$P_{cr} = \frac{k\pi^2 E}{12\left(1-\nu^2\right)}\left(\frac{t^3}{l}\right) \tag{3.12}$$

Eqn. (3.12) represents the buckling critical load expression of a simply supported plate.

Now focusing back on the general case of a rectangular plate with elastically restrained end conditions, the buckling condition of the plate depends on the value of the restraint coefficient of the common edges. The calculation of the restraint coefficient based on the deflection equation of the restraining wall is explained in the following sub-section.

3.3.2 Bending equation of the restraining walls

In this sub-section, the value of the restraint coefficient for a given tube is calculated based on the interaction of the buckling wall and the restraining wall along the common edge. This depends on the dimensional relation of the buckling and restraining walls. Figure 3.3 shows a representation of the restraining wall with dimensions and coordinate system used for the derivation process. The length and thickness of the restraining wall are considered as l_r and t'. The height of the restraining wall is equal to the height of the buckling wall h as these are the walls of the same tube. The ratio of the lengths of restraining wall and buckling wall (l_r/l) is termed as length ratio for further reference in this study.

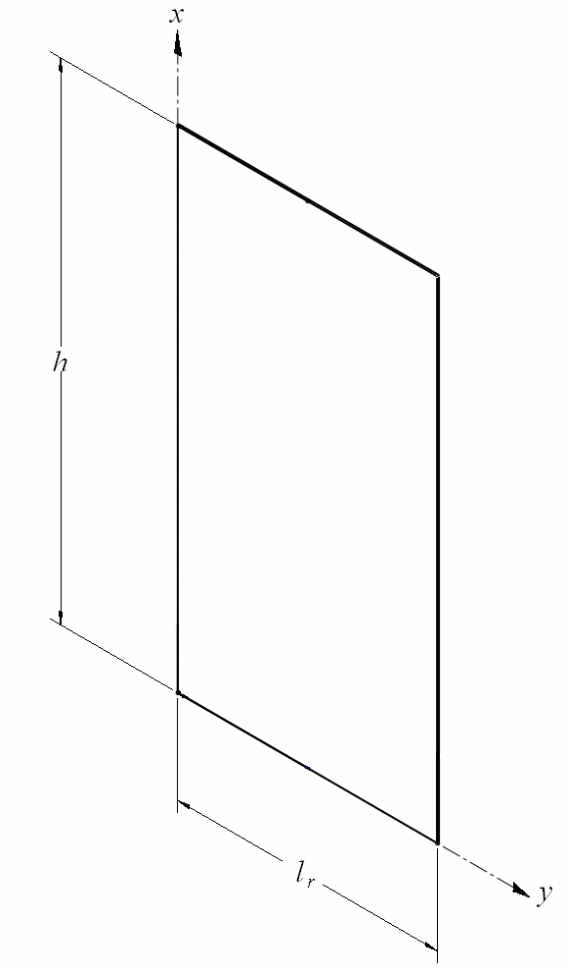

Figure 3.3 Schematic representation of one of the restraining walls of the tube with coordinate system and dimensions

With the buckling of the buckling wall of a rectangular tube, bending moments are induced on the restraining walls, resulting in the bending of the restraining walls. The restraining walls represent rectangular plates simply supported along all of the edges with a certain bending moment along the vertical edges. This implies that the bending of the restraining walls can be presented in the form of Eqn. (3.1). As the restraining wall does not buckle due to the longitudinal force, the longitudinal force acts as a compressive load and its effect is negligible on bending. With this reasoning, the terms associated with the acting loads are neglected from the plate bending equation. This modifies the plate bending equation of the restraining wall as,

$$\frac{\partial^4 w}{\partial x^4} + \frac{\partial^4 w}{\partial x^2 \partial y^2} + \frac{\partial^4 w}{\partial y^4} = 0 \tag{3.13}$$

where w is the out-of-plane deflection of the restraining wall. The boundary conditions of the above system are,

at $x = 0$ and $x = h$,

$$w = 0 \tag{3.14}$$

$$M_x = 0 \tag{3.15}$$

and, at $y = 0$ and $y = l_r$,

$$w = 0 \tag{3.16}$$

$$M_y = M \tag{3.17}$$

Solving Eqn. (3.13) using the boundary conditions from Eqns. (3.14), (3.15), (3.16) and (3.17), the expression of the out-of-plane deflection of the plate is obtained as, (*the details of this solution are shown in Appendix A*)

$$\begin{aligned} w = & -\frac{Ml_r h}{2m\pi D' \sinh^2 \frac{m\pi}{h} l_r} \left(1 - \cosh \frac{m\pi}{h} l_r\right) \sinh\left(\frac{m\pi}{h} y\right) \\ & - \frac{Mh}{2m\pi D'} y \sinh\left(\frac{m\pi}{h} y\right) - \frac{Mh}{2m\pi D' \sinh \frac{m\pi}{h} l_r} \left(1 - \cosh\left(\frac{m\pi}{h} l_r\right)\right) y \cosh\left(\frac{m\pi}{h} y\right) \end{aligned} \tag{3.18}$$

The angle of deflection of the wall at the edge is calculated by differentiating Eqn. (3.18) at $y = 0$. With the comparison of the expression of the angle of deflection with Eqn. (3.6) and Eqn. (3.7), the expression for the restraint coefficient on the buckling wall due to the restraining wall was derived as,

$$\zeta = -\left(\frac{\phi}{m}\right)\left(\frac{t}{t'}\right)^3 \frac{\left(\left(1 - \cosh\left(\frac{m\pi}{\phi} \frac{l_r}{l}\right)\right).\left(\frac{m}{\phi} \frac{l_r}{l} \pi + \sinh\left(\frac{m\pi}{\phi} \frac{l_r}{l}\right)\right)\right)}{\pi \sinh^2\left(\frac{m\pi}{h} \frac{l_r}{l}\right)} \tag{3.19}$$

Using this equation, the restraint coefficients of a given tube with fixed l_r/l ratio were calculated for different values of m/ϕ. The values of k of the buckling wall at different aspect ratios were then calculated using the values of restraint coefficient and Eqn. (3.8) for different m/ϕ ratio. Figure 3.4 shows the plot of k for an elastically restrained plate with the restraining wall having a l_r/l ratio of 0.5. The plate represents one of the two buckling walls of a rectangular tube with the restraining walls of half the length of the buckling wall. The plot was constructed using different m/ϕ ratios for different m values.

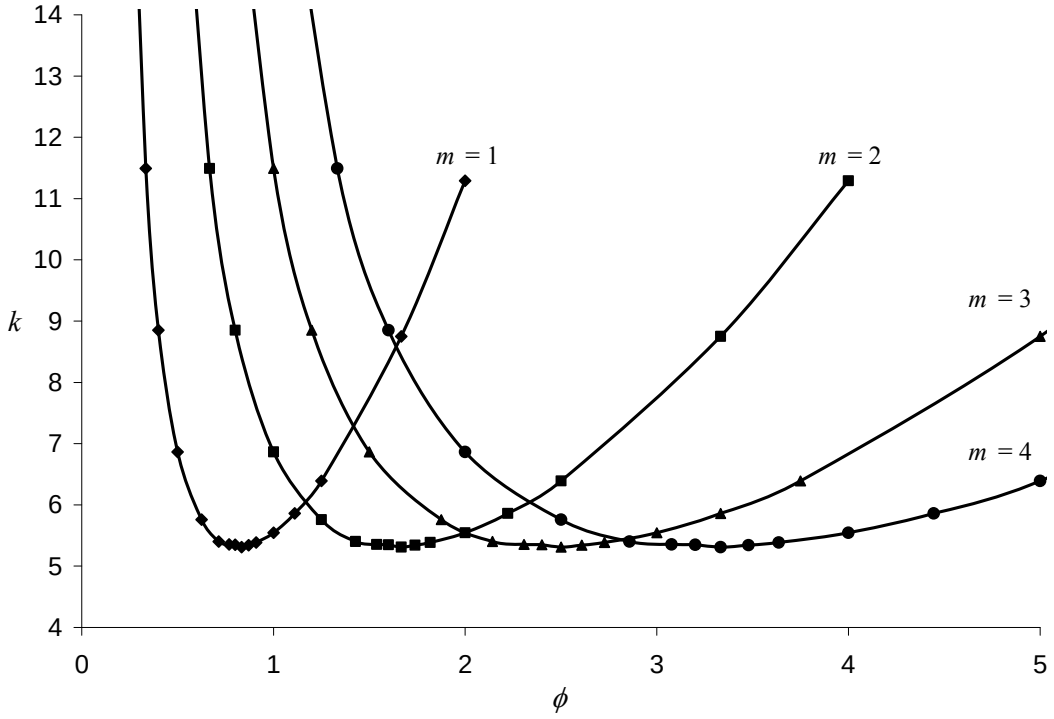

Figure 3.4 The plots of k for a wall with l_r/l ratio 0.5

The figure shows curves of the buckling factor k for four values of m. The intersection points of the curves of k for different m values are called transitional aspect ratios. More discussion on translational aspect ratios is discussed in the following sub-section.

3.3.3 Transition of Number of Half-Waves in Plate Buckling

In the elastic buckling phenomenon of any plate structure, the plate buckles with the formation of sinusoidal waves along the height and width direction. For the lowest energy mode of buckling, thus corresponding to the minimum buckling critical load, the number of half-waves formed along the width of the plate is always equal to 1. However, the number of half-waves formed along the height of the plate depends on the aspect ratio of the plate. For maintaining the lowest critical load, the plate may undergo buckling with more than one half-wave. This phenomenon is more clearly evident from the case of a simply supported plate. The expression of k for the simply supported plate presented in Eqn. (3.11) obtains a minimum value for certain aspect ratio. Thereafter, the value of k begins to increase for a constant m value. To maintain the lowest value of k, the plate transforms the buckling mode to form m+1 half-waves, thus maintaining the minimum possible buckling factor and critical load of buckling. This

phenomenon is also observed in supported plates representing buckling walls of a rectangular tube. This is obvious from the curves of k in Figure 3.4. It is observed that the value of k on the line of m =1 is higher that the corresponding values of k on the curve of m = 2 after a certain aspect ratio. This aspect ratio is called transitional aspect ratio. The buckled shape of a plate structure changes from m to m+1 number of half-waves after the transitional aspect ratio. For the case of the elastically restrained plate studied in the previous sub-section, the values of transitional aspect ratios for transitions from m = 1 to m = 2, m = 2 to m = 3, m = 3 to m = 4 were calculated as approximately 1.16, 2 and 2.82 respectively. The transitional aspect ratios of the buckling walls of a tube vary as the l_r/l ratio of the tube is varied. It was observed that the first transition occurs at a lower aspect ratio as the l_r/l ratio of the tube increases. For example, the transitional aspect ratio for transition from m = 1 to m = 2 is lowest for a plate built in along both vertical edges, at approximately 0.94 and highest for a simply supported plate, at the value of √2. For a simply supported plate, the transition aspect ratio is defined as, [2]

$$\phi_t = \sqrt{m(m+1)} \tag{3.20}$$

The value of k for simply supported plate is minimal at the integer values of aspect ratio, for which the number of half-waves is equal to the aspect ratio.

3.3.4 Buckling of square tubes

The buckling characteristic of a square tube is the simplest case of polygon tube buckling, where each wall buckles as a simply supported plate. For a square tube under a uniform axial compressive force with the top and bottom edges hinged or simply supported, the load is equally distributed on all of the walls. As all of the walls are identical in geometry and load, each plate has the same individual critical load, and the restraint coefficient along the common edges is ∞. Therefore, each of the walls reaches instability simultaneously. The half-waves on adjacent walls are formed in such a way that the common edges do not buckle. Walls rotate by the same amount and in the same direction about the common edge, and therefore the wall angle remains unchanged before and after buckling [4]. This results in zero restraining moments at the common edges for the walls and the tube behaves as four independent simply supported plates put together with common edges. The critical load of a square tube is therefore four times the value of the critical load of a single wall behaving as simply supported plate. From

the critical load expression of a simply supported plate presented in Eqn. (3.12), the critical load expression of the square tube is obtained as, [2]

$$P_{cr} = 4 \times \frac{k\pi^2 E}{12\left(1-\nu^2\right)}\left(\frac{t^3}{l}\right) \tag{3.21}$$

The value of k is determined by the aspect ratio of the tube and the number of half-waves formed, as was explained in the preceding section for the single simply supported plate. The values of k for each wall of a square tube or any simply supported plate with varying aspect ratio are represented in Figure 3.5. The intersection points of curves of certain number of half-waves m and m +1 represent the transitional aspect ratios.

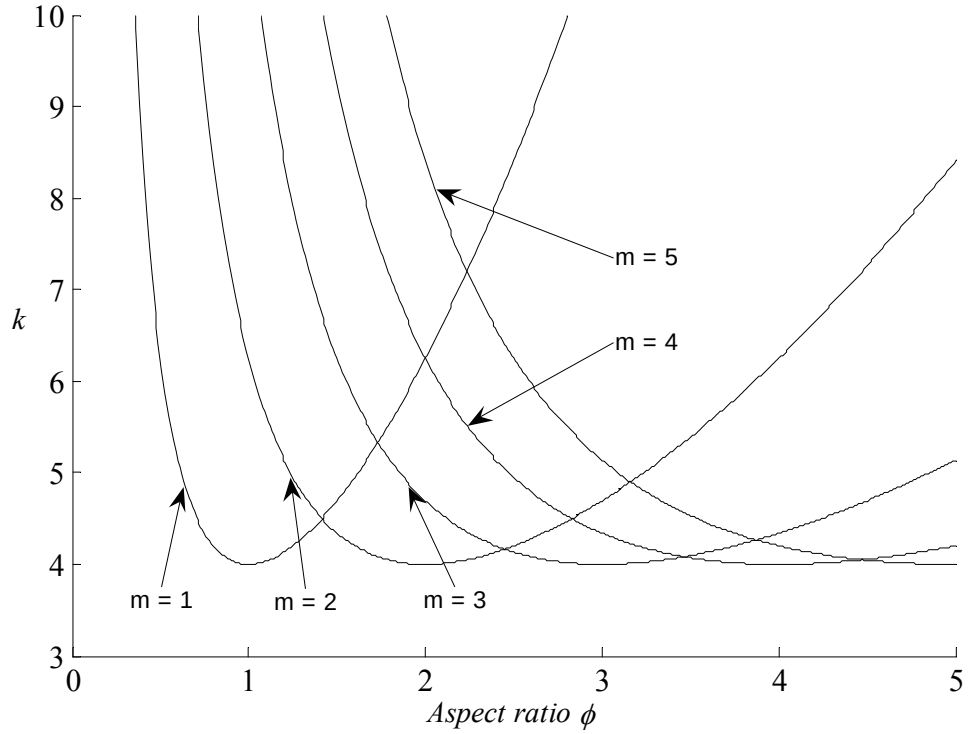

Figure 3.5 Plot of the values of *k* with varying aspect ratios of the walls of a square tube

3.3.5 Buckling of Rectangular Tubes

Apart from the dependency of the critical load of a given rectangular tube on the aspect ratio of the tube, the ratio of the lengths of the buckling wall and restraining walls also plays a role in the buckling behavior of the tube. At a given aspect ratio, the value of k of the buckling walls is higher for low l_r/l ratio and lowest for buckling and restraining walls of equal length,

representing a square tube. The values of k were calculated using the procedure presented in the preceding section for calculating the k values of the particular case with l_r/l ratio of 0.5.

It was observed that the values of k obtained from this procedure were accurate for low l_r/l ratios. For higher l_r/l ratios (ratios more than 0.5), however, the values of k were observed not to be accurate. This is assumed to be because of the effect of the longitudinal force on the stiffness of the restraining wall. To correct this error, Bleich [4] suggested an approximate correction method for the calculation of restraint coefficient ζ. The correction was expressed as,

$$\zeta_{corrected} = \frac{1}{1-\left(\frac{tl_r}{t'l}\right)^2}\zeta \tag{3.22}$$

where, $\zeta_{corrected}$ is the corrected value of restraint coefficient considering the effect of load on the resisting wall and ζ is the value of restraint coefficient obtained from Eqn. (3.19). The procedure of calculating the buckling factor of buckling walls was repeated as was performed previously, but, with the use of corrected values of restraint coefficients in Eqn. (3.8). Figure 3.6 shows the plot of k for different rectangular tubes of length ratios of the rectangle as 0.1, 0.3, 0.5, 0.7 and 0.9 (at each of three constant values of m - m = 1, m = 2, m = 3) with this corrected procedure.

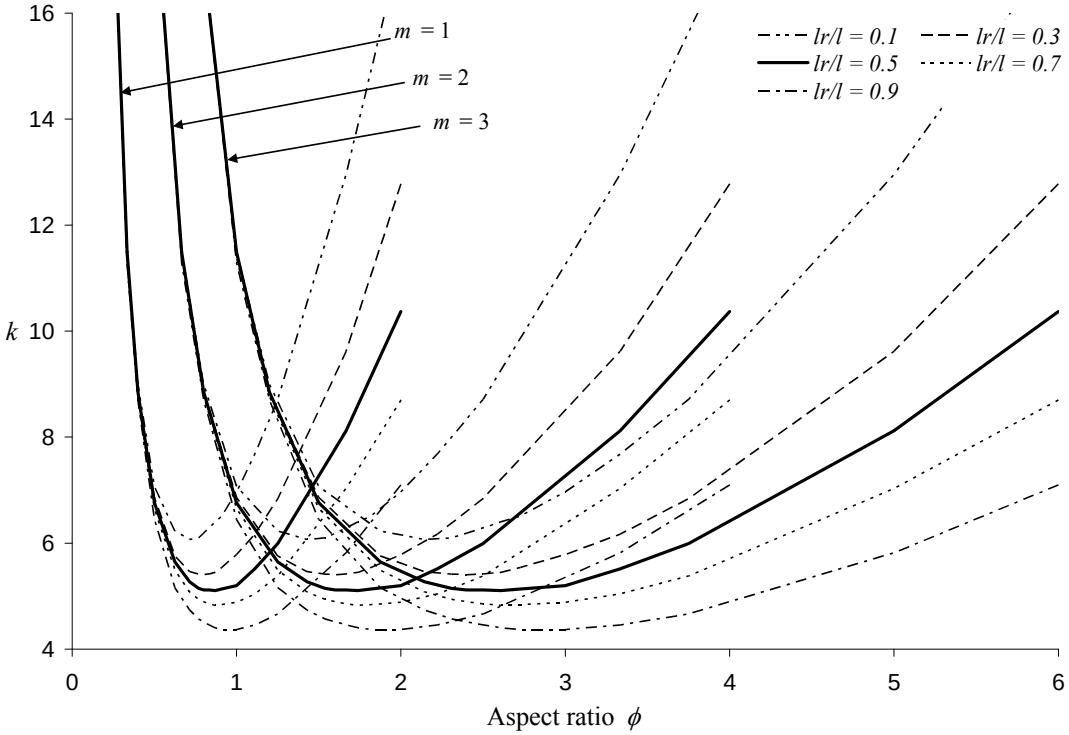

Figure 3.6 Plots of *k* of different rectangular tubes varying with aspect ratio

The minimum values of k with different length ratios are presented in Figure 3.7. The extremes $l_r/l = 0$ and $l_r/l = 1$ were considered as a plate fixed on both sides and simply supported plate respectively.

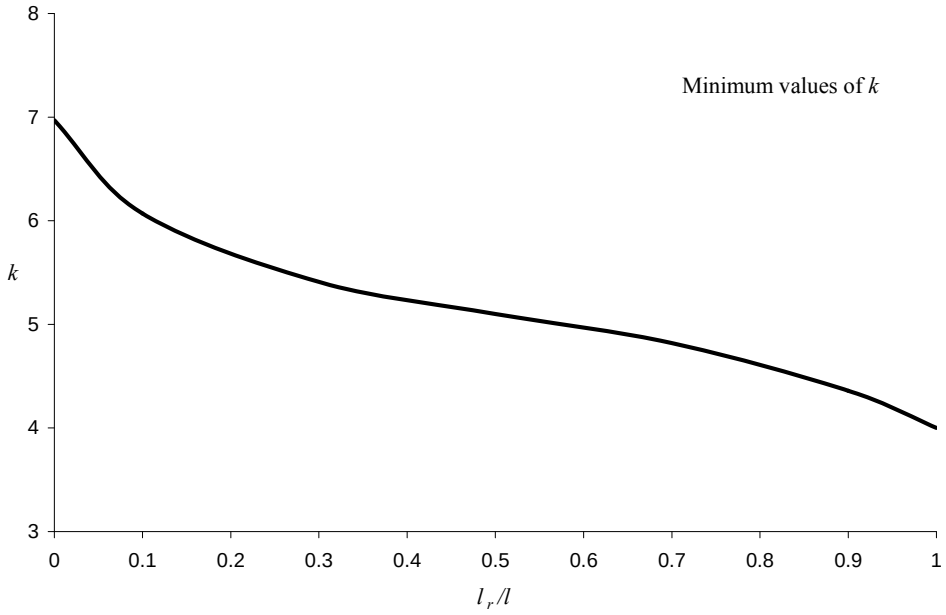

Figure 3.7 Minimum values of k for different l_r/l ratios

The critical load of the rectangular tube is expressed in the terms of the length ratio of the buckling wall and restraining wall of the rectangular tube as,

$$P_{rect} = 2\left(1+\frac{l_r}{l}\right)P_{cr} \tag{3.23}$$

where, P_{rect} is the critical load of the rectangular tube and P_{cr} is the critical load of the buckling wall using the specific k value (for a given l_r/l ratio) and Eqn. (3.12). The results of the critical load of certain rectangular tubes obtained from this theory were compared to computational results from finite element simulations. The comparisons are presented in following sections.

3.3.6 Buckling of Rhombic and Parallelogram Tubes

According to the theory of buckling of square and rectangular tubes, the angle between the walls of a quadrilateral tube does not affect the critical load of the tube if it is maintained in the buckled structure. This statement follows logically that the critical load of buckling of rhombic and parallelogram tubes would be same as that of square and rectangular tubes, respectively, with the same dimensions. Thus the critical loads of rhombic and parallelogram

tubes can be derived from the theory of square and rectangular tube buckling as explained in the preceding sections. For a rhombic tube, the critical load would be the load value calculated from Eqn. (3.21). For a parallelogram tube, the critical load would be the load value obtained from Eqn. (3.23) with the walls on the longer sides of the parallelogram considered as the buckling walls. However, in both rhombic and parallelogram tubes with very small angles, there exists a possibility of Euler buckling. A discussion on the Euler buckling of rhombic and parallelogram tubes is presented in the following sections. Finite element simulation results of rhombic and parallelogram tubes were compared with the theoretical results of respective square and rectangular tubes. Also, a few experiments were performed on rhombic tubes to compare the critical loads with the simulation models and corresponding square tubes. These results are presented in the section Results of this chapter.

3.3.6 Euler Buckling of Rhombic and Parallelogram Tubes

As mentioned in the previous section, the rhombic and parallelogram tubes have a possibility of buckling as a single structure in Euler mode. Some of the studies presented in [16,25] have discussed the possibility of Euler buckling in square and rectangular tubes. In this section, the Euler buckling of any generalized rhombic and parallelogram tubes are discussed. An equation for finding out the minimum height of a given tube to buckle in wall buckling mode is derived based on the lowest critical load. This study is important for post-buckling studies of tubes. Tubular structures have effective load carrying capacity in post-buckling. This is accounted to the load carrying capacity of the vertical edges of the tube when the tube buckles as four individual walls. For a tube buckling in Euler mode, the tube is ineffective as a post-buckling crash member as the load carrying capacity of a tube buckling in Euler mode decreases drastically in post-buckling regime. This makes the study of Euler buckling of the tubes an important aspect for effective design of structures which are designed to function in post-buckling.

The minimum height for a rhombic tube, over which the tube will buckle in Euler mode, was calculated by comparing the critical loads of the tube in Euler mode and wall buckling mode. Figure 3.8 shows the schematic representation of a general rhombic tube used in this derivation.

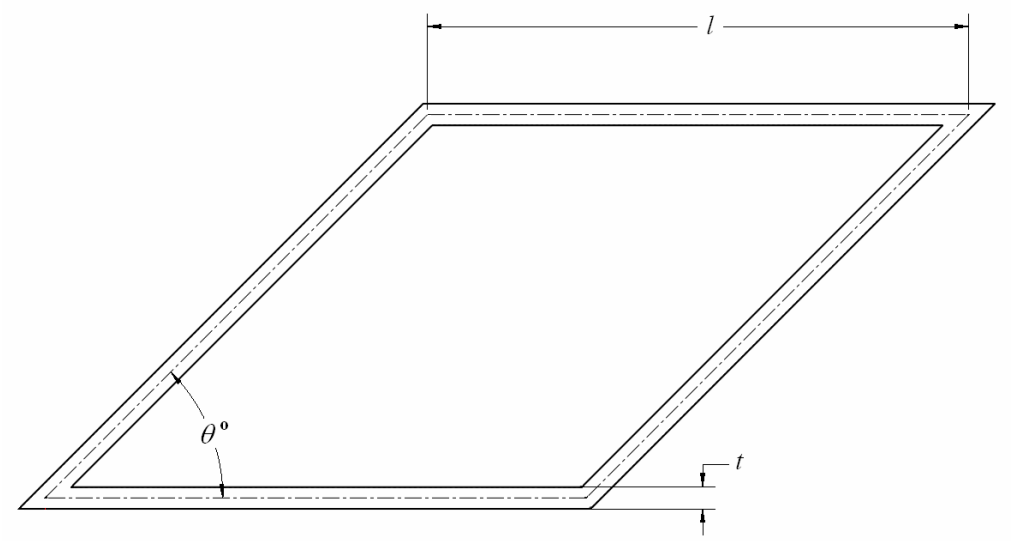

Figure 3.8 The representation of the cross-section of a general rhombic tube of each wall of width *l*, wall thickness of *t* and acute angle of rhombus as θ

The Euler buckling of a structure occurs along the axis with minimum moment of inertia and the critical load of buckling in Euler mode is expressed as,

$$P_{cr} = \frac{C\pi^2 EI_{\min}}{h^2} \tag{3.24}$$

where $I_{\min}$ is the minimum moment of inertia and h is the height of the body. The term C is a constant which depends on the end boundary conditions of the tube. For the hinged-hinged condition, the value of C is 1. In the case of a rhombic tube, the longer diagonal is always the axis of minimum moment of inertia. With the substitution of the expression for minimum inertia of the section, the expression for critical load of the tube in Euler mode with hinged-hinged condition along the longer diagonal is,

$$P_{cr} = \frac{\pi^2 Elt\left(t^2 + l^2 \sin^2\theta\right)}{3h^2 \cos^2\frac{\theta}{2}} \tag{3.25}$$

Comparing this to the critical load of the tube buckling in wall buckling mode expressed in Eqn. (3.21), the expression of the critical height is,

$$h_{cr} = \sqrt{\frac{l^2\left(1-\nu^2\right)\left(1+\left(\frac{l}{t}\right)^2 \sin^2\theta\right)}{k\cos^2\frac{\theta}{2}}} \tag{3.26}$$

The critical height of the tube depends on the dimensions of the tube and the value of k of the tube at the particular height. The value of k of the tube is generally assumed to be 4 for aspect ratios greater than 5. This modifies the expression of the critical height of the equal-sided tubes with high aspect ratios to,

$$h_{cr} = \frac{1}{2}\sqrt{\frac{l^2\left(1-\nu^2\right)\left(1+\left(\frac{l}{t}\right)^2 \sin^2\theta\right)}{\cos^2\frac{\theta}{2}}} \tag{3.27}$$

Based on this principle, the theoretical buckling behavior of a tube of a given angle was predicted with relation to various heights h of the tube. Figure 3.9 shows the critical loads of a tube with walls of width 2 *in*, angle $\theta = 60^o$ and wall thickness of 0.08 *in*. Material properties of ABS plastic were used for the tube material, having a Young's Modulus of 236000 *psi* and Poisson's ratio of 0.39. This was because of the tube specimens made of ABS plastic which were used for experimental studies.

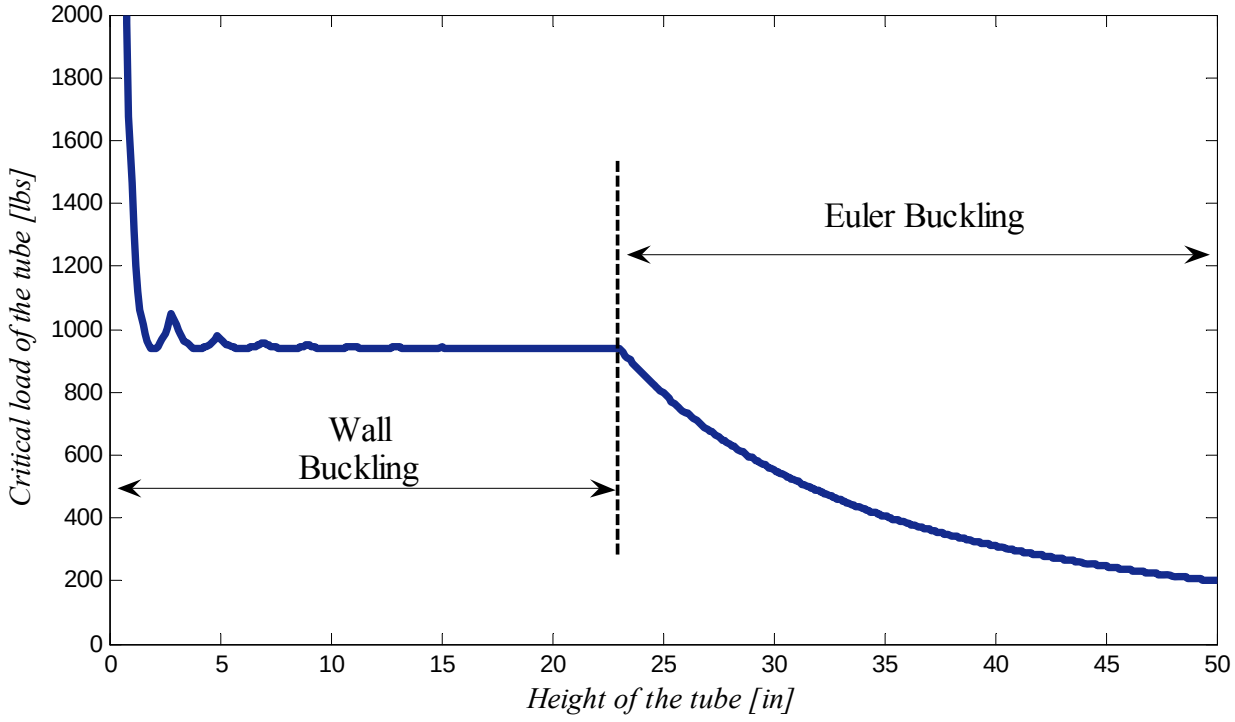

Figure 3.9 The critical load of a rhombic tube with l = 2 *in*, $\theta = 60^o$ *in* and t = 0.08 *in*

The figure shows initial critical load similar to the form of the k curve for a rectangular plate, but with a steep fall in the critical load after a certain height, which is due to Euler

buckling. This plot was created using a MATLAB program which calculated the critical load of the tube in both modes and selected the lower load as the critical load of the tube. From this method, the rhombic tube under study is expected to buckle in Euler mode at a height of 23 *in*. Investigation of Euler buckling of square tubes was also performed using this method by substituting the angle of the tube as 90^o. The value of critical height for the square tube with similar dimensions and material properties of the rhombic tube studied in this sub-section was obtained as 32.5 *in*.

Similar study on parallelogram tubes was conducted by considering a parallelogram tube with dimensions as shown in Figure 3.10. The lengths of the sides of the parallelogram were considered similar to the dimensions in the wall-buckling analysis of the rectangular tubes.

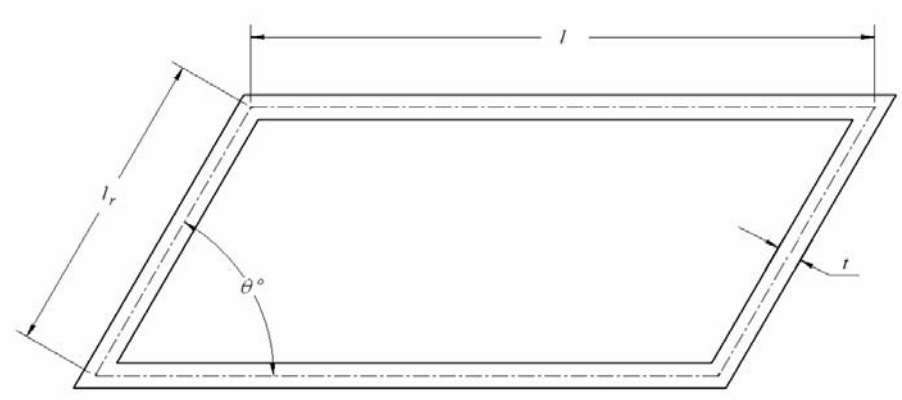

Figure 3.10 The representation of the cross-section of a general parallelogram tube with longer walls of length *l*, shorter walls of length l_r, wall thickness of *t* and angle of θ

The expression for the critical height of a tube with dimensions as shown in the figure was calculated in a similar fashion as was calculated for a square tube. The minimum moment of inertia of the cross-section was calculated using the principal moments. The expression of the critical height of Euler buckling of a parallelogram tube by comparing the two critical loads was obtained as,

$$h_{cr} = \sqrt{\frac{6I_{\min}\left(1-\nu^2\right)l}{kt^3\left(1+\alpha\right)}} \tag{3.28}$$

where, α is the ratio of the length of the sides (l_r/l) and $I_{\min}$ is the minimum moment of inertia of the parallelogram section. The derivation of the minimum moment of inertia is presented in *Appendix B*. The value of k is considered as the minimum value of k for the given l_r/l. This was

done as the value of k becomes almost constant after an aspect ratio of 3. Using this equation, the critical loads of a given tube were plotted by varying heights. The parallelogram tube for this theoretical analysis was chosen with the length of longer sides of 2 *in* and shorter sides 1 *in*. The value of k was considered to be constant and equal to the minimum value of k for a tube of l_r/l ratio of 0.5. The material of the tube was assigned a Young's Modulus of 236000 *psi* and a Poisson's ratio of 0.39, representing the properties of ABS plastic. The graph of critical loads is presented in Figure 3.11.

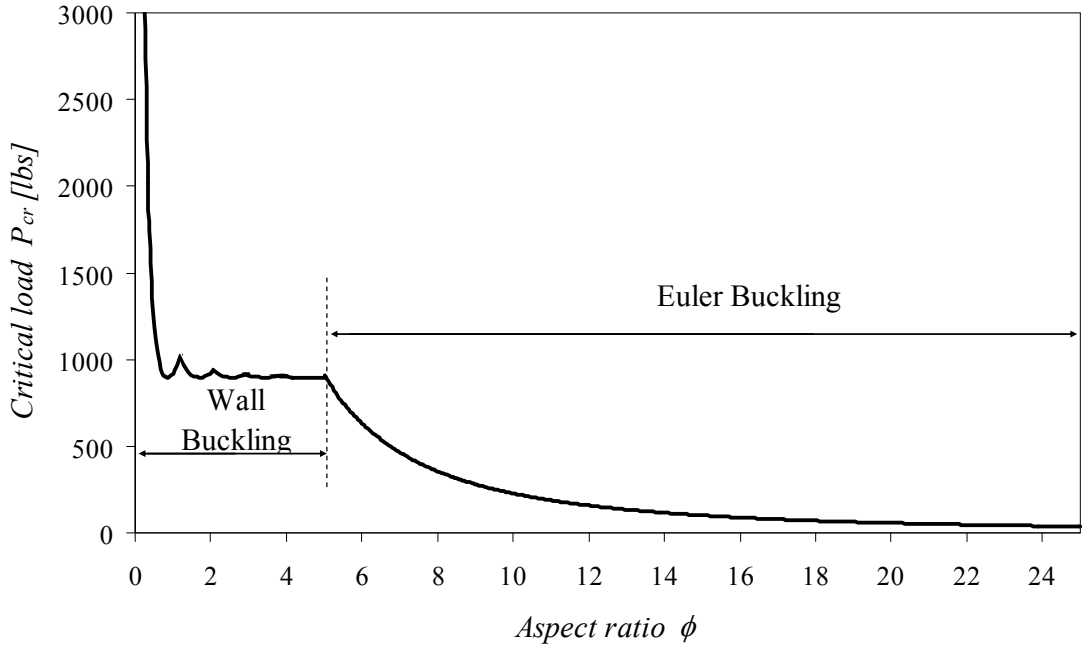

Figure 3.11 The critical load plot with different aspect ratios of a parallelogram tube with l = 2 *in*, l_r = 1 *in*, $\theta = 60^o$ and t = 0.08 *in*

The figure reveals that the tube under study is expected to buckle in Euler mode beyond an aspect ratio of approximately 5. The theoretical predictions explained in this section were compared with finite element elastic buckling simulations. The results of the simulations and their comparison with the theoretical results are presented in the following section.

3.4 Finite Element Buckling Simulations of Plate and Tubular Geometries

According to the theoretical prediction, a single, simply supported plate under compressive load buckles with the formation of single or multiple lobes along the height of the plate, called half-waves. The number of half-waves depends on the aspect ratio of the tube and

the dimension ratio of the walls. It is also predicted from the theory that open multi-wall structures with the open edges subjected to simply supported conditions (i.e. regular polygon tubes) have a critical load equal to the number of walls times the critical load of a single simply supported plate. The study of these structures using finite element simulation on certain geometries has been elaborately discussed and presented in [24]. In the present study, square, rhombus, rectangular and parallelogram tubes over a range of aspect ratios are simulated under elastic buckling conditions using SolidWorks simulations. Some important results are discussed in this section and the comparison of computational critical loads with the theoretical and experimental results are discussed in the section Results of this paper. The geometries used for simulations were modeled with the dimensions of the experimental specimens and were assigned material properties representing the properties of ABS plastic, which was used for fabricating the specimens.

3.4.1 Elastic Buckling Simulations of a Square Tube

It was postulated in [2] that a square tube under a uniformly distributed buckling load behaves as four individual simply supported plates. The theoretical critical load of a square tube is calculated based on this theory as was explained in the earlier sections. In this sub-section, the procedure of simulating the elastic buckling phenomenon using finite element method is presented. The square tube was modeled with sides of length 2 *in* and uniform wall thickness of 0.08 *in*. Simulations were performed on models of tubes over a range of heights, thus observing the behavior of the tube at different aspect ratios. The model of the tube with lowest height had an aspect ratio of 0.5 and the tallest tube had an aspect ratio of 3. The aspect ratios were chosen with special focus on the transitional aspect ratios and the aspect ratios corresponding to minima of k to observe the theoretically predictions at these ratios. The value of Young's Modulus of the tubes and the Poisson's ratio were assigned as 236,000 *psi* and 0.39, respectively. The models of the tubes were meshed using triangular shell elements. Each element had a total of six nodes with three on the vertices and three mid-edge nodes. The size of the elements ranged from 0.05 to 0.06 *in*. For the simulations, the bottom edges were subjected to simply supported restraint, thus restricting translation in all directions and allowing rotation along the edges. The top edges were subjected to restraints which only allowed vertical translation and rotation along the edges.

A parametric uniform compressive force was applied to the top edges of the geometries. Figure 3.12 shows the exaggerated buckled profile of the finite element model with an aspect ratio of 1.

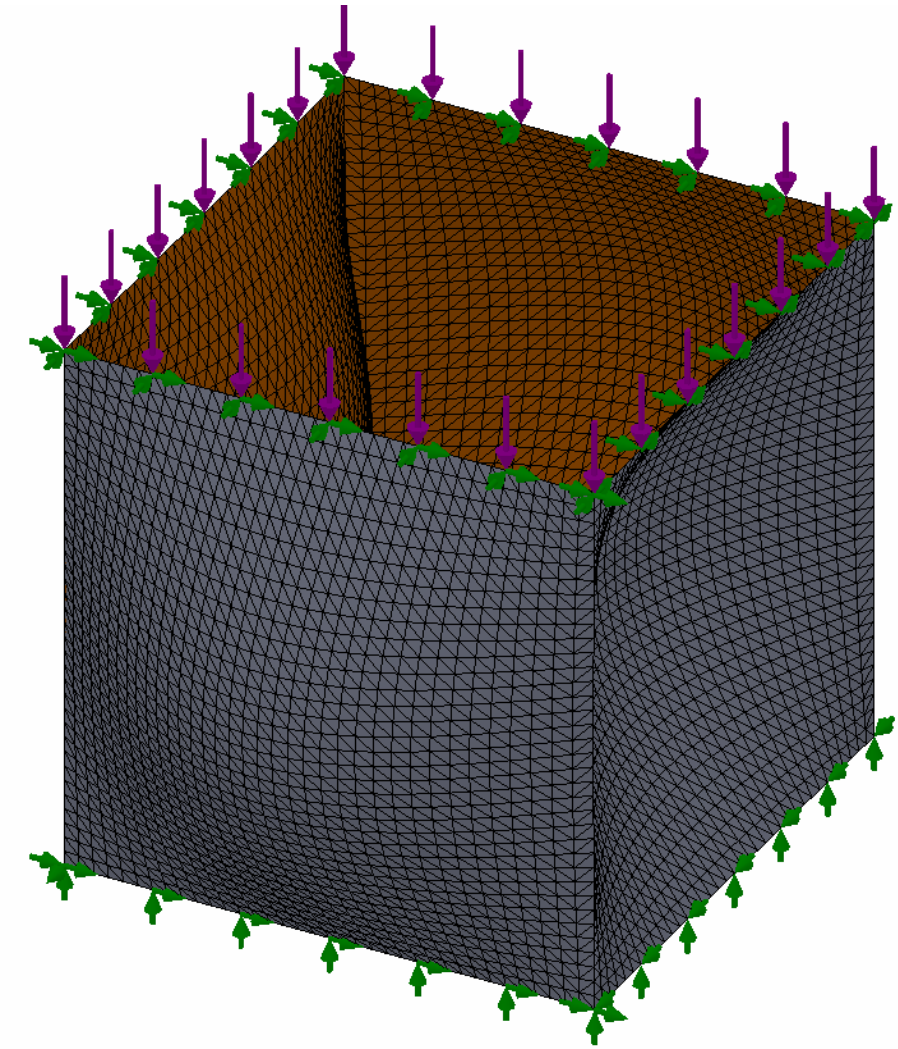

Figure 3.12 Finite element model of a square tube with sides of length 2 *in* and aspect ratio of 1, with exaggerated deformation

Using this method for simulations, the critical load readings for the tubes of different aspect ratios were recorded. The results of critical loads from simulations are presented and compared with theoretical and experimental results in the Results section of this paper. Also, the finite element simulation models were used to critically investigate the transitional aspect ratios by capturing the transition of half-waves in the tube. Figure 3.13 shows the first transition in the tube (m = 1 to 2).

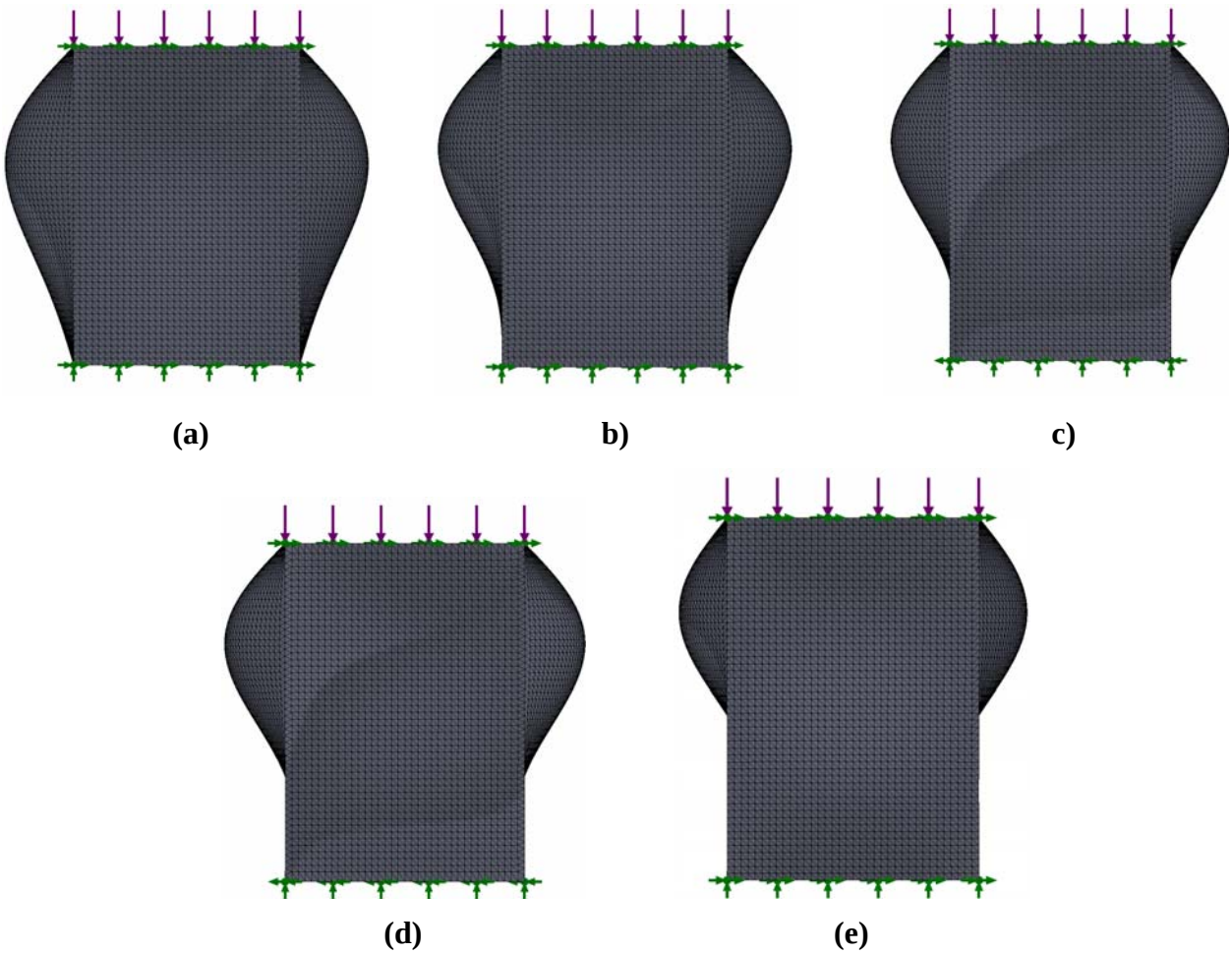

Figure 3.13 Front view of the buckled profile of finite element model of the tube at an aspect ratio of (a) 1.4, (b) 1.41, (c) 1.414, (d) 1.417 and (e) 1.45

The figure shows the initiation of the second wave at an aspect ratio of 1.414. This matches with the theory which predicts the transition to occur at an aspect ratio of √2. Subsequent transitions of number of half-waves were observed at the theoretically expected aspect ratios.

3.4.2 Finite Element Elastic Buckling Simulations of Rectangular Tubes

Similar to the method of finite element simulations of the square tubes, elastic buckling simulations were performed for a set of rectangular tubes. The tubes were modeled with $l = 2$ *in*, $l_r = 1$ *in* (l_r/l ratio = 0.5) and a uniform wall thickness of 0.08 *in*. The tubes were modeled over a range of heights for the aspect ratios ranging from 0.5 to 3 with special focus on minima and transitional aspect ratios. Triangular shell elements having six nodes each, similar to elements used in square tubes, were used to mesh the tubes with an average element size of 0.06 *in*. The

material of the tube was assigned a Young's Modulus of 236,000 *psi* and Poisson's ratio of 0.39. Similar boundary conditions and forces as applied to square tubes were applied on the rectangular tubes and the elastic buckling critical loads were recorded. Figure 3.14 shows the meshed model of the rectangular tube with an aspect ratio of the longer walls as 1.

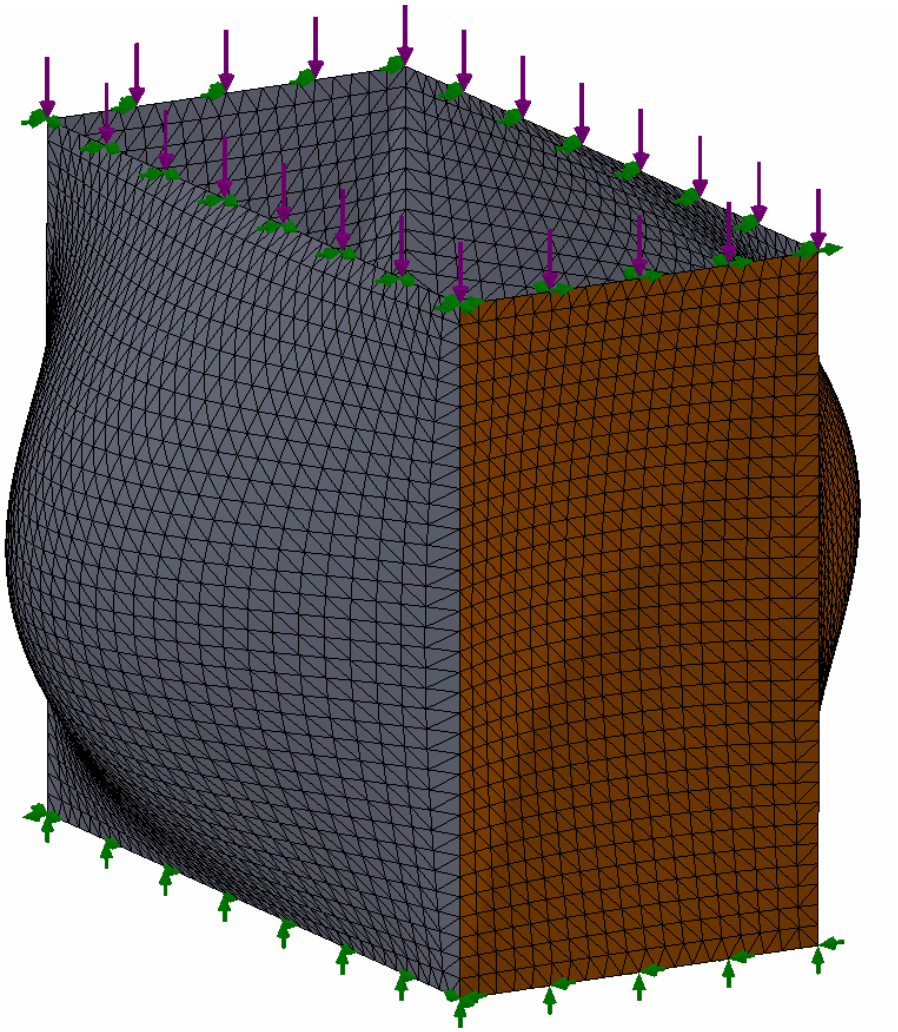

Figure 3.14 Isometric view of the buckled shape from the simulation of the rectangular tube model (l = 2 in, l_r = 1 in) of aspect ratio 1 with boundary conditions, applied forces, in an exaggerated scale

The critical load data of the simulations was compared to the theoretical results and the comparison of results is presented in the Results section. Similar to the investigation in square tubes, the transitional aspect ratios were critically examined in the rectangular tube under study using the finite element models. Figure 3.15 shows the simulation result at different aspect ratios showing the transition from m = 1 to 2.

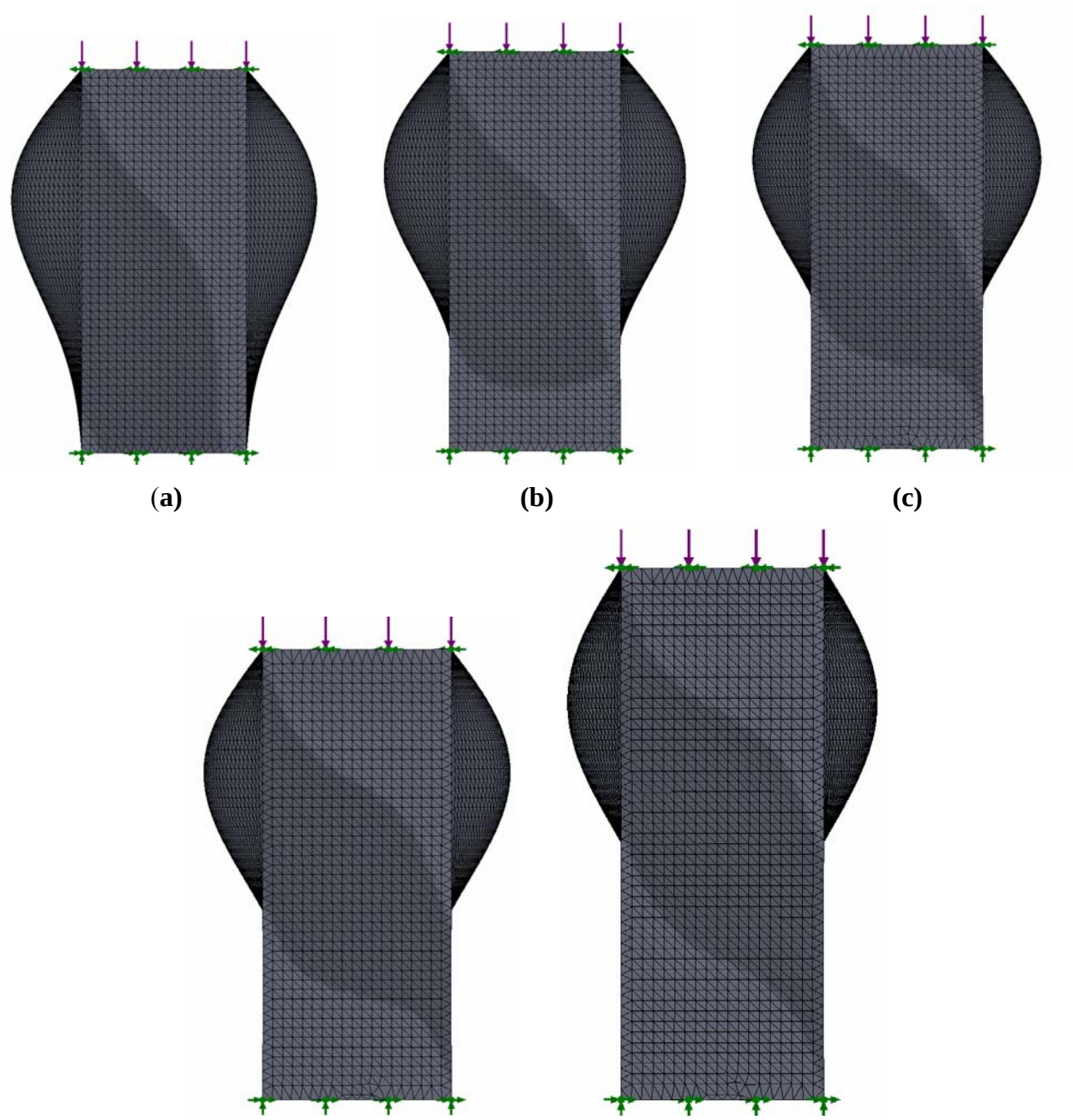

Figure 3.15 The exaggerated buckled shapes from the elastic buckling simulations at aspect ratios of (a) 1.18, (b) 1.19, (c) 1.2, (d) 1.21 and (e) 1.3

The transition of the number of half-waves in the buckling wall was observed at an aspect ratio of 1.19, which matches closely with the theory which predicts the first transition at aspect ratio of 1.2. Subsequent transitions of the number of half-waves were observed at the aspect

ratios of 2.05 and 3 for the transitions m = 2 to 3 and m =3 to 4 respectively. These match closely with the theoretically predicted values of transitional aspect ratios.

3.4.3 Finite Element Simulations of Rhombic and Parallelogram Tubes

The next set of simulations was performed on a few rhombic and parallelogram tubes to see the critical load behavior of these tubes. The goal of these simulations was to show that the critical load behavior was similar to that of the corresponding square and rectangular tubes. The geometries were selected with similar dimensions as that of the square and rectangular tubes. Figure 3.16 shows the buckled shapes of the finite element models of a rhombic and a parallelogram tube with $\theta = 45^{o}$. The rhombic tube had dimensions l = 2 *in* and h = 2 *in*. The parallelogram tube had dimensions l_r = 1 *in*, l = 2 *in* and h = 2 *in*. The parallelogram considered in the study was modeled with $\theta = 60^{o}$. Both tubes were modeled with t = 0.08 *in*. With the use of similar material properties and mesh parameters, buckling simulations were performed on these tubes for different heights. The critical loads of these tubes were compared at minima of k and the transition aspect ratios.

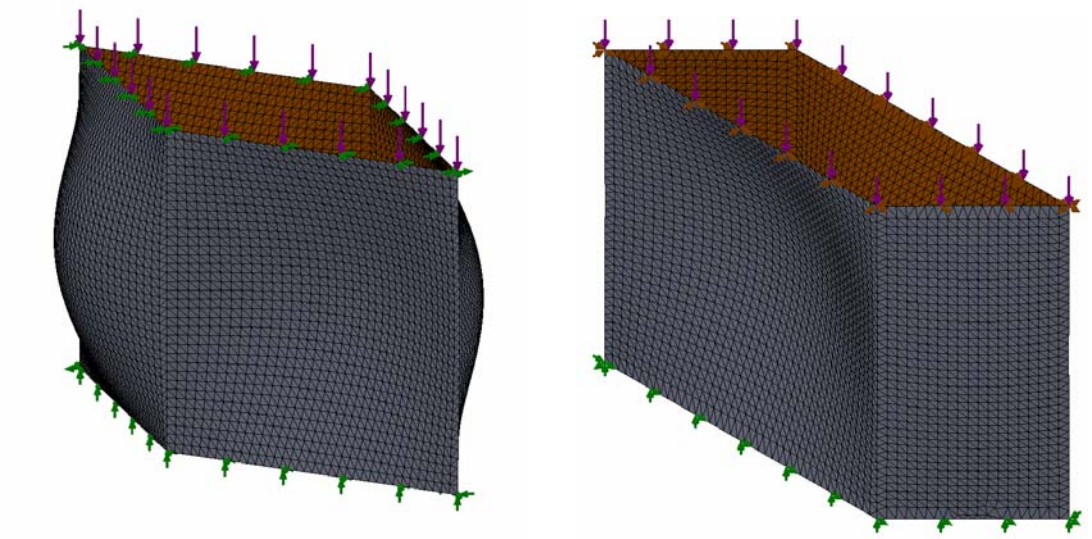

(a) **(b)**

Figure 3.16 Exaggerated buckled shapes from the finite element simulation of (a) a rhombic tube of aspect ratio 1 with θ = 45° and l = 2 in and (b) a parallelogram tube of aspect ratio of longer walls equal to 1 with θ = 60°, l = 2 and l_r/l = 0.5

According to the theory of tube buckling, the critical load and the buckling behavior of the tubes are independent on the angle of the tube. This means that the minimum values of k and the transition of half-waves are expected at the same aspect ratio as that expected from the theory of square or rectangular tubes. This theory was confirmed as the simulation results revealed that the buckling behavior of these tubes is similar to their corresponding 90° counterparts. From the simulations, transition of half-waves from $m = 1$ to 2 was observed at an aspect ratio of 1.41 for a rhombic tube and 1.2 for a parallelogram tube which matches well with the theoretically expected transitional aspect ratios. To properly achieve Euler buckling, the buckling simulations of rhombic and parallelogram tubes were performed in two parallel simulation models of the tubes. First model was subjected to boundary conditions representing simply supported conditions for the top and bottom edges of the tube. The other model was subjected to boundary conditions representing hinged-hinged condition, which relaxes the restraint and allows Euler buckling to occur. This was achieved by restraining the vertical translation of the ends of minimum moment axis of the bottom plane and allowing all other points of the top and bottom surface of vertical translation. With these considerations, restraints applied similar to the square tube were applied on the first model of rhombic tube. The second model was restrained by restricting the ends of the longer diagonals of the rhombus section at the non-loading end of tube in all directions. All of the top and bottom edges were restrained from motion along the horizontal plane only. In the case of parallelogram tubes, the first model of the tube was subjected to the boundary conditions used on the rectangular tubes. In the second model of the tube, the ends of the minimum moment axis were subjected to boundary conditions resembling the restraint applied to the end of longer diagonal of the rhombic tube. The edges of the tube were restrained from translation along the horizontal plane. The heights of the tubes were increased for each simulation and the critical loads of the tubes were recorded. Figure 3.17 shows the Euler buckling of the rhombic and parallelogram tubes after a height which matches well with the theoretically predicted critical heights. The results of critical load were compared with the theoretical prediction in Figure 3.9 and Figure 3.11 for the corresponding rhombic and parallelogram tube, respectively. This comparison is presented in the Results section of this paper.

(a) **(b)**

Figure 3.17 Initiation of Euler buckling in a (a) rhombic tube with l = 2 *in*, t = 0.08 *in* and θ = 60^{o} at h = 23.5 *in* and (b) parallelogram tube with l = 2 *in*, l_r = 1 *in*, t = 0.08 *in* and θ = 45^{o} at h = 9.5 *in*

The Euler buckling of the rhombic tube was observed at h = 23.5 *in* in the hinged-hinged model of the tube. In the parallelogram tube, the Euler buckling phenomenon was observed in the hinged-hinged model of the tube with h = 9.5 *in*. These heights match well with the theoretically predicted values of the critical heights for Euler buckling as were observed in Figure 3.9 and Figure 3.11. The results of the simulation were compared to the theory. These

comparisons of critical loads from the simulation of both of simply supported case and hinged-hinged case are presented in the Results section of this paper.

3.5. Buckling experiments in ABS plastic tube specimens

Following the theoretical and simulation studies of the various tubes, some square and rhombic tubes were tested experimentally. The goal of the experiments was to verify the theoretical and computational predictions of critical loads and number of half-waves. The tube specimens were made of ABS plastic with a Young's Modulus of 236,000 *psi* and Poisson's ratio of 0.39. All of the specimens were manufactured with $l = 2$ *in* and $t = 0.08$ *in* with variable height depending on the desired aspect ratio. Also, two rhombic tubes were manufactured with an aspect ratio of 1 and $\theta = 45^{o}$. The square tubes were manufactured to aspect ratios of 1, 1.41, 2, 2.44 and 3. The tube specimens with integer aspect ratios were expected to show the minimum critical loads and the non-integer aspect ratios were expected to exhibit the transition of half-waves.

The tubes were compressed in an Instron 8516 servo-hydraulic test frame with a maximum capacity of 50,000 *lbs*. The machine was connected to a digital data acquisition system recording load, LVDT displacement and time, simultaneously, at a rate of 3 *Hz*. All of the tubes were compressed at a uniform rate of 0.05 *in*/*min*. The critical loads of the tubes were calculated from the load-displacement plots of the tubes by determining the first non-linear point in the plots. The results of the measured critical load were compared with the theoretical and computational data. These comparisons are shown in the following section.

The tubes having integer aspect ratios exhibited formation of a number of half-waves equal to the aspect ratio of the given tube in order to maintain lowest critical load as expected theoretically. At the non-integer aspect ratios, the transition of half-waves was clearly observed. The buckled profiles of one specimen of each height are presented in Figure 3.18. The gridlines were drawn on the surfaces (at 0.5 *in* spacing) to make the deflections clear. The half-waves formed along the height of the tubes were clearly visible in the buckled tubes.

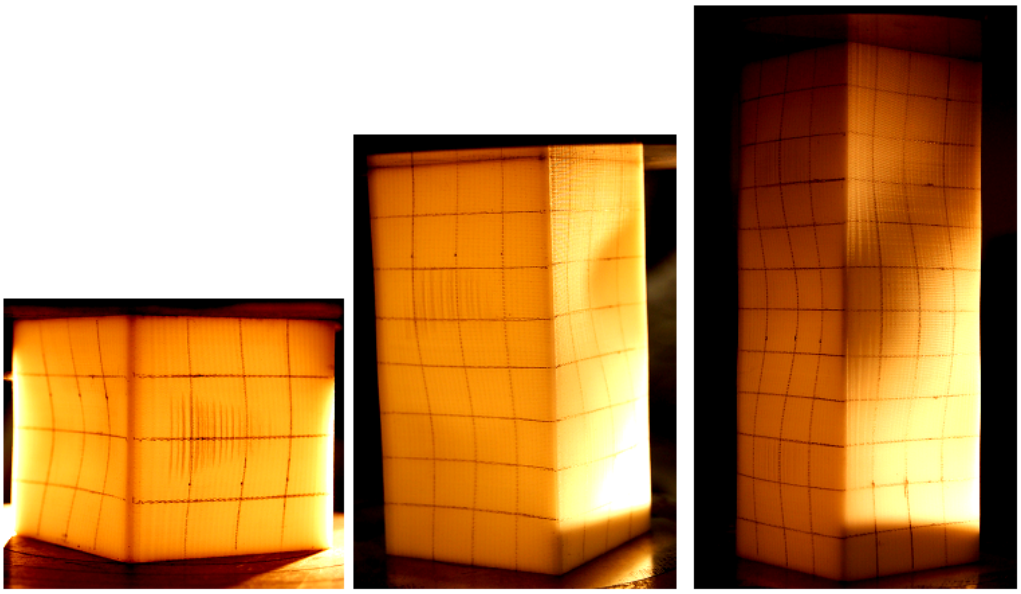

(a) **(b)** **(c)**

(d) **(e)**

Figure 3.18 The buckled profile of the ABS square tubes with aspect ratios (a) 1, (b) 2, (c) 3, (d) 1.41 and (e) 2.44

Similar tests on rhombic tubes of 45^{o} revealed the similarities between the rhombic tube and square tube. The half-wave form exhibited in the rhombic tube was observed similar to that of the square tube of same aspect ratio. Figure 3.19 shows the buckled profile of one of a rhombic tube tested, corresponding to the aspect ratio of the square tube in Figure 3.18(a).

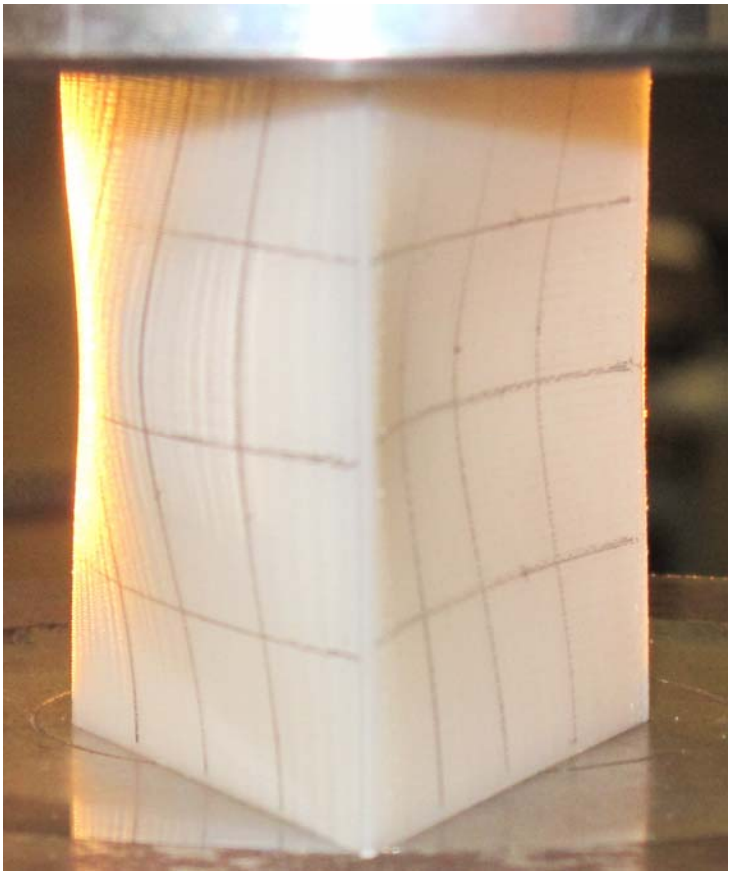

Figure 3.19 Buckled shape of a rhombic tube with aspect ratio of 1 and angle of 45^{o} with the cross section dimensions similar to that of the square tubes presented in Figure 3.18(a)

The experiments revealed that the critical load of the rhombic tubes were similar to that of the square tube data. The complete comparison of the results of the critical loads of the experiments is presented in the following section.

3.6 Results

In this section of the paper, the results of the theoretical expectations of all the tubes studied are compared with the simulation results. Also, the experimental results from the tests performed on certain tubes are compared with the theoretical and experimental results. The results of each of the tube geometries have been discussed separately in the following sub-sections.

3.6.1 Comparison of results for square tubes

In this sub-section, the theoretical critical load data of the square tubes was compared with the simulation and experimental results. The results from theory and experiments were

calculated using the material properties of the ABS plastic used for the experiments. The results of the critical loads of the tube were compared to each other by plotting the values of critical load against the aspect ratio of the tubes. The comparison is shown in Figure 3.20. The figure reveals the match of the data of the simulation and experiments from the theory.

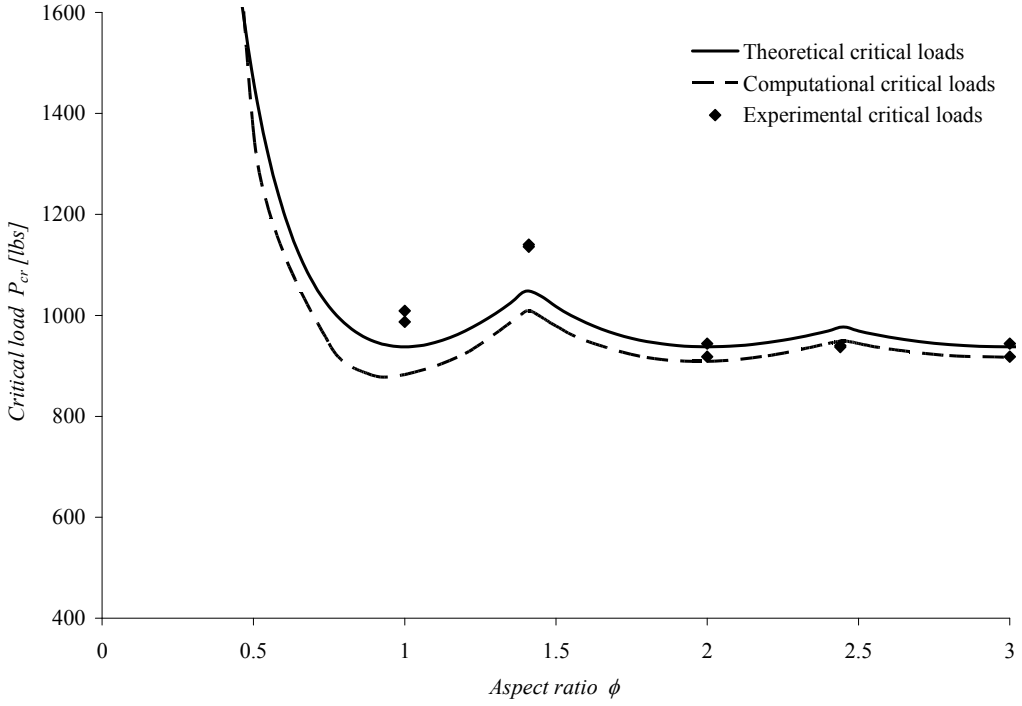

Figure 3.20 Comparison of theoretical, computational and experimental critical load variance with aspect ratio of a square tube with l = 2 *in* and t = 0.08 *in*

The comparison shows good match of all of the three results. The maximum discrepancy of the simulation results with theory was of 6 % at low aspect ratios. Similarly, maximum discrepancy between the experimental and theoretical data was of 8.7 % at the aspect ratio of 1.41 representing the transition of the number of half-waves from m = 1 to 2. The comparison shows good match of the theory and simulations.

3.6.2 Comparison of Results for Rectangular Tubes

The theoretical formulation of the curves of k and therefore the critical loads of a tube with the l_r/l ratio as 0.5 were compared with the simulation results. This comparison is presented in Figure 3.21. The model of the tube had l = 2 *in,* l_r = 1 *in* and t = 0.08 *in*.

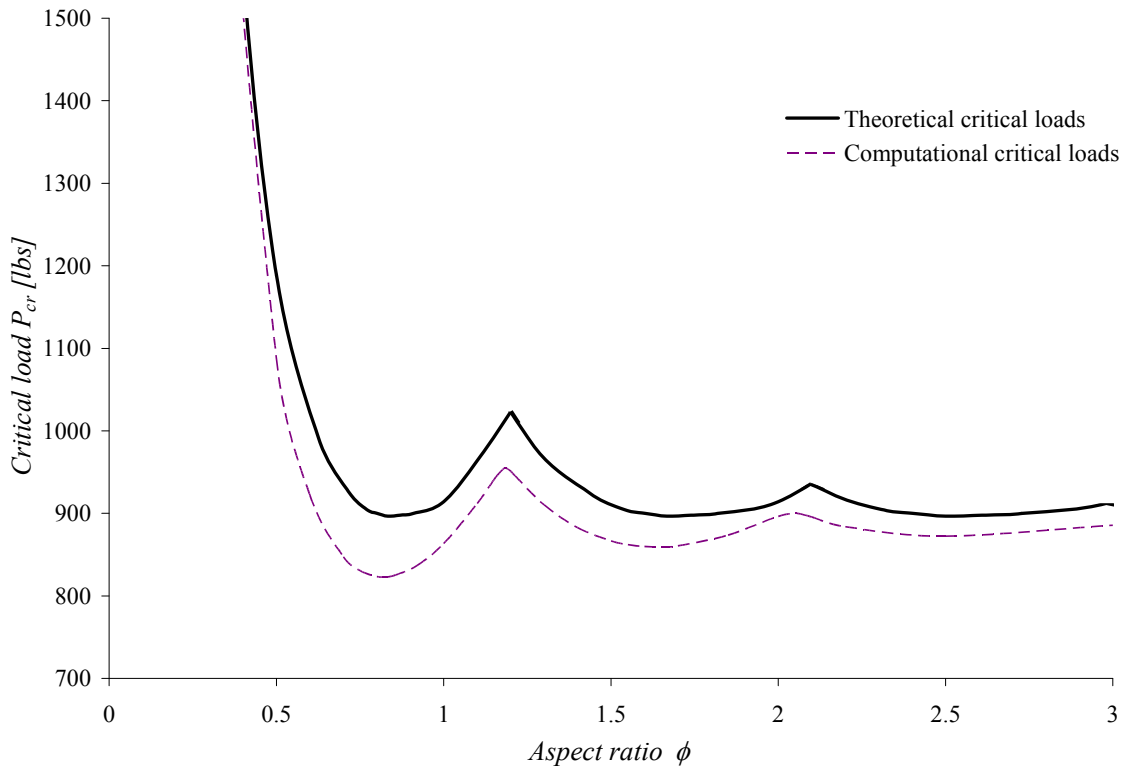

Figure 3.21 The comparison of theoretical expectations and simulation results of the buckling critical loads of a rectangular tube with l = 2 *in*, l_r = 1 *in* and t = 0.08 *in*, over different aspect ratios

The comparison revealed good agreement of the theoretical results with the computational plots. However, at the second transition, the transition was observed in simulation ratio which was off from the theoretically expected aspect ratio. The theoretical ratio is expected to be 2.1 but the simulation model exhibited the transition at 2.05. These aspect ratios are very close to each other and can be considered comparable. The reason for the small offset is unknown and is expected to be because of simulation errors. Transitions are difficult to match exactly.

3.6.3 Comparison of results of Rhombic and Parallelogram tubes

The theoretical results of rhombic and parallelogram tube buckling loads were compared to the data from the simulations. The theory postulates that the critical load behavior of rhombic and parallelogram tubes is the same as the corresponding square and rectangular tubes and thus the theoretical critical load values of the rhombic and parallelogram tubes are expected to be the same as that of the theoretical square and rectangular tubes prediction presented in Figure 3.20

and Figure 3.21, respectively. It was observed from the simulation results that the critical load data of a rhombic tube with $l = 2$ *in*, $t = 0.08$ *in* and $\theta = 45^{o}$ was the same as that of the critical load data of a square tube with same dimensions and the plot of critical loads was indistinguishable when compared to the plot of square tube shown in Figure 3.20. Similar results were observed in a parallelogram tube with $l = 2$ *in*, $l_r = 1$ *in*, $t = 0.08$ *in* and $\theta = 60^{o}$. Thus, the assumption of similar buckling behavior of the tubes of any angle buckling in wall buckling mode was verified. Also, experiments were performed on two rhombic tubes with the dimensions of the simulation models and an aspect ratio of 1. Table 3.1 shows the experimental critical load comparison of these tubes with the theoretical and simulation loads.

Table 3.1. The critical load data of a rhombic tube with $l = 2$ *in*, $t = 0.08$ *in* and $\theta = 45^{o}$, from theoretical, computational and simulation methods

Theoretical result [*lbs*]	Computational result [*lbs*]	Experimental result [*lbs*]	
		Tube 1	Tube 2
936.6	868.7	1003.5	1150.6
		Average = 1077	

The comparison revealed that the Tube 1 closely matched the theoretical result but the result of the Tube 2 had a larger error in comparison to theoretical load than Tube 1 (18 % approximately).

Apart from the study of wall buckling of the tube, the Euler buckling behavior of a rhombic tube of same dimensions as the previous models with an angle of 60^{o} was also studied using simulations. The critical loads of the tubes were compared to the theoretically expected critical load curve, which was presented in Figure 3.9. The comparison is presented in Figure 3.22.

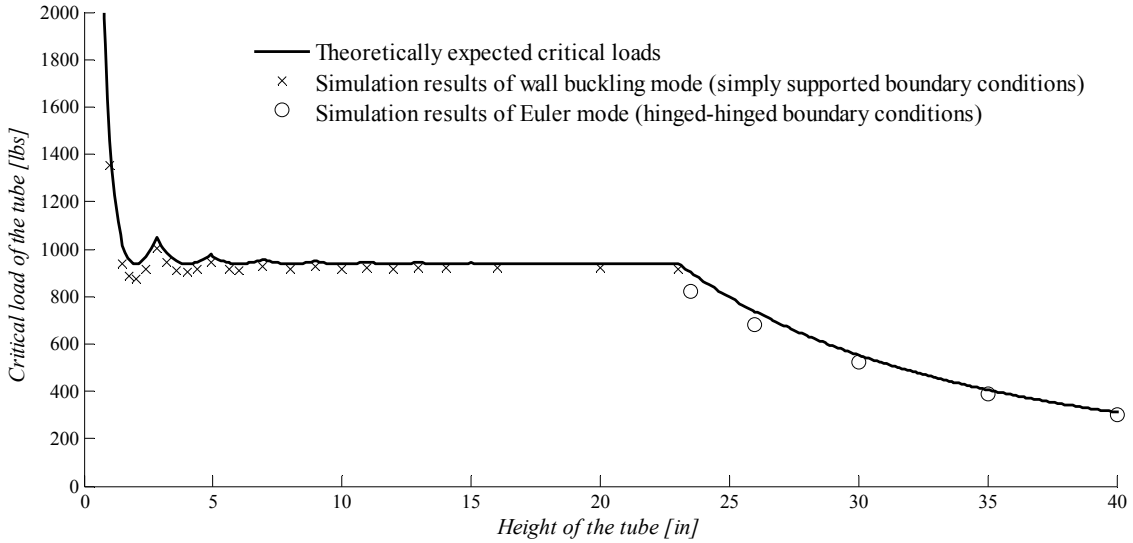

Figure 3.22. The critical load behavior of a rhombic tube with angle 60^{o} with the consideration of Euler buckling after the critical height of the tube

The study revealed an excellent match with the theoretical expectation with the observation of Euler buckling after the critical height of the tube. The beginning of the Euler buckling mode was observed at the height of 23.5 as was presented in Figure 3.17(a). A similar simulation study was performed on the parallelogram tube model studied theoretically. The comparison of the critical loads by considering the Euler buckling is presented in Figure 3.23.

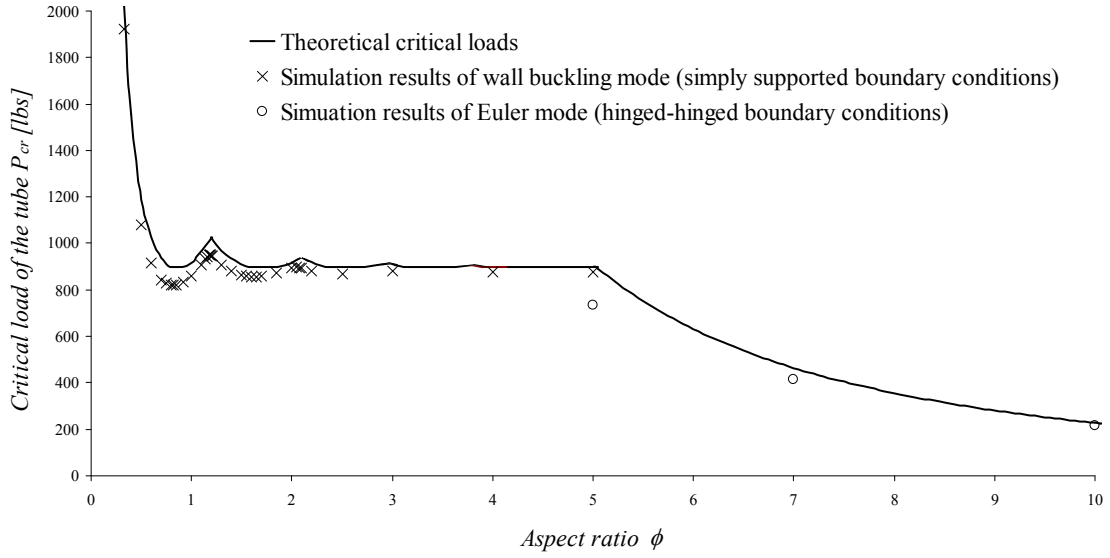

Figure 3.23 The critical load behavior of the parallelogram tube with the consideration of Euler buckling after the critical height of the tube

The simulation results show good comparison between the critical loads, however, the aspect ratio at which the Euler buckling is expected to begin was observed to be lower than the theoretical prediction. A possible reason for this is the localized effects on the finite element simulation model from the end conditions, which resulted in higher load in wall buckling mode thus resulting in the Euler buckling of the tube.

3.7 Conclusions

The present study was intended to study the buckling behavior of different kinds of quadrilateral tubes. Finite element simulations of elastic buckling were performed on different tubes and these were compared with existing theory on the buckling of tubes to critically examine the elastic buckling phenomenon of these tubes. Also, the possibility of Euler buckling in different rhombus and parallelogram tubes and good agreement with the theoretical predictions were observed from simulation results. Apart from finite element simulations, some experiments were carried out on square and rhombic tubes with tube specimens made of ABS plastic. The experimental results of the tubes exhibited good match with the theoretical and simulation results with some minor exceptions.

3.8 References

[1] G. H. Bryan. "On the stability of a plane plate with thrusts in its own plane with applications to the buckling of the sides of the ship", Proceeding of London Mathematical Society, 1891, Vol 22.

[2] Timoshenko S. P, Gere J. M. "*Theory of elastic stability*", New York, McGraw-Hill, 1961.

[3] Lundquist E. E. "Local Instability of Symmetrical Rectangular Tubes Under Axial Compression", Nat. Advisory Comm. Aeronaut. 1939 Tech note No. 686.

[4] Bleich F. "*Buckling strength of metal structures*", New York, McGraw-Hill, 1952.

[5] Bulson P. S. "*The stability of flat plates*", London, Chatto and Windus, 1970.

[6] Kandil K. S, Callandine C. R. "Classical local buckling of tubes having rectangular cross sections", International Journal of Mechanical Sciences 1986, Vol 28.

[7] Pizhong Q, Luyang S. "Explicit local buckling analysis of rotationally restrained composite plates under biaxial loading", International Journal of Structural Stability and Dynamics, World Scientific Publishing Company, 2007, Vol 7.

[8] Hosseini-Hashemi S, Khorshidi K, Amabili M. "Exact solution for linear buckling of rectangular Mindlin plates", Journal of Sound and Vibration, 2008 Vol 315.

[9] Aliabadi M. H, Baiz P. M, Albuquerque E. L. "Stability analysis of plates", Recent Advances in Boundary Element Method, 2009.

[10] Swartz S. E, O'Neill R. J. "Linear elastic buckling of plates subjected to combined loads", Thin-Walled Structures, Elsevier 1995. Vol 21.

[11] Rasmussen K. J. R, Burns T, Bezkorovainy P, Bambach M. R. "Numerical modeling of stainless steel plates in compression", Journal of constructional steel research, Elsevier 2003, Vol 59.

[12] Meng Q., Al-Hassani S. T. S. and Soden P. D, "Axial Crushing of Square Tubes", International Journal of Mechanical Sciences, 1983 Vol: 25 Issue: 9, pp. 747–773.

[13] von Karman T, Sechler E. E, Donell L. H. "Strength of thin plates in compression", Transaction of ASME, 1932, Vol 54.

[14] Winter G. "Strength of thin steel plates in compression", Transaction of ASCE, 1947, Vol 112.

[15] Cox L. H. "Buckling of thin plates in compression", Aeronautical Research Community R&M No. 1554, 1934.

[16] Mahmood H. F, Paluzny A. "Design of thin walled columns for crush energy management – their strength and mode of collapse", International Conference on Vehicular Structural Mechanics – Proceedings 1981.

[17] Li. S and Reid S. R, "The plastic buckling of axially compressed square tubes", Journal of applied Mechanics, 1992 Vol 59 No 2.

[18] Abramowicz W, Weirzbicki T, "Axial crushing of multi-corner sheet metal columns", Journal of Applied Mechanics, 1989 Vol 56.

[19] Wierzbicki T, Akerstorm T. "Dynamic crushing of strain rate sensitive box columns", International Conference on Vehicular Structural Mechanics – Proceedings 1977.

[20] Weirzbicki T, Abramowicz W. "On the crushing mechanics of thin walled structures", Journal of Applied Mechanics 1983, Vol 50.

[21] Zhang X W, Su H, Yu T X, "Energy absorption of an axially compressed square tube with a buckling initiator", International Journal of Impact Engineering - Elsevier, 2009 Vol 30.

[22] Karagiozova D, Jones N. "Dynamic buckling of elastic plastic square tubes under axial impact – II: Structural response", International Journal of Impact Engineering 2004, Vol 30.

[23] Rhodes J. "Buckling of thin plates and members – and early work on rectangular tubes", Thin Walled Structures 2002, Vol 40.

[24] Chattopadhyay A. P, Frink E, Lease K, Xin X. J, "Effects of aspect ratios and side constraints on the elastic buckling behavior of multi wall structures", Proceedings of ASME Manufacturing Science and Engineering Conference, 2011 (Accepted)

[25] Abramowicz W and Jones N, "Transition from initial bending to progressive buckling of tubes loaded statically and dynamically", International Journal of Impact Engineering, 1997 Vol 19.

Chapter 4 - Elastic Buckling Characteristics of Triangular Tubes under Uni-Axial Loading

4.1 Abstract

Tubular structures play an important role in energy absorbing components and structural members requiring high strength-to-weight ratio. The theory of buckling of circular, square, and rectangular tubes is relatively well established in the literature. The study of buckling of triangular tubes, however, has not been researched as extensively. In this paper, an analytical solution for the elastic buckling of isosceles triangular tubes was obtained by considering the buckling characteristics of individual walls of the triangular tube, with appropriate edge conditions. The results from this analytical solution were compared with previously published work in literature and finite element simulations and good agreement was found.

4.2 Introduction

The buckling behavior of plate, tubular and cellular structures has been an important area of study in the field of solid mechanics. This is mainly because of their widespread application in various fields including aeronautical, marine and civil applications. The load carrying properties of plate structures make them useful in construction of structures like ship hulls, whereas the high strength to weight ratio of cellular structures like honeycombs make them a very efficient design in aviation industry. On the other hand, the post buckling properties of tubes to form plastic folds and absorb the kinetic energy in a crash, plays an important role in the design of crash safety structures in automobiles. Buckling of plate and tubular structures has been extensively studied in the past. The following sub-sections present a brief review on the buckling of the plate and tubular structures of different shapes and discuss the goals of the present study.

4.2.1 Buckling of plate structures

The walls of any polygon tubular structure behave as supported plates under buckling loads, with different boundary conditions along the edges of the structure. The boundary conditions of the walls depend on the geometry of the structure, and these conditions determine the behavior of the wall under the compressive loads. The simplest case of buckling of a

supported plate is the condition of a plate simply supported along all of the edges with uniform loads acting along the opposite edges. Study of this kind of plate was first performed by Bryan [1]. The study of the plate buckling problem has intrigued many researchers since then. Subsequent works on elastic buckling of plates with different kinds of edge conditions have been presented in [2-4]. Studies of the supported plates revealed that the addition of support along the vertical edges of a plate structure enhances the load carrying capacity in comparison to that of an unsupported plate buckling in simple Euler buckling. Following the analysis of elastic buckling of a plate, significant work on post buckling behavior of plates have been undertaken by various researchers. Some of the important theoretical studies on post-buckling behavior of plates have been presented in [5-7]. Some of the recent theoretical studies on the elastic buckling of plates are presented in [8-10]. Methods like the Ritz Method and the Boundary Element Method were employed in these studies. Apart from theoretical solutions, extensive research has been performed on the plate buckling problem using experimental methods and computational methods using finite element solutions. Some of the works illustrating experimental and computational work has been presented in [11-14]. Bambach and Rasmussen [13] have provided an efficient design description of a test rig to test a plate under uniform compressive load for buckling and post-buckling analysis.

Despite extensive research on the plate buckling, the case of plate buckling under uni-axial force with one of the vertical non-loading edges under a restraining moment and the other simply supported has not been studied in the past. In the present study, this case of elastic buckling has been studied on account of its direct relation with the triangular tube buckling problem. The solution of buckling of this plate was derived using classical plate mechanics.

4.2.2 Buckling of square and rectangular tubes

Based on the study of plates under various conditions, extensive research has been carried out on the buckling of square and rectangular tubes. Solution of the elastic buckling of square tubes was presented by Timoshenko and Gere [2] based on the direct relation of tube buckling with the buckling of simply supported plates. It was postulated that, in the buckling of a square tube, each wall of the tube behaves as a simply supported plate. This proposition reduced the study of the whole square tubular structure to the study of buckling of four individual walls and simplified the critical load of the tube being four times of the critical load of the single wall.

Using a similar procedure, the buckling characteristics of rectangular tubes were studied by imposing proper boundary conditions on the longer walls of the rectangle. It was proposed in [15] that the longer walls of the rectangular section buckle while the smaller walls try to restrain the longer walls from buckling. Based on this proposition, the theory of elastic buckling of rectangular tubes was later studied and presented in [4] and further modified in [16]. A review of various theoretical solutions on the elastic buckling and post buckling of supported plates and rectangular tube structures has been presented in [17].

Apart from quasi-static loading of square and rectangular tubes, the behavior of these tubes in post buckling under impact loading has been studied by various researchers. The study of response of tubular structures to impact loading is an important aspect due to their applications in vehicular safety. Studies [18-22] show some of the theoretical, experimental and computational work on dynamic behavior of square and rectangular tubes.

4.2.3 Buckling behavior of circular tubes

Apart from box-columns, circular tubes are also used widely used in the design of energy absorbing structures in vehicular safety. The structural behavior of circular tubes in buckling and post-buckling conditions has been studied extensively in the past. The elastic buckling behavior of circular tubes has been presented in [2]. Post-buckling behaviors of circular tubes under quasi-static and impact loading has been studied subsequently. Some of the work on the crushing characteristics of circular tubes is presented in [23-25].

4.2.4 Buckling of triangular tubes

Despite of exhaustive research of the buckling properties of square, rectangular and circular tubes, the study on the behavior of triangular tubes has not been extensive in literature. Early theoretical works on triangular tubes were presented in [4, 26-28], which provided the solution of the buckling of a triangular tube using general plate mechanics. Also, some experimental and finite element method studies on the investigation of triangular tube buckling and post bucking have been presented in literature [29-30]. It was proposed by Wittrick and Curzon [28] that in the buckling of an equilateral triangular tube, the lowest critical load may result in two different mode shapes of buckling. In this paper, one of the two modes was used to produce explicit solutions of the buckling problem of an equilateral triangle, using classical plate mechanics. This theory was extended to any isosceles triangular tube with the length of the third

side equal to or less that the other two equal sides. The study was based on the formulation of buckling of the critical walls of the tube and establishing the relation between the main walls and the restraining wall at the common edges. The theoretical results were compared with results of finite element simulations in the present study. Certain special cases were compared with published results from literature. Theoretical predictions of the number of half waves formed along the height of the tube and the transition of the number of half waves were critically examined and compared with the computational results. The comparisons revealed excellent agreement of the theoretical results with the results of simulations.

4.3 Theoretical Buckling phenomenon of Triangular Tubes

General buckling of a tubular structure occurs by the buckling of the individual walls of the tube. The conditions for the buckling of each wall are defined by the shape of the tube and dimensional relations between the walls in the tube. In a square tube or other regular polygon tubes with an even number of sides, all of the walls reach instability at the same load in the lowest energy mode. As a result, alternating inward and outward lobes are formed in the adjacent walls of the buckled structure. Such an alternating pattern of inward-outward lobes enables the angles between the adjacent walls to remain unchanged before and after buckling. The lobes are generally referred to as half sine waves because of their shape closely resembling a sine wave between 0 and π. The buckling analysis of evenly-sided regular polygon tubes is therefore reduced to that of a single wall [2], and the total critical bucking load for the tube is the critical load of a single wall times the total number of walls. In the case of an even-sided polygon tube with walls of unequal length such as a rectangular tube, the longer walls of the tube have lower critical load compared to the shorter walls. Thus, under the application of a uniform distributed load, the longer walls buckle first while the shorter walls act as restraining walls.

However, this buckling-restraining phenomenon is possible only in the case of a polygon tube with an even number of walls. When the polygon has an odd number of sides, the alternating pattern of an entirely inward lobe of one wall followed by an entirely outward lobe in the next wall results in change of at least one original angle and is therefore energetically unfavorable. This phenomenon is illustrated schematically in Figure 4.1 using an even-sided (hexagonal) tube and an odd-sided (pentagonal) tube. The angle θ_f represents the angle between

the walls in the buckled structure. In the regular pentagonal tube, the buckling of the bottom wall in a complete inward or outward lobe changes the initial wall angle of 72^o to a new value.

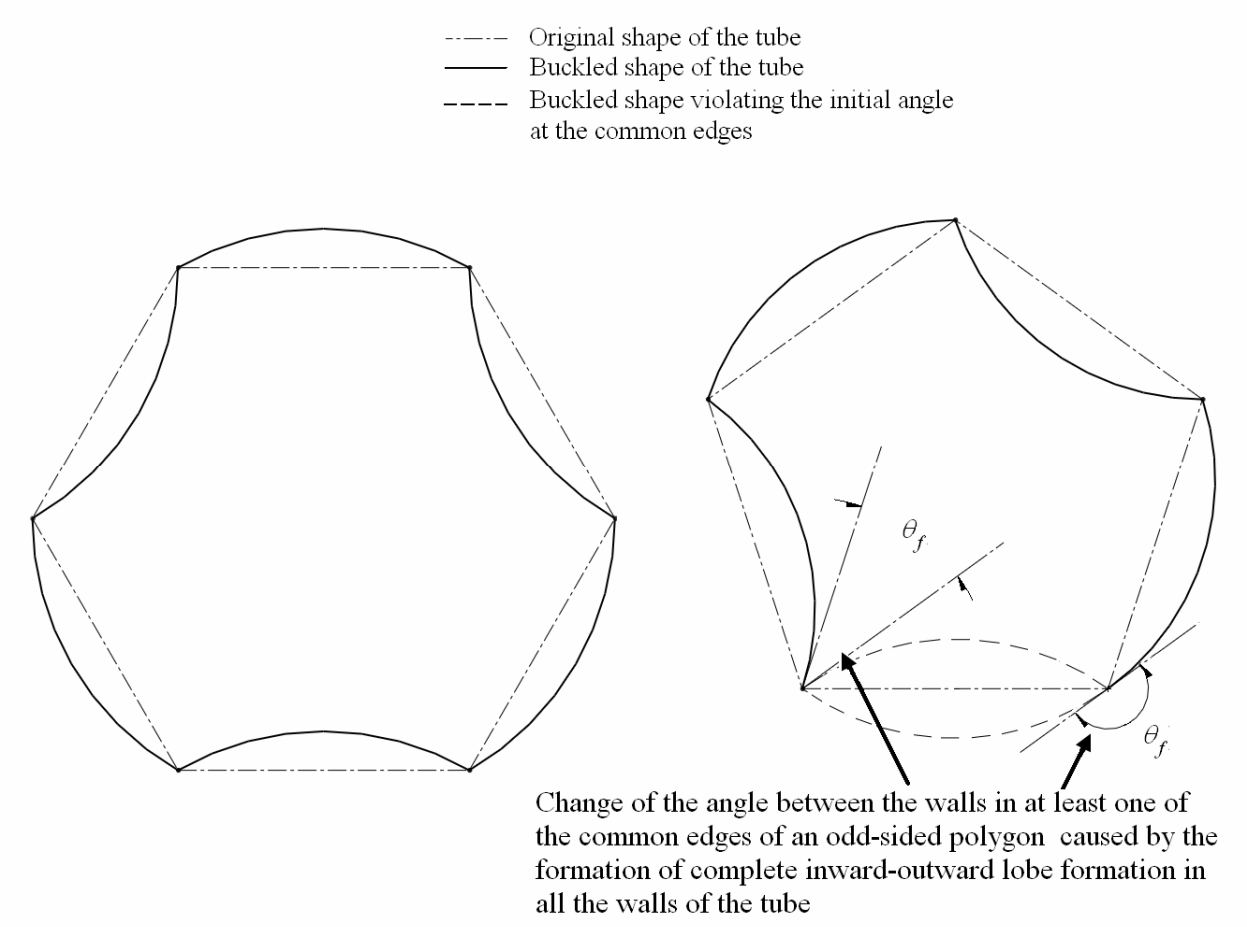

Figure 4.1 The schematic representation showing the formation of single lobe in all the walls violating the initial angle between the walls of the tube

To avoid this high energy configuration, one wall is expected to form an inward lobe on half of the wall and an outward lobe on the other half. This inward-outward lobe on the same wall is expected in any regular odd-sided polygon tube.

It was suggested in [28] that in the buckling of an equilateral triangular tube (hereafter referred to as an equilateral tube), the lowest critical load can possibly form two different mode shapes as are illustrated in Figure 4.2. In the present study, the formulation of critical load of equilateral tubes was derived based on the mode shape presented in Figure 4.2(a). It was also proposed that any isosceles tube with the unequal side shorter than the equal sides (hereafter referred to as a *short-sided isosceles tube*) will buckle as in illustrated in Figure 4.2(a). On the

other hand, an isosceles triangular tube with third side longer than the equal sides (hereafter referred to as a *long-sided isosceles tube*) will buckle as illustrated in Figure 4.2(b).

The theoretical critical load formulation of equilateral tubes presented in this paper was then used to determine the theoretical behavior of short-sided isosceles tubes, with this proposition.

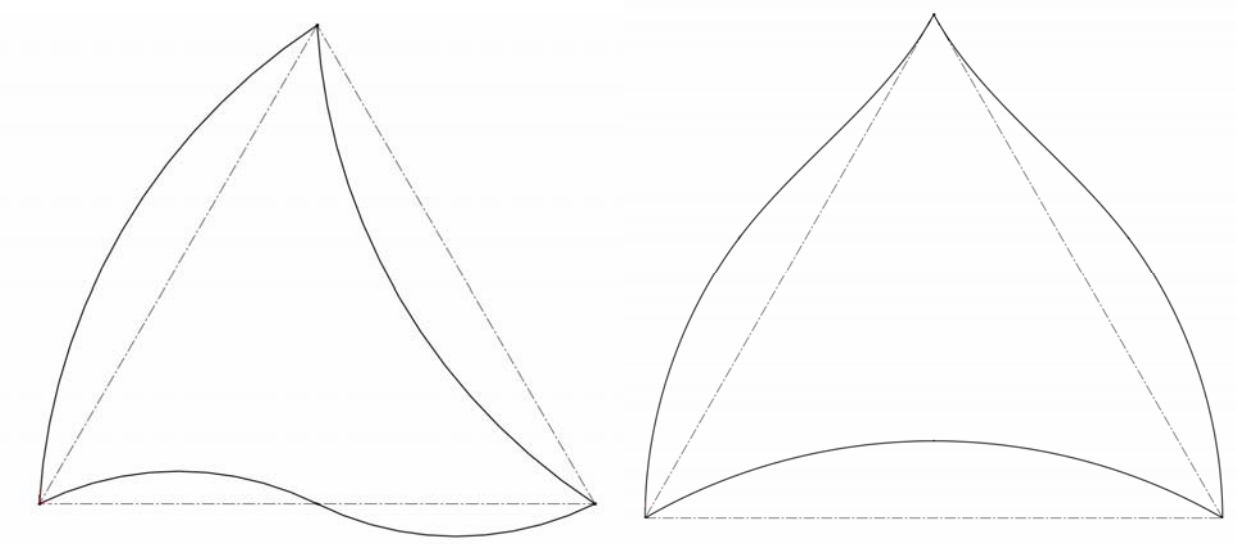

(a) **(b)**

Figure 4.2 Schematic representation of the top views of possible lowest critical load buckling patterns of an equilateral triangular tube. The dotted lines represent the original shape and solid lines represent the assumed buckled shape (for the present theoretical study, shape (a) was considered)

For the theoretical determination of the critical buckling load of a triangular tube, the tube was divided into two equal half-tube sections with one long wall and one short wall (hereafter referred to as an *angle section*). Figure 4.3 shows the top view of the two angle sections. The total critical load of the triangular tube was assumed to be the sum of the critical loads of the two identical angle sections under proper boundary conditions for the open edges.

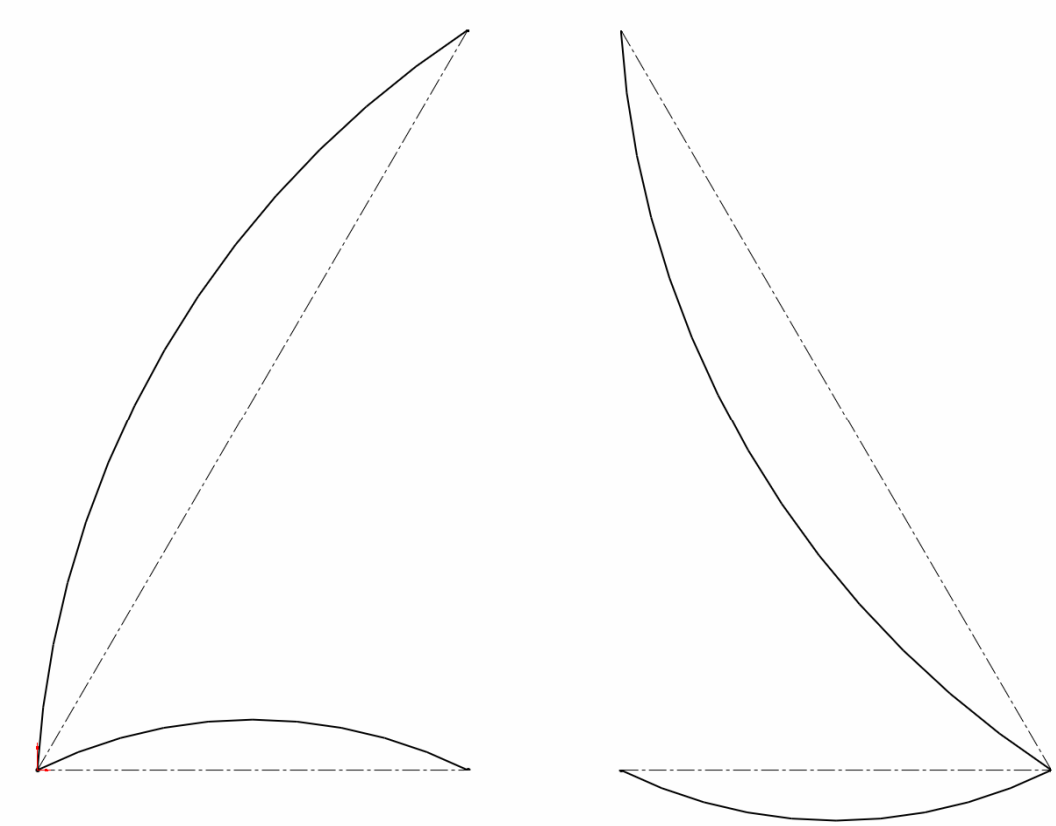

Figure 4.3 Division of the triangular tube into two half triangular tube sections called as angle sections

As the direction of the lobe formation at buckling changes along the centerline of the bottom wall of the triangular tube as shown in Figure 4.2(a), the moment and out-of-plane deflection along this line are zero. This makes the open edges of the smaller walls of the angle sections behave as a hinged (or simply supported) end. For deciding the boundary conditions of the other open edge of the angle section, conditions of this edge in the complete tube section were considered. The walls adjacent to this common edge in the tube are of same length, which results in equal critical loads of both of these walls. According to the theoretical prediction, one wall is expected to bulge inwardly and the other outwardly in the buckled shape to maintain the original wall angle. This results in a zero moment and a zero out-of-plane deflection at common edge. Therefore, both of the open vertical edges of the angle sections are considered to be hinged. The solution of the critical load of buckling for the angle sections was carried out with these boundary conditions. In the following section, the critical load formulation of an angle section is presented. This formulation is then applied to equilateral and short-sided isosceles tubes under elastic buckling in subsequent sections.

4.4 Critical Load of Buckling of an Angle Section

The critical load equation of a plate equally restrained along both of the edges has been presented in [3]. In this study, critical load formulation of a plate elastically restrained along one non-loading edge and simply supported along the other the other non-loading edge is derived and is extended to critical load formulation of an angle section. The expression for the buckling critical load of the longer wall of the section (hereafter referred to as the *main wall*) was derived in terms of an elastic restraint coefficient. The value of elastic restraint coefficient defines the amount of restraint provided by the shorter wall (hereafter referred to as the *restraining wall*) on the main wall and depends on the length ratio of main wall and restraining wall. The derivation process of the critical load of main wall of the angle section is shown in the following sub-section.

4.4.1 Equation of Deflection of the Main Wall

The theory of buckling for the angle section of an equilateral tube was derived considering the condition that the main wall buckles and the restraining wall acts as a restraint, thus inducing a resisting or restraining moment along the common edge. This makes the main wall behave as a plate simply supported along the loading edges and one of the vertical edges, and elastically restrained along the other vertical edge. A schematic representation of the angle section is presented in Figure 4.4. The problem to be solved is therefore transformed into the case of a supported plate as shown in Figure 4.5.

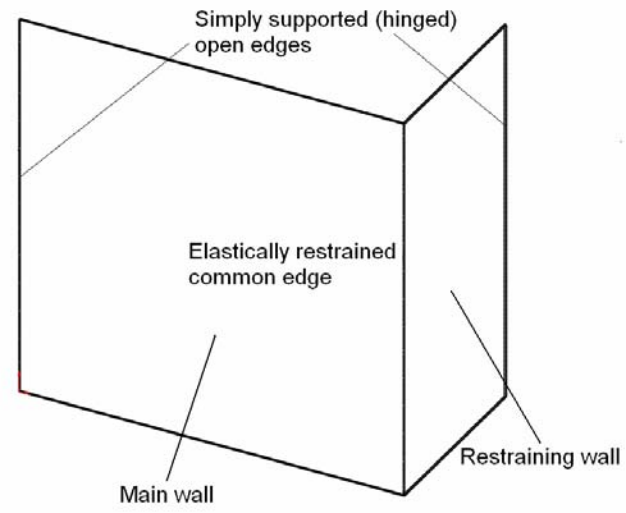

Figure 4.4 Schematic representation of the angle section with illustration of main wall and restraining wall

Based on the classical plate theory [2,3] for a unit length of a plate, the out of plane deflection w along the z-axis follows the condition.

$$\frac{EI}{1-\nu^2}\left(\frac{\partial^4 w}{\partial x^4}+2\frac{\partial^4 w}{\partial x^2 \partial y^2}+\frac{\partial^4 w}{\partial y^4}\right)+t\left(\sigma_x \frac{\partial^2 w}{\partial x^2}+\sigma_y \frac{\partial^2 w}{\partial y^2}+2\tau_{xy}\frac{\partial^2 w}{\partial x \partial y}\right)=0 \qquad (4.1)$$

where, E is the Young's Modulus of the material of the plate, ν is the Poisson's ratio, I is the moment of inertia of the cross-section about the bending axis and t is the thickness of the plate. The equation is considered over unit length of the plate. Here σ_x, σ_y are the normal in-plane stresses in x and y directions acting on the top and side edges of the plate due to the applied load respectively and τ_{xy} is the shear stress in the xy direction, acting along the edges of the plate. In the present case, all of the stresses other than σ_x are zero as a uniform in-plane force is applied only on the top edges of the angle section.

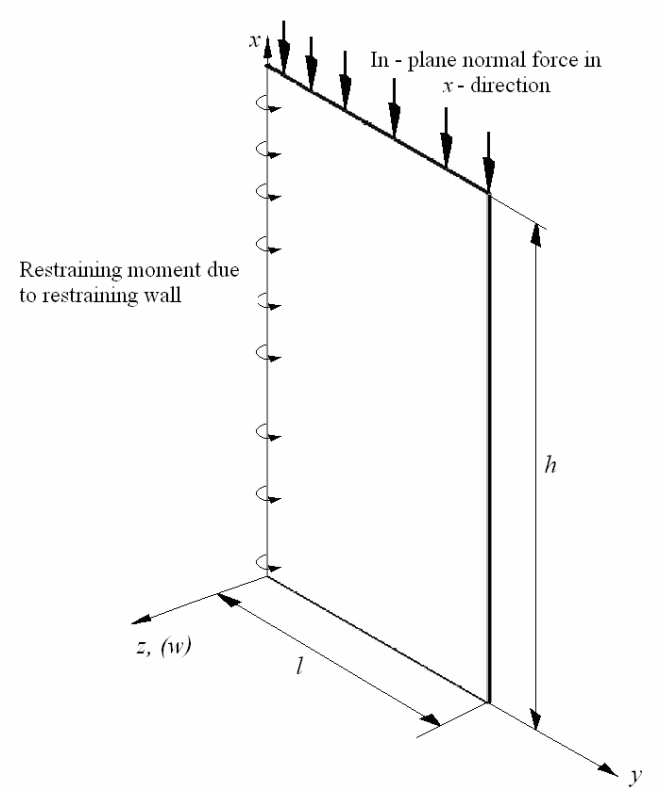

Figure 4.5. Representation of the main wall with coordinate axes and dimensions, showing the simply supported condition along one vertical edge and elastically restrained condition along the other vertical edge

The term $EI/(1 - \nu)^2$ is called the flexural stiffness of a wall. By considering the cross section of the geometry, the flexural stiffness of the plate over unit length is expressed as,

$$D = \frac{Et^3}{12\left(1-\nu^2\right)} \tag{4.2}$$

Substituting Eqn. (4.2) in Eqn. (4.1),

$$D\left(\frac{\partial^4 w}{\partial x^4} + 2\frac{\partial^4 w}{\partial x^2 \partial y^2} + \frac{\partial^4 w}{\partial y^4}\right) + t\left(\sigma_x \frac{\partial^2 w}{\partial x^2}\right) = 0 \tag{4.3}$$

The boundary conditions of the top and bottom edges of this wall, with reference to Figure 4.5 are,

at $x = 0$ and h,

$$w = 0 \tag{4.4}$$

and,

$$M_x = 0 \tag{4.5}$$

Using Eqn. (4.3) and the boundary conditions from Eqn. (4.4) and Eqn. (4.5), the general solution of the out-of-plane deflection of a supported plate with hinged top and bottom edges is, (*the details of this solution are shown in Appendix C*)

$$w = \sin\frac{m\pi x}{h}(A_1 \cosh k_1 y + A_2 \sinh k_1 y + A_3 \cos k_2 y + A_4 \sin k_2 y) \tag{4.6}$$

Here, m is the number of half sine waves formed along the height of the plate. The terms k_1 and k_2 are defined as

$$\begin{aligned} k_1 &= \frac{m\pi}{h}\sqrt{\mu+1} \\ k_2 &= \frac{m\pi}{h}\sqrt{\mu-1} \end{aligned} \tag{4.7}$$

where μ is a parameter expressed as

$$\mu^2 = \frac{\sigma_c t}{D}\left(\frac{h}{m\pi}\right)^2 \tag{4.8}$$

Here, σ_c is the critical buckling stress of the plate. The constants A_1, A_2, A_3, A_4 are calculated using the boundary conditions of the main walls, which are,

at $y = l$,

$$w = 0 \tag{4.9}$$

$$M_y = 0 \tag{4.10}$$

and, at $y = 0$,

$$w = 0 \tag{4.11}$$

$$M_y = -\bar{\zeta}\theta \tag{4.12}$$

In Eqn. (4.12), $\bar{\zeta}$ was assumed to be the proportionality constant between the resisting moment and the angle of rotation of the walls at the common edge. The parameter corresponds to the stiffness of the restraining wall against bending at the buckling point of the main wall. At this buckling point, the main wall bends due to buckling and tries to bend the un-buckled restraining wall by the same amount to maintain the angle between the walls at the edge. The restraining wall tries to resist against bending from the main wall, thus offering stiffness to the structure against bending. This phenomenon results in an increase in the critical load of the structure in comparison to a simply supported plate. The assumption of the introduction of the parameter $\bar{\zeta}$ was considered in accordance with the work presented in [3].

The moment acting along the *y*-axis at any point is given by, [2]

$$M_y = -D\left(\frac{\partial^2 w}{\partial y^2} + \nu\frac{\partial^2 w}{\partial x^2}\right) \tag{4.13}$$

Along the vertical edges, the term $\frac{\partial^2 w}{\partial x^2}$ is zero due to zero out-of-plane displacement. Therefore,

$$M_y = -D\left(\frac{\partial^2 w}{\partial y^2}\right) \tag{4.14}$$

Using Eqn. (4.12) and Eqn. (4.14), in the expression for defining the angle of rotation at y=0, expressed as $\left(\partial w/\partial y\right)_{y=0}$, the boundary condition at $y = 0$ is restated as,

$$\frac{D}{\bar{\zeta}}\left(\frac{\partial^2 w}{\partial y^2}\right) - \frac{\partial w}{\partial y} = 0 \tag{4.15}$$

For simplicity of the derivation, a term ζ, referred to as the restraint coefficient [3], was introduced, which is defined as,

$$\zeta = \frac{1}{l}\frac{D}{\bar{\zeta}} \tag{4.16}$$

The restraint coefficient in this equation corresponds to the compliance of the structure at the common edge between the main wall and the restraining wall. Using Eqn. (4.16), Eqn. (4.15) is modified as,

$$l\zeta\left(\frac{\partial^2 w}{\partial y^2}\right)-\frac{\partial w}{\partial y}=0 \tag{4.17}$$

By applying the boundary conditions from Eqns. (4.9), (4.10), (4.11) and (4.17), along with the use of Eqn (4.7) to re-substitute expressions for k_1 and k_2, the non-trivial solution of the equation of deflection is: (*the details of this are shown in Appendix D*):

$$\tan\left(\frac{m\pi}{\phi}\sqrt{\mu-1}\right)\left(\zeta\left(\frac{m\pi}{\phi}\frac{2\mu}{\sqrt{\mu+1}}\right)\tanh\left(\frac{m\pi}{\phi}\sqrt{\mu+1}\right)+1\right)-\sqrt{\frac{\mu-1}{\mu+1}}\tanh\left(\frac{m\pi}{\phi}\sqrt{\mu+1}\right)=0 \tag{4.18}$$

The above characteristic equation represents the buckling condition of the main wall of the angle section under study. This equation shows that the value of μ^2 defining the critical load of the wall varies with ζ. The values of μ^2 were plotted with respect to the various restraint coefficients ζ at different values of m/ϕ of the angle section. Figure 4.6 shows the variation of μ^2 with ζ when the ratio m/ϕ was set as 1.

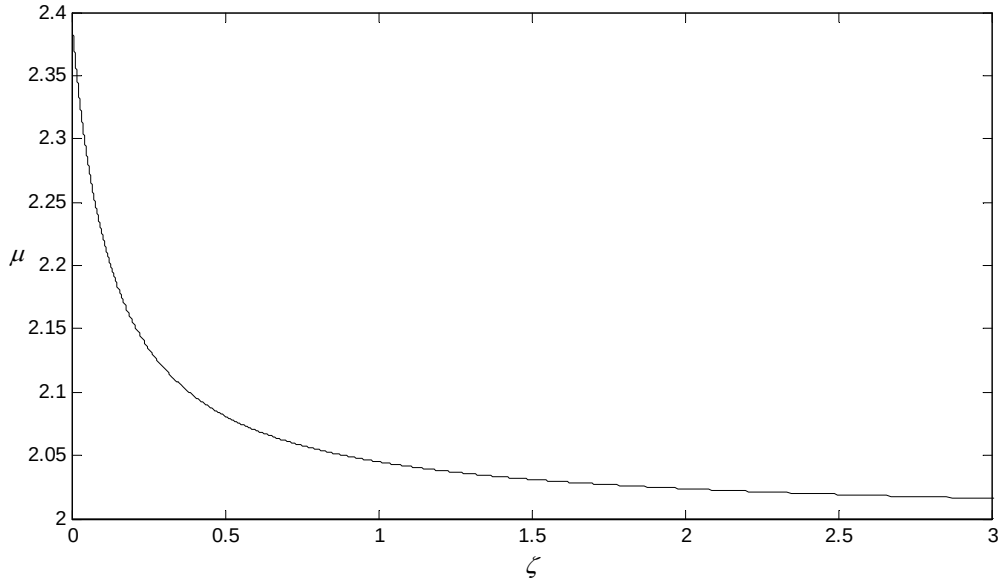

Figure 4.6 Variation of μ^2 with ζ when m/ϕ is 1

The simplest case of a plate buckling corresponds to a plate with all four edges simply supported. From Eqn. (4.12) and Eqn. (4.16), this is represented by ζ approaching ∞. At this condition, the curve approaches asymptotically to the line $y = 2$ in Figure 4.6. Therefore, using Eqn. (4.8),

$$\mu^2 = 4 = \frac{\sigma_c t}{D}\left(\frac{h}{m\pi}\right)^2$$

or
$$\sigma_c = \frac{4\pi^2 D}{t}\left(\frac{m}{\phi l}\right)^2 \tag{4.19}$$

Substituting the value of m/ϕ as 1 and the expression for D from Eqn. (4.2) into Eqn. (4.19), the expression of critical stress becomes,

$$\sigma_c = \frac{4\pi^2 E}{12\left(1-\nu^2\right)}\left(\frac{t}{l}\right)^2 \tag{4.20}$$

From the established equation of critical stress of a plate under any general boundary condition, the critical stress takes the form, [3]

$$\sigma_c = \frac{k\pi^2 E}{12\left(1-\nu^2\right)}\left(\frac{t}{l}\right)^2 \tag{4.21}$$

Comparing Eqn. (4.20) and Eqn. (4.21), the value of k for a plate simply supported along both of its edges is observed as 4 from the present study, which is in agreement with many previously published works [2-4]. Substituting the value of ζ as approaching ∞ in Eqn. (4.18),

$$\frac{m\pi}{\phi}\sqrt{\mu-1} = n\pi \qquad n=0,1,2,..$$

(4.22a)

Neglecting the trivial solution of $n = 0$ which gives $\mu = 1$ the next smallest value of n in this solution gives,

$$\mu^2 = \left(\frac{\phi}{m}\right)^4 + 2\left(\frac{\phi}{m}\right)^2 + 1 \tag{4.22b}$$

Substituting this into Eqn. (4.8) leads to:

$$\sigma_c = \left(\frac{\phi}{m}+\frac{m}{\phi}\right)^2 \frac{\pi^2 E}{12\left(1-\nu^2\right)}\left(\frac{t}{l}\right)^2 \tag{4.23}$$

The force acting over the cross-section of the plate of length l and thickness t is therefore,

$$P_{cr} = \left(\frac{\phi}{m}+\frac{m}{\phi}\right)^2 \frac{\pi^2 E}{12\left(1-\nu^2\right)}\left(\frac{t^3}{l}\right) \tag{4.24}$$

Comparing this with the general expression for the critical load of a plate with any edge conditions represented as:

$$P_{cr} = \frac{k\pi^2 E}{12\left(1-\nu^2\right)}\left(\frac{t^3}{l}\right) \tag{4.25}$$

the expression of k is,

$$k = \left(\frac{\phi}{m} + \frac{m}{\phi}\right)^2 \tag{4.26}$$

The expression of k obtained here is in agreement with the expression presented in literature [2]. In the general case of the angle sections of different equilateral tubes, different values of ζ affect the values of k. The value of ζ as a function of ϕ/m was calculated using the equation of deflection of the restraining wall. This is discussed in following sub-section.

4.4.2 Calculation of Restraint Coefficient using the Deflection Equation of the Restraining Wall

The equation of bending of the restraining wall has the same form as that of the main wall, which was expressed in Eqn. (4.1). A schematic representation of the dimensions and coordinate system of the restraining wall used for the derivation is presented in Figure 4.7.

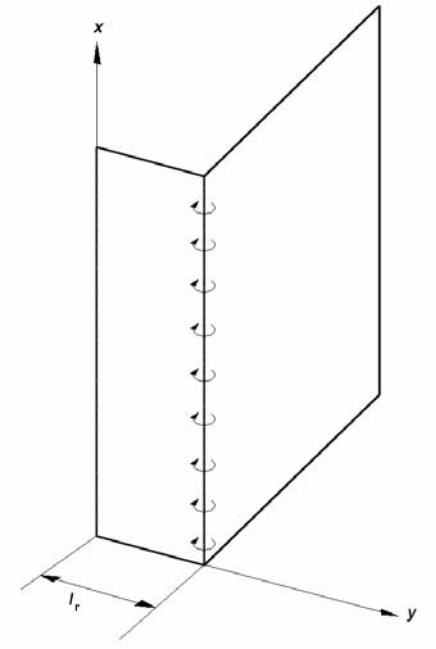

Figure 4.7 Geometry of the restraining wall with a diagrammatic representation of bending moment acting along the common edge due to buckling of main wall

Since the buckling load for the main wall is lower than that of the restraining wall, under the action of a uniformly distributed load, the restraining wall remains unbuckled at the point of buckling of the main wall. Thus, the in-plane load acting on the top edges causes negligible effect on the bending of the restraining wall. The bending of the restraining wall occurs only due to the bending moment exerted along the common edge by the lobe formation of the main wall. Therefore, in the equation of bending of the plate shown in Eqn. (4.1), the terms consisting of the longitudinal, transverse and shear forces are neglected. Therefore, the expression of deflection of the restraining wall is expressed as,

$$\frac{\partial^4 w}{\partial x^4} + \frac{\partial^4 w}{\partial x^2 \partial y^2} + \frac{\partial^4 w}{\partial y^4} = 0 \tag{4.27}$$

where w is the out-of-plate deflection of the restraining wall. The displacement and moment along the bottom and top edges ($x = 0$ and $x = h$, respectively) are zero because the plate is simply supported along the top and bottom edges. With these conditions, using the similar process used to derive Eqn. (4.6), the solution for the deflection of the plate is,

$$w = \sin\frac{m\pi x}{h}\left(C_1 \sinh\frac{m\pi}{h} y + C_2 \cosh\frac{m\pi}{h} y + C_3 y \sinh\frac{m\pi}{h} y + C_4 y \cosh\frac{m\pi}{h} y \right) \tag{4.28}$$

where, C_1 to C_4 are constants which depend on the boundary conditions of the restraining wall. These boundary conditions are,

at $y = 0$, l_r,

$$w = 0 \tag{4.29}$$

At the open vertical edge of the restraining wall, the moment along the y-axis is zero. Therefore, using the equation of moment along the vertical edges of a plate under bending as explained in Eqn. (4.14), the condition obtained at $y = 0$ is,

$$\frac{\partial^2 w}{\partial y^2} = 0 \tag{4.30}$$

At the common edge, the moment acting on the restraining wall is due to the bending of the main wall. The magnitude of this moment is equal to the restraining moment offered by the restraining wall. Therefore, at $y = l_r$,

$$\frac{\partial^2 w}{\partial y^2} = -\frac{M_y}{D'} \tag{4.31}$$

where, M_y is the moment at the common edge as was presented in Eqn. (4.12), which is considered constant for an angle section at a given height and D' is the flexural stiffness of the restraining wall. Solving Eqn. (4.28) with the boundary conditions from Eqns. (4.29), (4.30) and (4.31), the solution of the deflection of the restraining wall was derived as, (the details of this solution are shown in *Appendix E*)

$$w = \frac{M_y}{2D'\left(\frac{m\pi}{h}\right)\sinh\left(\frac{m\pi}{h}l_r\right)}\left[l_r\frac{\cosh\left(\frac{m\pi}{h}l_r\right)}{\sinh\left(\frac{m\pi}{h}l_r\right)}\sinh\left(\frac{m\pi}{h}y\right) - y\cosh\left(\frac{m\pi}{h}y\right)\right]\sin\frac{m\pi x}{h} \tag{4.32}$$

The angle of rotation at the common edge of the two walls with respect to the coordinate system of the restraining wall is given by,

$$\bar{\theta} = \left[\frac{\partial w}{\partial y}\right]_{y=l_r} \tag{4.33}$$

Therefore, the angle of rotation obtained by substituting the expression of w from Eqn. (4.32) in Eqn. (4.33) is,

$$\bar{\theta} = -\frac{M_y}{2D'}\left(\frac{h}{m\pi}\right)\left[l_r\frac{m\pi}{h} + \coth\left(\frac{m\pi}{h}l_r\right) - l_r\left(\frac{m\pi}{h}\right)\coth^2\left(\frac{m\pi}{h}l_r\right)\right] \tag{4.34}$$

The relation between the angle of rotation and the moment at the common edge was assumed in Eqn (4.12) as,

$$\bar{\theta} = -\frac{1}{\bar{\zeta}}M_y \tag{4.35}$$

It follows from comparison of Eqn. (4.34) and Eqn. (4.35),

$$\frac{1}{\bar{\zeta}} = \frac{l}{2D'}\frac{\phi}{m}\left[\frac{l_r}{l}\frac{m}{\phi} + \frac{1}{\pi}\coth\left(\frac{m\pi}{\phi}\frac{l_r}{l}\right) - \frac{l_r}{l}\left(\frac{m}{\phi}\right)\coth^2\left(\frac{m\pi}{\phi}\frac{l_r}{l}\right)\right] \tag{4.36}$$

Substituting Eqn. (4.36) in Eqn. (4.16),

$$\zeta = \frac{l}{2}\left(\frac{t}{t'}\right)^3\left[\frac{\phi}{m}\left\{\frac{l_r}{l}\frac{m}{\phi} + \frac{1}{\pi}\coth\left(\frac{m\pi}{\phi}\frac{l_r}{l}\right) - \frac{l_r}{l}\left(\frac{m}{\phi}\right)\coth^2\left(\frac{m\pi}{\phi}\frac{l_r}{l}\right)\right\}\right] \tag{4.37}$$

Equation (4.37) defines the dependence of ζ on the ratios l_r/l and m/ϕ. For a given angle section or triangular tube, the ratio l_r/l is constant, and the value of the restraint coefficient ζ depends only on the value of m/ϕ. In the present case of study of an equilateral triangular tube,

the ratio l_r/l is 0.5. A graph showing the different values of the restraint coefficient for different values of m/ϕ with $l_r/l = 0.5$ is shown in Figure 4.8. From this plot, the values of ζ varying with m/ϕ ratios were calculated.

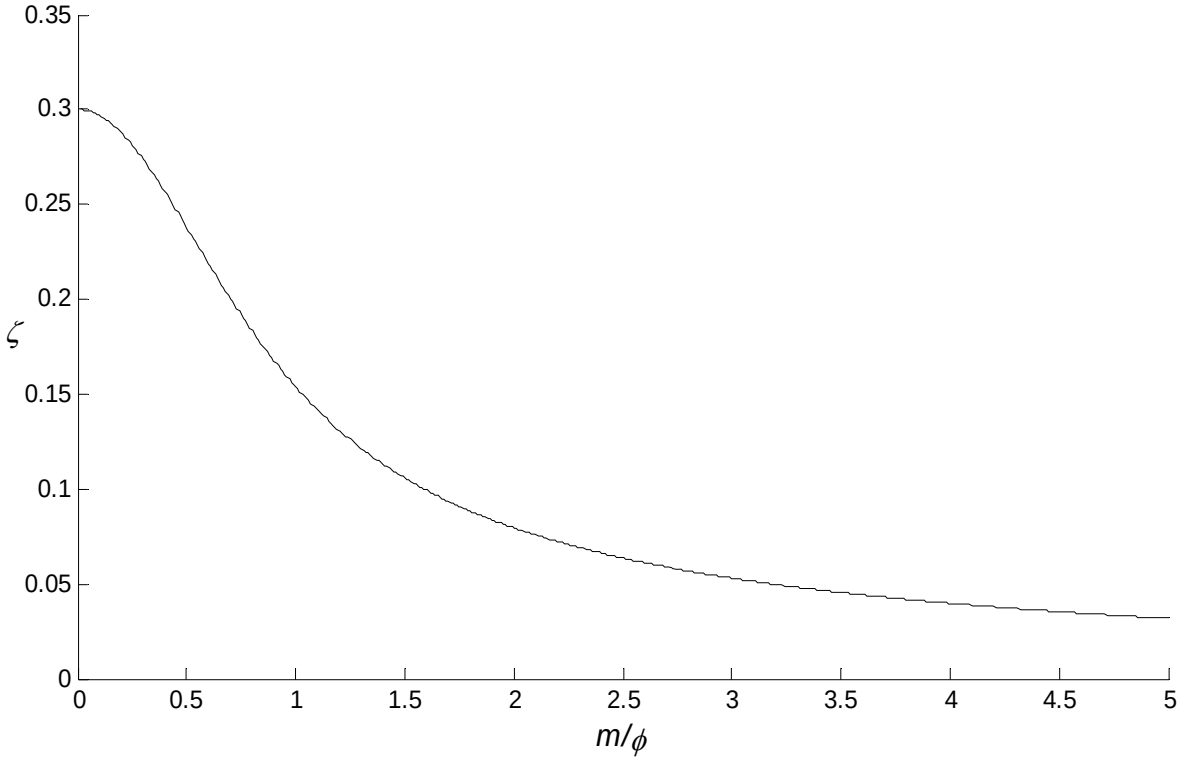

Figure 4.8 Plot showing the variation of coefficient ζ with the change of ratio m/ϕ for l_r/l = 0.5

Substitution of the expression of flexural stiffness D in Eqn. (4.8) and expressing it in the form of Eqn. (4.21) leads to the relation,

$$k = \mu^2 \left(\frac{m}{\phi} \right)^2 \tag{4.38}$$

Using Eqn. (4.38), the values of buckling factor k of the main wall of the angle section of an equilateral tube were calculated for the different values of aspect ratios. The values of ζ were calculated at different values of the ratio m/ϕ from Eqn. (4.37). With these values of ζ, the values of μ were calculated for these values of the ratio m/ϕ using Eqn. (4.18). The aspect ratios at these values of m/ϕ were calculated, by substituting the number of half waves as 1, 2, 3 and so on. Table 4.1 shows the values of k calculated for a main wall using this procedure for m = 1.

Table 4.1 Theoretical calculation of the values of *k* for different values aspect ratios for *m*=1

m/ϕ	ϕ	ζ	μ	$k=\mu^2\left(\frac{m}{\phi}\right)^2$
0.5	2.00	0.154	6.02	9.06
0.6	1.67	0.149	4.48	7.21
0.8	1.25	0.138	2.91	5.42
0.9	1.11	0.132	2.49	5.04
1	1.00	0.126	2.20	4.85
1.1	0.91	0.121	1.98	4.76
1.15	0.87	0.118	1.90	4.75
1.2	0.83	0.114	1.82	4.77
1.25	0.80	0.112	1.75	4.78
1.3	0.77	0.109	1.69	4.84
1.4	0.71	0.103	1.59	4.98
1.6	0.63	0.094	1.45	5.36
2	0.50	0.078	1.28	6.56
2.5	0.40	0.063	1.18	8.64
3	0.33	0.053	1.12	11.31
3.5	0.29	0.046	1.09	14.50
4	0.25	0.040	1.07	18.21

Using a similar calculation as shown in Table 4.1 for different number of half waves generates the set of curves of *k* for different number of half waves formed along the height of the main wall. Figure 4.9 shows the set of *k* curves for *m* equal to 1, 2, 3 and 4.

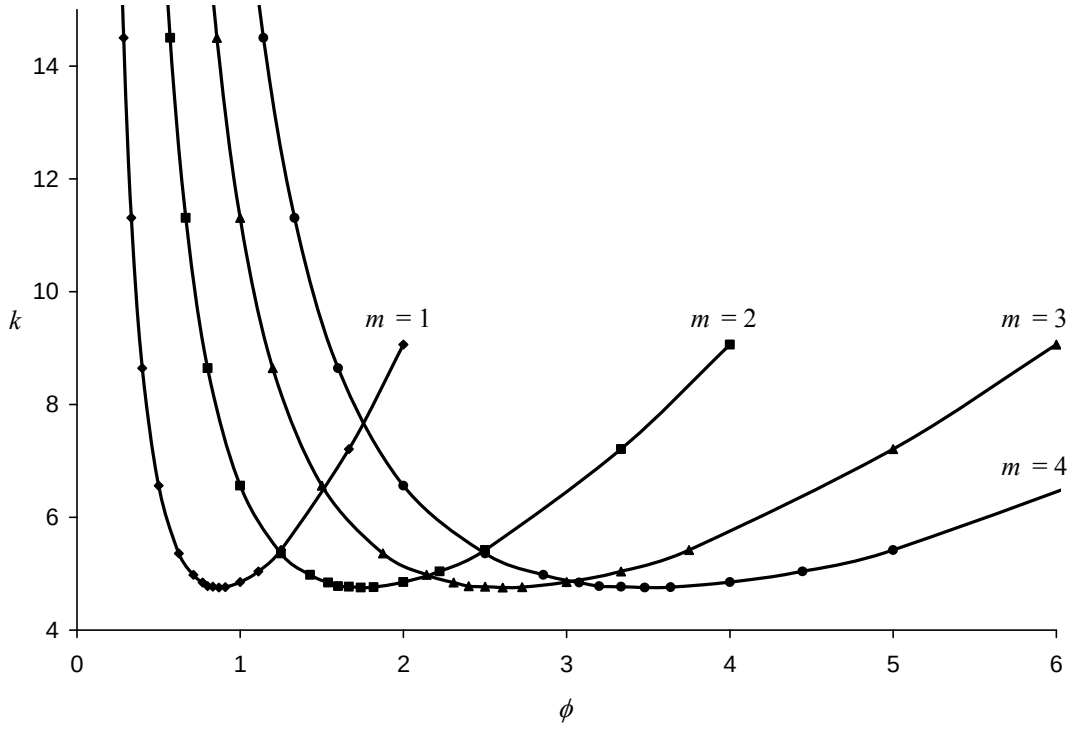

Figure 4.9 Plot showing the curves of *k* for different number of half sine waves varying with the values of aspect ratios

It is observed from Eqn. (4.25) that the critical load of bucking of a plate is directly proportional to the buckling factor *k*. Looking at the plot of *k* in Figure 4.9, this relationship implies that the number of half waves formed along the height of the wall is transformed to $n+1$ from n after a certain aspect ratio to maintain the minimum value of the buckling factor *k*. This is a phenomenon which is observed in any plate structure under buckling action. This phenomenon suggests that the minimum value of *k* of any supported plate, multi-walled and tubular structure recurs at certain aspect ratios of the structure. For the calculation of the critical load of the main wall with a certain aspect ratio, the value of *k* is read from the curve with the *m* value corresponding to the least value of *k* at that aspect ratio.

As the load acting upon the angle section was considered to be uniform, the critical load of the angle section becomes,

$$P_{cr_{half-section}} = 1.5P_{cr} \tag{4.39}$$

where P_{cr} is the elastic buckling critical load of the main wall and was calculated using Eqn. (4.25). Similarly, the total critical load of an equilateral tube is,

$$P_{cr_{equilateral}} = 3P_{cr} \tag{4.40}$$

The obtained theoretical values of k of the main wall at different aspect ratios of an angle section corresponding to an equilateral tube were compared to finite element simulation results. These comparisons are presented in the following sections.

4.5 Critical Load Derivation of an Isosceles Tube

The derivation of the critical load solution presented in the previous section can be easily extended to the case of an isosceles tube. The only difference between an isosceles tube and an equilateral tube lies in the difference in l_r/l ratio of the corresponding angle section. For an isosceles tube, this ratio lies between 0 and 1. However, the present study is confined to the short-sided isosceles tubes. In the case of a long-sided isosceles tube, the buckling mode shape will follow the pattern illustrated in Figure 4.2(b). In this deformation mode, the long wall acts as the buckling main wall and the equal shorter walls act as restraining walls. The common edge between the short walls does not undergo any rotation to maintain the initial wall-angle. Edges between the shorter walls and the long wall act as elastically restrained joints providing equal restraint on both of the edges during buckling. This proposition was verified computationally by performing a finite element simulation on a long-sided isosceles tube. The lowest critical load mode shape for this tube was recorded from the simulation results. Figure 4.10 shows the model of the buckled shape on an exaggerated scale from simulation result, which appears similar to Figure 4.2(b).

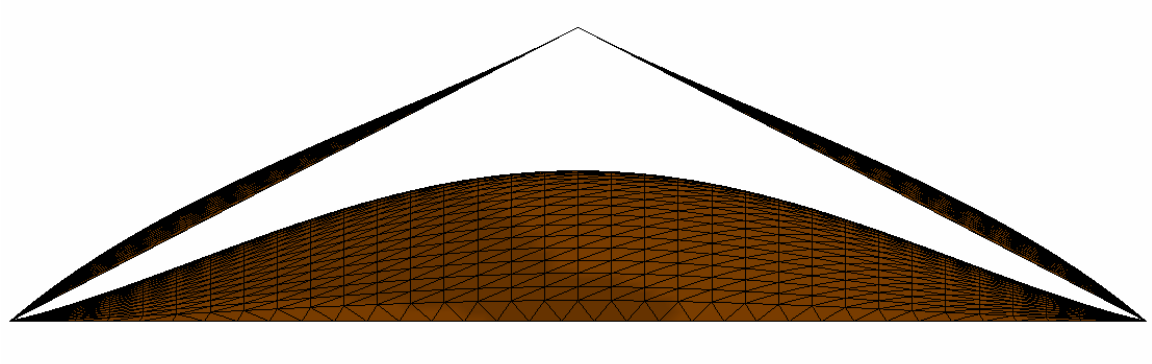

Figure 4.10 Simulation result of buckling of a long-sided isosceles tube showing the buckling of the walls at an exaggerated scale

The critical load of long-sided isosceles tubes can be derived by considering the main wall as an equally restrained plate and defining the relation of the main wall with the restraining

walls. This is not considered in this study, as the derivation of the critical load of a plate equally restrained along both the edges exists in the literature [2-4].

In the present study, the values of k for short-sided isosceles tubes were derived in the same fashion, as was carried out for the equilateral tube. Using Eqn. (4.37), the values of ζ were calculated for various angle sections corresponding to different short-sided isosceles tubes. The values of l_r/l ratios of the studied angle sections were 0.01, 0.1, 0.3 and 0.5. With the values of restraint coefficients of these sections at different m/ϕ ratios, the curves of k of the main wall were plotted against the aspect ratios. In this study, the values of m/ϕ were selected to critically examine the important points of the k curves like the transition of m and the minima of k. These plots are presented in Figure 4.11.

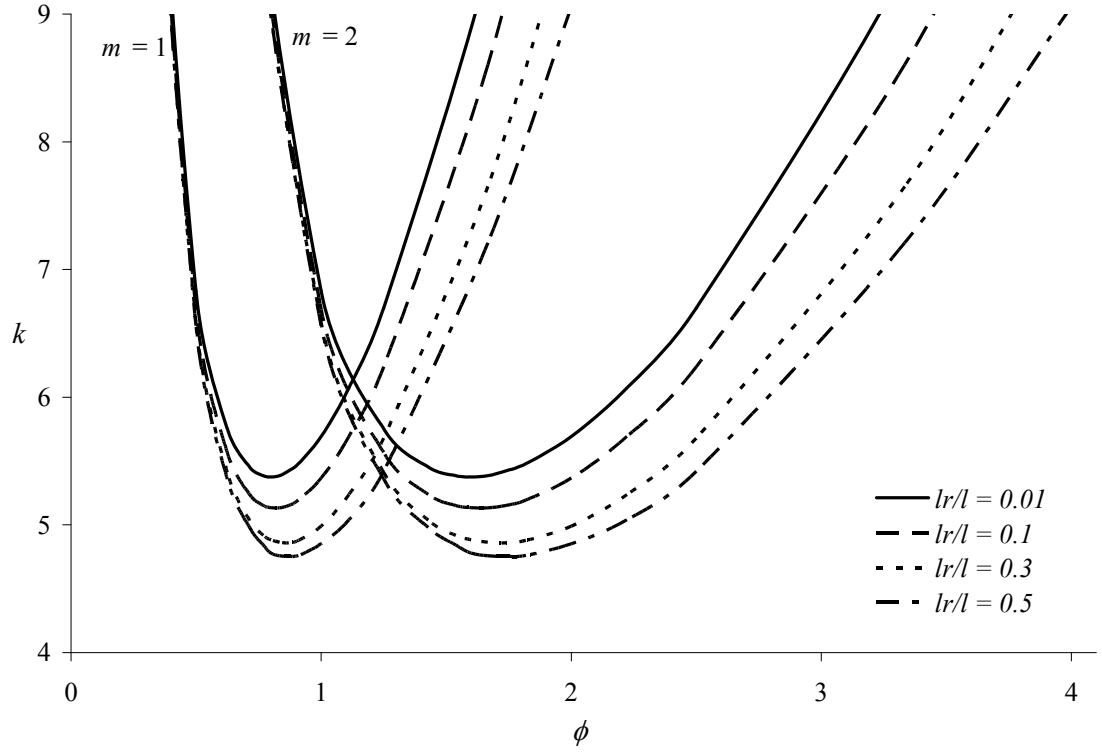

Figure 4.11 Plots of k curves for various l_r/l ratios varying with aspect ratio ϕ

The case $l_r/l = 0.01$ closely resembles the case of a plate fixed on one side and simply supported on other side. From a previous study in [4], the buckling factor k for such a plate has been presented in an empirical form as,

$$k = \frac{1}{\phi^2} + 2.5\phi^2 + 2.25 \tag{4.41}$$

Equation (4.41) predicts k to be 5.75 for an aspect ratio of 1. From the curves of k in Figure 4.11, the value of k on the curve for length ratio $l_r/l = 0.01$, at an aspect ratio of 1 is 5.7. This is comparable to value of k of 5.75 obtained from the equation. Also, it was observed in Figure 4.11 that k reaches a minimum of 5.37 for this angle section at an aspect ratio of 0.8. Equation (4.41) generates a k value of 5.41 at this aspect ratio. These results verify the validity of the solution obtained in the current study for the angle section of any ratio of l_r/l less than 0.5. Based on results from Figure 4.11, the minimum values of k as a function of l_r/l are plotted in Figure 4.12.

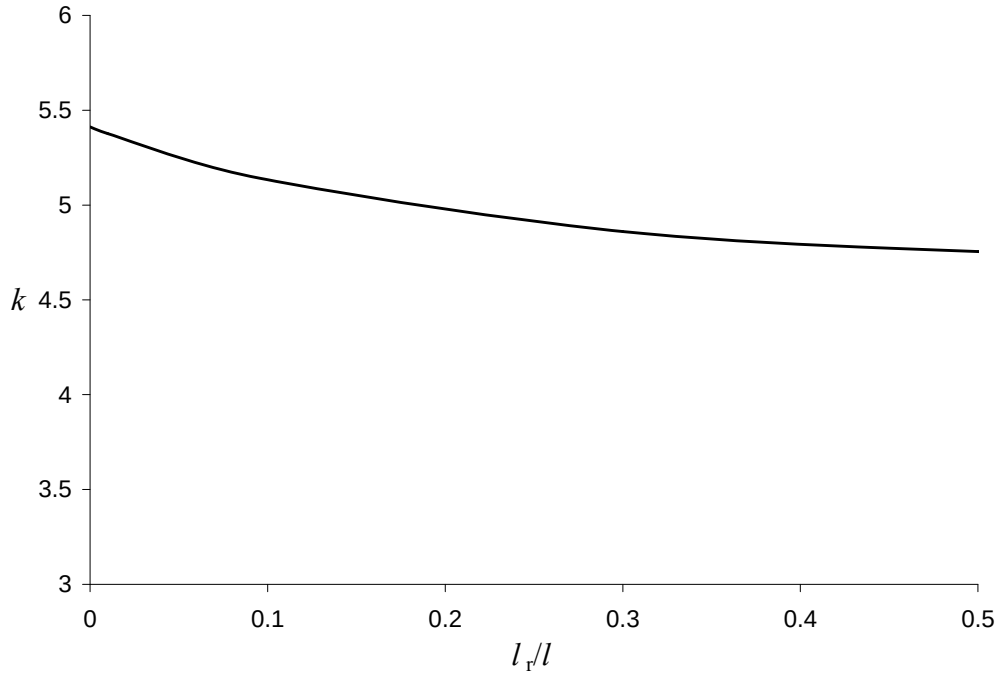

Figure 4.12 Curve showing the minimum values of buckling factor k of the main wall of an angle section for different length ratios l_r/l

Since the applied load was considered uniformly distributed along the length of the walls of the angle section, the critical buckling load of the whole isosceles tube is expressed as,

$$P_{cr_{isoscles}} = 2\left(l_r/l + 1\right)P_{cr} \tag{4.42}$$

where l_r/l is the length ratio of the sides of the angle section corresponding to the isosceles tube and P_{cr} is the critical load of the main wall of the angle section, calculated using Eqn. (4.25). Theoretical values of k of the main wall of a few different angle sections corresponding to

various short-sided isosceles tubes were compared with FEM simulation results. These comparisons are presented in the following section.

4.6 Finite Element Simulation of Buckling of Different Triangular Tubes

In this section, results of finite element simulations for buckling of angular sections and triangular tubes are presented. The first pair of simulations was performed on an equilateral tube and its corresponding angle section. This was carried out to confirm the assumption that the angle sections with simply supported boundary conditions along the open vertical edges, behave as half of the whole triangular tube. Following this, buckling simulations of angle sections of equilateral and isosceles tubes were performed over a range of aspect ratios, to verify the postulates of the derived theory.

4.6.1 Finite Element Simulations of an Equilateral Tube and Corresponding Angle Section

The goal of these simulations was to show that the critical load of the triangular tube is twice that of the corresponding angle section. Simulations were performed on an equilateral tube and its corresponding angle section. The triangular tube was modeled with walls of length 5 *mm* and wall thickness of 0.1 *mm*. The height of the tube was chosen to be 10 *mm* to produce an aspect ratio of 2. The angle section was created with the longer side of length 5 *mm* and shorter side of length 2.5 *mm*, with the same wall thickness and height. Figure 4.13 shows the shapes of the structures after a buckling simulation in an exaggerated scale. Material properties were assigned to the geometries with Young's Modulus E of 100 *GPa* and Poisson's ratio ν of 0.3, for all FEM simulations. SolidWorks Simulation software was used for performing the simulations, which uses linearized Eigen value problem to solve for the buckling critical loads. The models of both of the geometries were meshed using a shell mesh. A total of 9408 triangular elements, each of size approximately 0.18 *mm* were used in the mesh of the equilateral tube. Each element had three corner nodes and three mid-edge nodes making a total of six nodes per element. The angle section was meshed using a total of 4704 triangular elements having a similar size as that of the elements used in the tube. The open edges of the angle section were restricted from translatory motion in the out-of-plane direction. However, rotation was allowed along the vertical open edges. The top and bottom edges were subjected to zero translation restraint with rotations allowed about the edges.

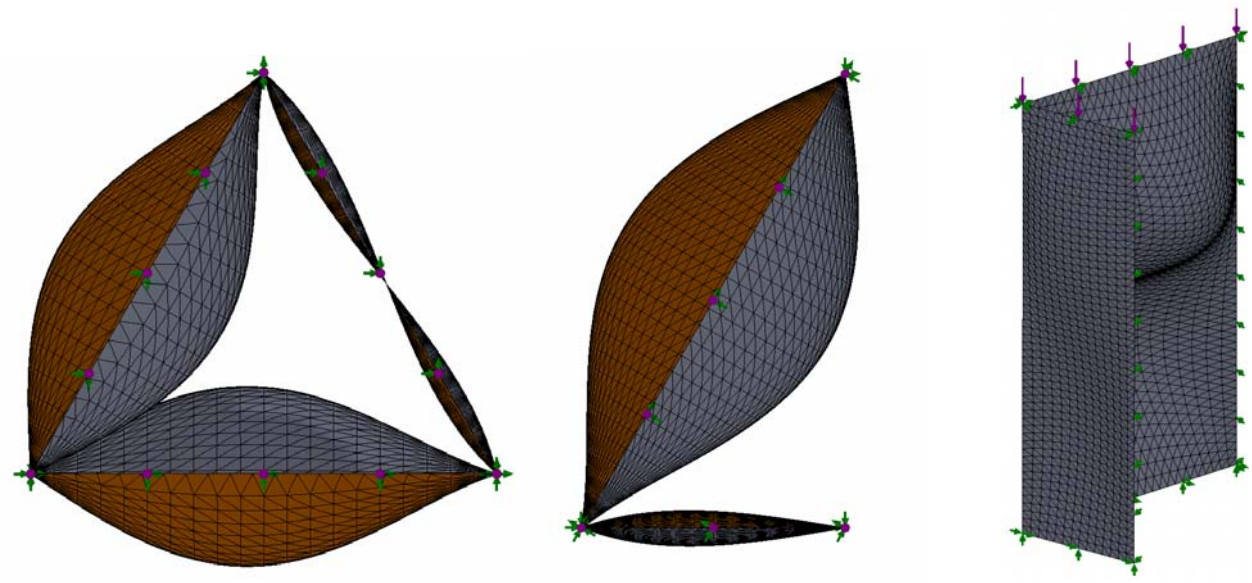

(a) **(b)** **(c)**

Figure 4.13 Finite element simulation results showing top views of the buckled shapes of (a) a triangular tube, (b) corresponding angle section and (c) trimetric view of the angle section at an exaggerated scale

This figure shows the formation of two lobes in one of the plates of a triangular tube with zero deflection along the centerline of the plate. The critical load and the buckling mode shape results from the simulation confirmed the assumption of the hinged support of the open edges in the angle section. Table 4.2 shows the critical load data from the simulation results of the two structures. It was observed from the results that the critical load of the whole tube was twice the critical load of the half tube or angle section.

Table 4.2 Critical loads of the two sections from the result of FEM simulations

Section	Critical load P_{cr} [*N*]
Equilateral tube	252.24
Corresponding angle section	125.89

The results support the initial assumption that the angle section behaves as half of the whole tube structure under similar loading conditions. This simulation thus verifies the assumed boundary conditions of the open edges used in the theoretical derivation process. Based on this result, all further simulation for testing triangular tubes were performed on their corresponding angle sections with the explained boundary conditions.

4.6.3 Simulation Results of the Angle Section of an Equilateral Tube

The next set of simulations was performed on a series of angle structures representing the angle sections of equilateral tubes. The length l of the main wall was chosen as 3.175 *mm* thus making the length of the restraining wall l_r equal to 1.5875 *mm* to maintain the ratio l_r/l as 0.5. The height h was changed for different simulations in order to vary the aspect ratios from 0.25 to 3. The thickness t was set to 0.025 *mm*. Meshing of the geometries was performed using triangular shell mesh elements of sizes ranging from 0.15 *mm* to 0.2 *mm*. As an example, Figure 4.14 shows the top and trimetric views of the exaggerated buckled shape of a model which has an aspect ratio of 1.

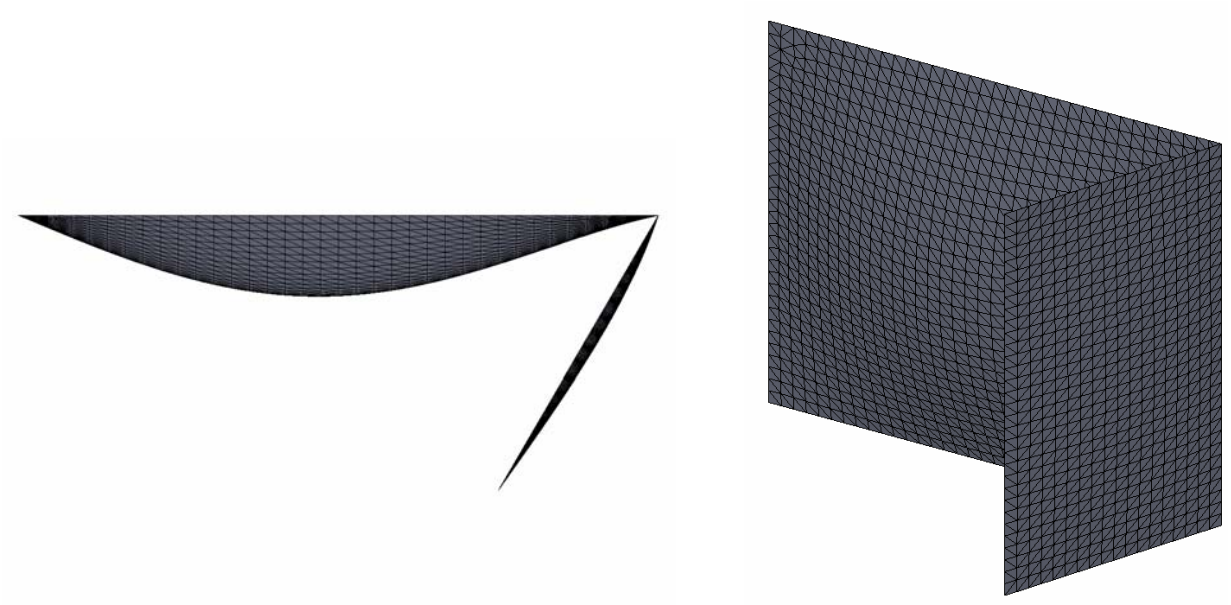

(a) **(b)**

Figure 4.14 (a) Top view and (b) trimetric view of the deformed model of a two legged angle section with aspect ratio of 1, at an exaggerated scale after buckling simulation

The total critical load of the section from the simulation of this case was 3.02 *N*. The critical load of the structure was calculated theoretically using Eqn. (4.25) and Eqn. (4.39) as 3.23 *N*. This shows good agreement between the simulation and theoretical results with a discrepancy of approximately 6.5 % for this aspect ratio. Table 4.3 shows the values of k from the results of simulations and the corresponding theoretical values at certain aspect ratios of the angle section of an equilateral tube with sides equal to 3.175 *mm*.

Table 4.3 Theoretical and simulation results of *k* of the angle section of equilateral tube, with main wall of length 3.175 *mm* and restraining wall of length 1.5875 *mm*

Aspect ratio ϕ	Total critical load [*N*]	Critical load of the main wall [*N*]	Buckling factor *k* (simulation result)	Buckling factor *k* (theoretical result)	% Error
0.25	11.29	7.52	16.92	18.21	7.08
0.29	9.12	6.08	13.66	14.50	5.79
0.40	5.47	3.65	8.20	8.64	5.09
0.50	4.10	2.74	6.15	6.56	6.25
0.63	3.31	2.21	4.97	5.36	7.28
0.71	3.09	2.06	4.63	4.98	7.03
0.77	3.00	2.00	4.50	4.84	7.02
0.80	2.98	1.98	4.46	4.78	6.69
0.83	2.96	1.97	4.44	4.77	6.92
0.87	2.95	1.97	4.43	4.75	6.74
0.91	2.96	1.97	4.44	4.76	6.72
1.00	3.02	2.02	4.53	4.85	6.60
1.11	3.16	2.11	4.74	5.04	5.95
1.25	3.40	2.27	5.10	5.36	4.85
1.67	3.05	2.03	4.57	4.77	4.19
2	3.11	2.07	4.65	4.85	4.12

Theoretical and computational values of *k* of the angle section were plotted against the aspect ratio of the section. These graphs are presented in Figure 4.15. The figure shows good agreement between theoretical results and the results of the finite element simulations with a maximum discrepancy of approximately 7 %.

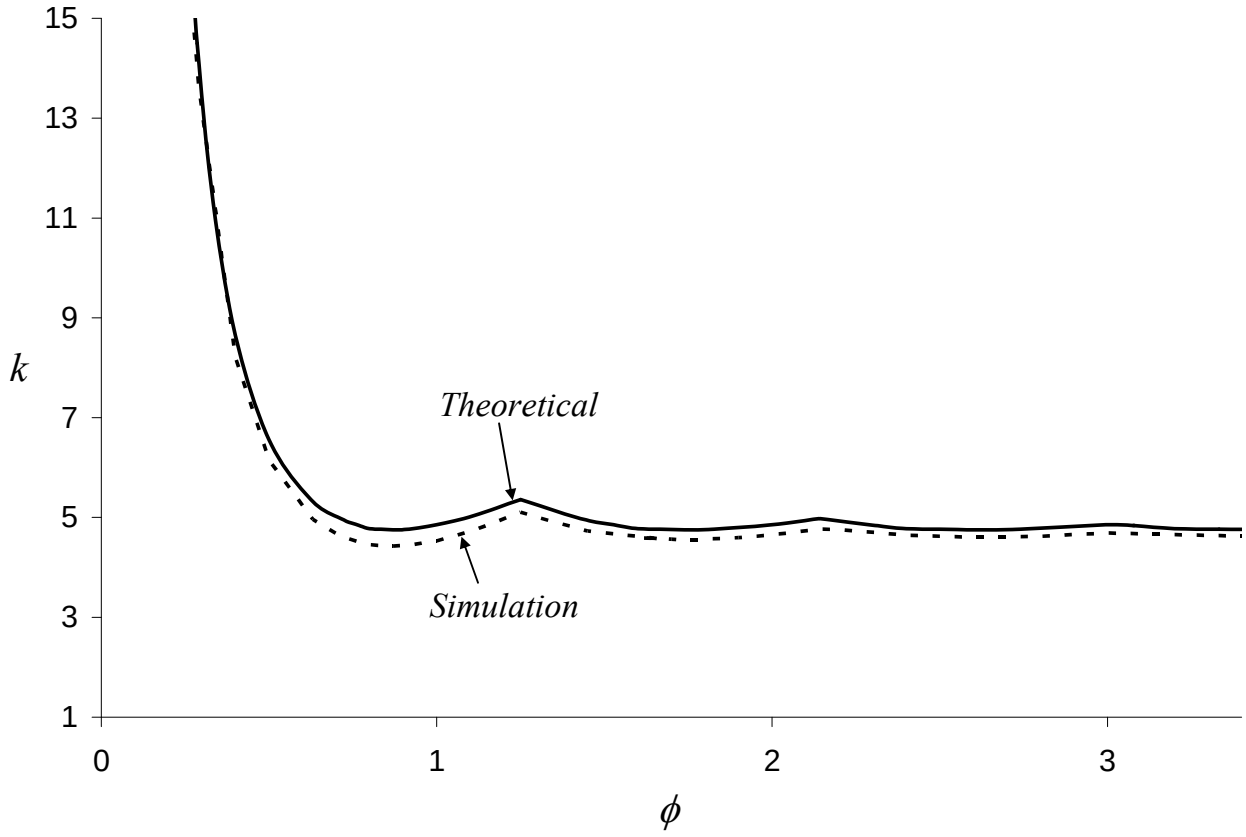

Figure 4.15 Comparison of the *k* curves obtained from theoretical and computational results over different aspect ratios

Apart from good agreement between the theoretical and computational *k* values, the transition of the number of half waves in the simulation results was observed at the theoretically expected aspect ratios. As an example, Figure 4.16 shows the change of the number of half waves from 1 to 2 in the main wall of the angle section plotted in an exaggerated scale buckled shape of the section. The transition was observed to start at an aspect ratio of 1.25 and the formation of two waves in the main wall was observed to begin at an aspect ratio of 1.26. This agrees with the theoretical results derived. At the aspect ratio of 1.29, two fully developed half waves were observed in the simulation results presented.

(a) **(b)** **(c)**

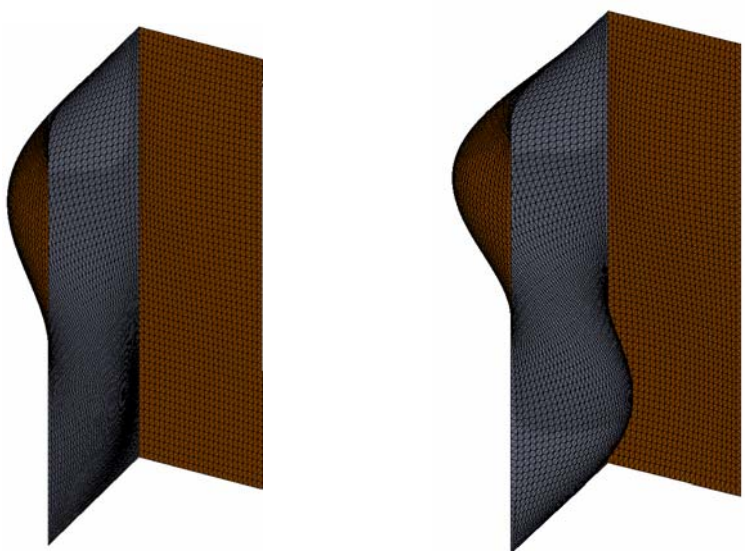

(d) **(e)**

Figure 4.16 Exaggerated scale simulation results of the angle section of an equilateral tube at aspect ratio of (a) 1.23, (b) 1.24, (c) 1.25, (d) 1.26 and (e) 1.29

Similarly, the transition of number of half waves in the main wall, from 2 to 3, was observed at an aspect ratio of approximately 2.48.

4.6.3 Simulations on Angle Section of Short-Sided Isosceles Tubes

The expected theoretical results of short-sided isosceles tubes were verified using finite element simulations on a few different isosceles triangular tube geometries at certain aspect ratios. The simulations were performed on the angle sections of short-sided isosceles tubes with

the main wall representing one of the two long walls of the tube. Similar boundary conditions as those applied to the angle section of the equilateral tubes were applied to these geometries. Simulations were performed on three different angle sections, each having a longer wall of length of 3.175 *mm*. The geometries were modeled with the length of the restraining walls l_r representing l_r/l ratios of 0.01, 0.1 and 0.3. As an example of these simulations, Figure 4.17 shows the exaggerated scale deformed shapes of the structures after buckling at an aspect ratio of 1.

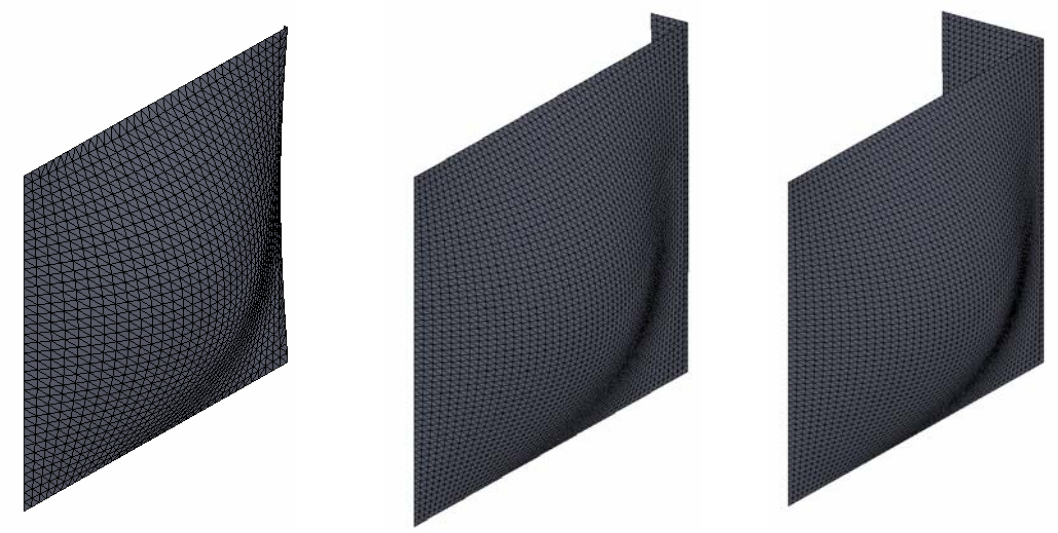

(a) **(b)** **(c)**

Figure 4.17 An exaggerated scale deformed shape of angle sections with l_r/l ratios as (a) 0.01, (b) 0.1 and (c) 0.3 after buckling simulation at aspect ratio of 1

It was observed from the simulation results that the common edge between the main wall and restraining wall did not remain unbuckled for angle section with the length ratio of 0.01. This implies that the buckling of the angled section with l_r/l ratio of 0.01 in the finite element simulation occurred in a mixed mode of wall buckling and global Euler buckling under hinged-hinged condition. This was not considered in the present theory and hence, the values of the buckling factor obtained from simulation for this angle section did not match the expected results from the tube buckling theory. In the other two angle sections, the values of k were close to the theoretical expectations. Table 4.4 shows the theoretical and simulation results of the critical loads and the buckling factors of the angle sections shown in Figure 4.17, at two different aspect ratios of each of the geometries. First aspect ratio of the angle sections was selected as 1 and the second ratio corresponding to first minimum of k curve.

Table 4.4 Simulation results of the buckling analysis on the sections shown in Figure 4.17

l_r/l	ϕ	P_{cr} [N] Total	P_{cr} [N] Main wall	k (simulation)	k (theoretical)	% Error
0.01	1	1.91	1.90	4.26	5.69	25.13
	0.8	1.95	1.93	4.34	5.37	19.18
0.1	1	2.47	2.25	5.05	5.37	5.96
	0.82	2.35	2.13	4.80	5.13	6.43
0.3	1	2.72	2.09	4.70	4.99	5.81
	0.83	2.63	2.02	4.55	4.86	6.38

The values of k obtained from simulations were in good agreement with the theoretical values thus supporting the derived theory for the case of short-sided isosceles tubes. However, for a very short unequal side, the present theory is invalid after certain heights, due to the mixed mode of buckling of the tube. In the present study, the mixed mode of buckling observed in the angle section with l_r/l ratio = 0.01 lowered the critical load of the structure. This resulted in a larger error between the theoretical and simulation results.

4.7 Discussion of Results

The theoretical solution presented in this paper was obtained by simplifying the problem of buckling of the whole triangular tube sections into the corresponding angle sections. Buckling behavior of the walls of the tubes was identified and, appropriate boundary conditions were applied to the end edges of the angle sections. Results from the theoretical formulations were compared with finite element simulations. Values of k of the critical wall (main wall) of any angle section and therefore, of the corresponding equilateral or short-sided isosceles tube, had a constant discrepancy or a shift of approximately 5-6 % with the simulation results. Also, a special case of the angle section was considered in the present study having the restraining wall of length 0.01 times the main wall. This section was expected to behave similar to a plate with one vertical edge simply supported and the other vertical edge fixed. The theoretical values of k for this case, over certain aspect ratios were calculated. These values were compared with the values of k obtained from an existing theoretical equation for a plate simply supported along one vertical edge and fixed along the other edge, available in the literature. The values of buckling factor obtained from these two methods had a discrepancy of less than 1% which can be

considered as an excellent match. However, the simulation result of this geometry did not match well with the theoretical prediction due to a mixed mode of individual wall buckling and global Euler buckling, observed in simulation result. Also, using the present form of the theoretical formulation, the critical load of triangular tubes with different wall thickness ratios can be calculated by setting different values of the thickness ratio in the equation for calculating ζ.

4.8 Conclusion

An analytical solution to find the critical load of isosceles triangular tubes with the base side not exceeding the equal length sides was derived. This was performed by dividing the triangular tube into two halves, each called as an angle section. The buckling behavior of each of the angle sections was studied by identifying the behavior of each of the walls of the section and applying appropriate boundary conditions to the edges. The results from the theoretical derivation from this study were compared with the existing theoretical formulas for some particular cases from literature. The theoretical solutions were also compared to a series of systematic finite element simulations. The comparisons showed good agreement of the theoretical predictions with the finite element simulation results.

4.9 References

[1] G. H. Bryan. "On the stability of a plane plate with thrusts in its own plane with applications to the buckling of the sides of the ship", Proceeding of London Mathematical Society, 1891, Vol 22.

[2] Timoshenko S. P, Gere J. M. "*Theory of elastic stability*", New York, McGraw-Hill, 1961.

[3] Bleich F. "*Buckling strength of metal structures*", New York, McGraw-Hill, 1952.

[4] Bulson P. S. "*The stability of flat plates*", London, Chatto and Windus, 1970.

[5] von Karman T, Sechler E. E, Donell L. H. "Strength of thin plates in compression", Transaction of ASME, 1932, Vol 54.

[6] Winter G. "Strength of thin steel plates in compression", Transaction of ASCE, 1947, Vol 112.

[7] Cox L. H. "Buckling of thin plates in compression", Aeronautical Research Community R&M No. 1554, 1934.

[8] Pizhong Q, Luyang S. "Explicit local buckling analysis of rotationally restrained composite plates under biaxial loading", International Journal of Structural Stability and Dynamics, World Scientific Publishing Company, 2007, Vol 7.

[9] Hosseini-Hashemi S, Khorshidi K, Amabili M. "Exact solution for linear buckling of rectangular Mindlin plates", Journal of Sound and Vibration, 2008 Vol 315.

[10] Aliabadi M. H, Baiz P. M, Albuquerque E. L. "Stability analysis of plates", Recent Advances in Boundary Element Method, 2009.

[11] Swartz S. E, O'Neill R. J. "Linear elastic buckling of plates subjected to combined loads", Thin-Walled Structures, Elsevier 1995. Vol 21.
[12] Rasmussen K. J. R, Burns T, Bezkorovainy P, Bambach M. R. "Numerical modeling of stainless steel plates in compression", Journal of constructional steel research, Elsevier 2003, Vol 59.
[13] Bambach M. R, Rasmussen K. J. R. "Experimental techniques for testing unstiffened plates in compression and bending", Tech note, Experimental Mechanics, Society of Experimental Mechanics, 2004.
[14] Chen D. H, Ozaki S. "Axial plastic collapse behavior of plates", Thin-Walled Structures, Elsevier, 2010, Vol 48.
[15] Lundquist E. E. "Local Instability of Symmetrical Rectangular Tubes Under Axial Compression", Nat. Advisory Comm. Aeronaut. 1939 Tech note No. 686.
[16] Kandil K. S, Callandine C. R. "Classical local buckling of tubes having rectangular cross sections", International Journal of Mechanical Sciences 1986, Vol 28.
[17] Rhodes J. "Buckling of thin plates and members – and early work on rectangular tubes", Thin Walled Structures 2002, Vol 40.
[18] Lowe W. T, Al-Hassani S. T. S, Johnson W. "Impact behavior of small scale model motor coaches", Proceedings – Institute of Mechanical Engineers 1972, Vol 186.
[19] Wierzbicki T, Akerstorm T. "Dynamic crushing of strain rate sensitive box columns", International Conference on Vehicular Structural Mechanics – Proceedings 1977.
[20] Mahmood H. F, Paluzny A. "Design of thin walled columns for crush energy management – their strength and mode of collapse", International Conference on Vehicular Structural Mechanics – Proceedings 1981.
[21] Weirzbicki T, Abramowicz W. "On the crushing mechanics of thin walled structures", Journal of Applied Mechanics 1983, Vol 50.
[22] Karagiozova D, Jones N. "Dynamic buckling of elastic plastic square tubes under axial impact – II: Structural response", International Journal of Impact Engineering 2004, Vol 30.
[23] Soden P. D, Al-Hassani S. T. S, Johnson W. "The crumpling of polyvinyl chloride tubes under static and dynamic loads", Conference on Mechanical Properties at High Rates of Strain, Institute of physics - London 1974, Conference series No. 21.
[24] Johnson W, Soden P. D, Al-Hassani S. T. S. "In-extensional collapse of thin walled tubes under axial compression", Journal of Strain Analysis 1977, Vol. 12.
[25] Gupta N. K, Sekhon G. S, Gupta P. K. "A study of fold formation in axisymmetric collapse of round tubes", International Journal of Impact Engineering 2002, Vol 27.
[26] Merchant W, Saafan S. A. "Critical pressures and buckling modes of regular polygon prismatic tubes", International Journal of Mechanical Sciences 1961, Vol 3.
[27] Wittrick W. H, Curzon P. L. V. "Stability function for the local buckling of thin walled structures with the walls in combines shear and compression", Aeronautical Quarterly 1968, Vol 19.
[28] Wittrick W. H, Curzon P. L. V. "Local buckling of long polygon tubes in combined compression and torsion", International Journal of Mechanical Sciences 1968, Vol 10.
[29] Yamashita A, Hattori T, Nishimura N, Tange Y. "Quasi-static and dynamic axial crushing of various polygon tubes", Key engineering Materials 2007, Vol 340 – 341.

[30] Younes M. M. “Finite element modeling of crushing behavior of thin tubes with various cross sections”, 13th international conference on aerospace and aviation technology, May 2009.

Chapter 5 - Conclusions and Scope of Future work

The goal of the study presented in this thesis was to review some of the existing theories and establish some new theoretical solutions on the elastic buckling of supported plate and tubular structures, and compare it with computational and experimental results. In this chapter, the final conclusions from the study are presented. Also, the scope of future work based on the present study is discussed.

In the second chapter of this thesis, the solution of buckling of a simply supported plate using energy method was reviewed from literature. This theory was extended to square tubes and multi-wall open structures. The theoretical predictions were then compared with finite element simulation results. The aspects of number of lobes formed along the height of the walls of a buckled structure and the buckling load of the structure were critically investigated and compared to the theory. It was observed that the simulation results were highly consistent with the theoretical predictions. The transitions of number of half waves in a plate were observed at theoretically expected aspect ratios and the critical load of the plate was in good agreement with the theoretically expected values. It was observed from the simulations that the critical load of multi-wall structures is equal to the critical load of a single simply supported plate times the number of walls in the structure. Also, the critical loads of these structures were observed to be independent of the angle between the walls of the structure. This was supported by the critical load results of a rhombic tube, which was equal as the critical load of the corresponding square tube.

The studies on square tube were then extended to various quadrilateral tube sections in Chapter 3. The buckling behavior of square, rectangular, rhombus and parallelogram tubes were explicitly studied. The critical load derivation of the tubes was illustrated using the classical plate bending mechanics. Also, the Euler buckling mode of the tubes was investigated. The theoretical results obtained were compared with finite element simulation results and experimental observations. The comparisons revealed good consistency of the simulation and experimental results with the theoretical predictions.

Following the study of square and rectangular tubes, the buckling behavior of isosceles triangular tubes was also studied. The critical load of triangular tubes was calculated by

assuming a possible buckling shape of the tube and deriving the theoretical critical load of the tube by considering the boundary conditions of the assumed shape. The assumed buckling shape, however, holds true only for isosceles tubes with the third side shorter than the equal sides and thus, the study was limited to these tubes. The predicted theories were validated using computation results from extensive finite element simulations. The observations from simulations proved that the buckled profile of the tubes considered in the study follows the assumed buckling shape. Also, the critical load comparison of the tubes from simulations matched well with the theoretical predictions. The transition of number of half waves was observed at the theoretically expected aspect ratios. These comparisons validated the consistency of the theoretical and simulation results.

Based on the explained theoretical methods, the study of any isosceles tubes can be derived using the similar procedures in future. Also, the buckling properties of a pseudo-square honeycomb structures can be derived by studying the behavior of walls of the cells of the structure under the buckling action. The future goals of this project are to derive the solution of buckling of any isosceles tube and the pseudo-square honeycomb structures. The theoretical solution would then be compared with finite element simulations. Also, short term goals include the experimental validation of the theory of the triangular tube buckling presented in this thesis.

Appendix A - Deflection Equation of the Restraining Walls of a Rectangular Tube

Out-of-plane deflection of the restraining wall takes place due to the bending moment imparted on the restraining wall by of the buckling of the buckling wall. As the width of restraining plate is very small compared to the buckling wall, effect of the compressive forces are negligible on the bending.

$$\frac{\partial^4 w}{\partial x^4}+\frac{\partial^4 w}{\partial x^2 \partial y^2}+\frac{\partial^4 w}{\partial y^4}=0 \tag{A.1}$$

The boundary conditions of the to and bottom edges are,

at $x = 0, h$

$$w=0 \tag{A.2}$$

and

$$M_x=0 \tag{A.3}$$

Solving the differential equation with these boundary conditions, the equation of deflection of the restraining wall is obtained as,

$$w=\sin\frac{m\pi x}{h}\left(C_1\sinh\frac{m\pi}{h}y+C_2\cosh\frac{m\pi}{h}y+C_3 y\sinh\frac{m\pi}{h}y+C_4 y\cosh\frac{m\pi}{h}y\right) \tag{A.4}$$

C_1 to C_4 were calculated using the boundary conditions for the vertical edges. Using the expressions of moments on a plate under bending, the boundary conditions presented in Eqn. (3.15) and (3.17) were modified. The modified boundary conditions of the restraining walls were reframed as,

$$\left[w\right]_{y=0,l_r}=0 \tag{A.5}$$

and,

$$\left[\bar{M}_y\right]_{y=0,l_r}=\left[M_y\right]_{y=l/2} \tag{A.6}$$

=>

$$\left[\frac{\partial^2 w}{\partial y^2}\right]_{y=l_r}=-\frac{M_y}{D'} \tag{A.7}$$

and,

$$\left[\frac{\partial^2 w}{\partial y^2}\right]_{y=0} = -\frac{M_y}{D'} \tag{A.8}$$

Differentiating Eqn. (A.4) wrt y twice,

$$\frac{\partial w}{\partial y} = \sin\frac{m\pi x}{h}\left[\begin{array}{l}\left(C_1\frac{m\pi}{h}+C_4\right)\cosh\left(\frac{m\pi}{h}y\right)+\left(C_2\frac{m\pi}{h}+C_3\right)\sinh\left(\frac{m\pi}{h}y\right)\\ +C_3\frac{m\pi}{h}y\cosh\left(\frac{m\pi}{h}y\right)+C_4\frac{m\pi}{h}y\sinh\left(\frac{m\pi}{h}y\right)\end{array}\right] \tag{A.9}$$

and,

$$\frac{\partial^2 w}{\partial y^2} = \sin\frac{m\pi x}{h}\left[\begin{array}{l}\left(C_1\left(\frac{m\pi}{h}\right)^2+2C_4\frac{m\pi}{h}\right)\sinh\left(\frac{m\pi}{h}y\right)+\left(C_2\left(\frac{m\pi}{h}\right)^2+2C_3\frac{m\pi}{h}\right)\cosh\left(\frac{m\pi}{h}y\right)+\\ C_3\left(\frac{m\pi}{h}\right)^2 y\sinh\left(\frac{m\pi}{h}y\right)+C_4\left(\frac{m\pi}{h}\right)^2 y\cosh\left(\frac{m\pi}{h}y\right)\end{array}\right] \tag{A.10}$$

The value $(m\pi/h)$ is substituted as N for ease of solving. Solving these equations with the boundary conditions, the expressions $C_{1\text{ to }4}$ were obtained as,

$$C_1 = -\frac{M_y l_r}{2ND'\sinh^2 Nl_r}\left(1-\cosh Nl_r\right) \tag{A.11}$$

$$C_2 = 0 \tag{A.12}$$

$$C_3 = -\frac{M_y}{2ND'} \tag{A.13}$$

$$C_4 = -\frac{M_y}{2ND'\sinh kl_r}\left(1-\cosh Nl_r\right), \tag{A.14}$$

Therefore, the equation of deflection of the plate is,

$$\begin{array}{l} w = -\dfrac{M_y l_r h}{2m\pi D'\sinh^2\dfrac{m\pi}{h}l_r}\left(1-\cosh\dfrac{m\pi}{h}l_r\right)\sinh\left(\dfrac{m\pi}{h}y\right)\\ -\dfrac{M_y h}{2m\pi D'}y\sinh\left(\dfrac{m\pi}{h}y\right)-\dfrac{M_y h}{2m\pi D'\sinh\dfrac{m\pi}{h}l_r}\left(1-\cosh\left(\dfrac{m\pi}{h}l_r\right)\right)y\cosh\left(\dfrac{m\pi}{h}y\right)\end{array} \tag{A.15}$$

Appendix B - Minimum Moment of Inertia of a Parallelogram Tube Cross-Section

The minimum moment of inertia of a section is expressed as,

$$I_{\min} = \frac{I_x + I_y}{2} - \sqrt{\left(\frac{I_x - I_y}{2}\right)^2 + I_{xy}{}^2} \tag{B.1}$$

where, I_x, I_y and I_{xy} are the moment of inertia about x and y axis and the product of inertia, respectively, with respect to the coordinate axes which pass through the centroid of the geometry. For a parallelogram section, the expressions of moment of inertia and product of inertia are expressed as,

$$I_x = \frac{ll_r{}^3 \sin^3\theta}{12} \tag{B.2}$$

$$I_y = \frac{l^3 l_r \sin\theta + bd^3 \sin\theta\cos^2\theta}{12} \tag{B.3}$$

and,

$$I_{xy} = -\frac{ll_r{}^3 \sin^2\theta\cos\theta}{12} \tag{B.4}$$

For the hollow parallelogram tube cross-section illustrated in Figure 3.10,

$$l_{out} = l + \frac{t}{2}\tan\frac{\theta}{2} + \frac{t}{2}\cot\frac{\theta}{2} \tag{B.5}$$

$$l_{in} = l - \frac{t}{2}\tan\frac{\theta}{2} - \frac{t}{2}\cot\frac{\theta}{2} \tag{B.6}$$

$$l_{r_{out}} = l_r + \frac{t}{2}\tan\frac{\theta}{2} + \frac{t}{2}\cot\frac{\theta}{2} \tag{B.7}$$

$$l_{r_{in}} = l_r - \frac{t}{2}\tan\frac{\theta}{2} - \frac{t}{2}\cot\frac{\theta}{2} \tag{B.8}$$

where, l_{out} and l_{in} and $l_{r_{out}}$ and $l_{r_{in}}$ are the lengths of outer and inner surface of the buckling and restraining walls respectively. The moment of inertia of the parallelogram tube cross-section is calculated as,

$$I_{x_{net}} = I_{x_{out}} - I_{x_{in}} \tag{B.9}$$

$$I_{y_{net}} = I_{y_{out}} - I_{y_{in}} \tag{B.10}$$

$$I_{xy_{net}} = I_{xy_{out}} - I_{xy_{in}} \tag{B.11}$$

where, I_{out} and I_{in} are the moment of inertias of the outer and inner parallelograms. These are calculated by substituting the dimensions of outer and inner parallelograms from Eqns. (B.5), (B.6), (B.7) and (B.8) in (B.2), (B.3) and (B.4). The minimum moment of inertia of the parallelogram section is given as,

$$I_{\min} = \frac{I_{x_{net}} + I_{y_{net}}}{2} - \sqrt{\left(\frac{I_{x_{net}} - I_{y_{net}}}{2}\right)^2 + I_{xy_{net}}^2} \tag{B.12}$$

This value of $I_{\min}$ was used in Eqn. (3.28) to calculate the buckling critical height of a parallelogram tube.

Appendix C - General Deflection Equation of the Main Wall of a Triangular Tube

The general equation of deflection of the bending of plate is,

$$D\left(\frac{\partial^4 w}{\partial x^4}+2\frac{\partial^4 w}{\partial x^2 \partial y^2}+\frac{\partial^4 w}{\partial y^4}\right)+t\left(\sigma_x \frac{\partial^2 w}{\partial x^2}\right)=0 \tag{C.1}$$

The boundary conditions of top and bottom edges are, at $x = 0$ and $x = h$, $w = 0$ and $M = 0$.
The moment along x on the plate is given by,

$$M_x=-D\left(\frac{\partial^2 w}{\partial x^2}+\nu\frac{\partial^2 w}{\partial y^2}\right) \tag{C.2}$$

The edge of the wall under consideration does not undergo any deformation along the edges with respect to y. Therefore, $\partial^2 w/\partial y^2 = 0$. This modifies the boundary conditions along the horizontal edges of the plate as,

$$\begin{aligned} w &= 0 \text{ at x = 0} \\ \frac{\partial^2 w}{\partial x^2} &= 0 \text{ at x = h} \end{aligned} \tag{C.3}$$

The solution of the Eqn. (C.1) obeying these conditions was assumed as,

$$w=Y\sin\left(\frac{m\pi x}{h}\right) \tag{C.4}$$

In this equation, Y is a function varying with y values only. Substituting this condition into Eqn. (C.1), the differential equation of deflection takes the form of,

$$\sin\left(\frac{m\pi x}{h}\right)\left[Y''''+2Y''\left(\frac{m\pi}{h}\right)^2+\left(\frac{m\pi}{h}\right)^4\left(1-\sigma_c\frac{t}{D}\left(\frac{h}{m\pi}\right)^2\right)\right]=0 \tag{C.5}$$

Substituting the expression,

$$\mu^2=\left(1-\sigma_c\frac{t}{D}\left(\frac{h}{m\pi}\right)^2\right) \tag{C.6}$$

and solving the differential equation, the solution of the equation is obtained as,

$$Y = A_1 \cosh\left(\frac{m\pi}{h}\sqrt{\mu+1}\right)y + A_2 \sinh\left(\frac{m\pi}{h}\sqrt{\mu+1}\right)y + A_3 \cos\left(\frac{m\pi}{h}\sqrt{\mu-1}\right)y + A_4 \sin\left(\frac{m\pi}{h}\sqrt{\mu-1}\right)y \tag{C.7}$$

Replacing the expressions $\left(\frac{m\pi}{h}\sqrt{\mu+1}\right)$ and $\left(\frac{m\pi}{h}\sqrt{\mu-1}\right)$ as k_1 and k_2 respectively in Eqn. (C.7) and substituting the expression of Y into Eqn. (C.4), the deflection equation of the main wall was obtained as Eqn. (4.6)

Appendix D - Buckling Condition of the Main Wall of a Triangular Tube

Along the vertical edges, $\frac{\partial^2 w}{\partial x^2} = 0$. This makes the boundary conditions as,

At $y = 0$,

$$w = 0$$
$$l\zeta\left(\frac{\partial^2 w}{\partial y^2}\right) - \frac{\partial w}{\partial y} = 0 \tag{D.1}$$

and, at $y = l$,

$$w = 0$$
$$\frac{\partial^2 w}{\partial y^2} = 0 \tag{D.2}$$

Substitution of these boundary conditions in the equation of deflection yields,

$$\begin{bmatrix} \cosh k_1 l - \cos k_2 y + B\sinh k_1 l & C\sinh k_1 l - \sin k_2 l \\ k_1^2\cosh k_1 l + k_2^2\cos k_2 l + Bk_1^2\sinh k_1 l & Ck_1^2\sinh k_1 l + k_2^2\sin k_2 l \end{bmatrix} \times \begin{bmatrix} A_3 \\ A_4 \end{bmatrix} = 0 \tag{D.3}$$

Solution of determinant, |Det| = 0 gives the non trivial buckling condition of the main wall of the angle section of a triangular tube. This condition is presented in Eqn. (4.18).

Appendix E - Out-of-plane Deflection Equation of the Restraining Wall of an Angle Section

The expression of the out-of-plane deflection of the restraining wall is,

$$w = C_1 \sinh\frac{m\pi}{h} y + C_2 \cosh\frac{m\pi}{h} y + C_3 y \sinh\frac{m\pi}{h} y + C_4 y \cosh\frac{m\pi}{h} y \tag{E.1}$$

C_1 to C_4 are calculated using the boundary conditions for the vertical edges. The boundary conditions are:

At $y = 0$,

$$w = 0 \tag{E.2}$$

$$\frac{\partial^2 w}{\partial y^2} = 0 \tag{E.3}$$

At $y = l_r$

$$w = 0 \tag{E.4}$$

$$\frac{\partial^2 w}{\partial y^2} = -\frac{M_y}{D'} \tag{E.5}$$

With these boundary conditions

From Eqn. (E.2)

$$C_2 = 0 \tag{E.6}$$

From Eqn. (E.3)

$$C_3 = 0 \tag{E.7}$$

From Eqn. (E.4)

$$C_1 \sinh\left(\frac{m\pi}{h} l_r\right) + C_4 l_r \cosh\left(\frac{m\pi}{h} l_r\right) = 0 \tag{E.8}$$

From Eqn. (E.5)

$$\left(C_1\left(\frac{m\pi}{h}\right)^2 + 2C_4\frac{m\pi}{h}\right)\sinh\left(\frac{m\pi}{h} l_r\right) + C_4\left(\frac{m\pi}{h}\right)^2 l_r \cosh\left(\frac{m\pi}{h} l_r\right) = -\frac{M_y}{D'} \tag{E.9}$$

Solving Eqn. (E.8) and Eqn. (E.9)

$$C_4 = -\frac{M_y}{2D'\left(\frac{m\pi}{h}\right)\sinh\left(\frac{m\pi l_r}{h}\right)} \tag{E.10}$$

$$C_1 = \frac{M_y l_r \cosh\left(\frac{m\pi l_r}{h}\right)}{2D'\left(\frac{m\pi}{h}\right)\sinh^2\left(\frac{m\pi l_r}{h}\right)} \tag{E.11}$$

Therefore,

$$w = \frac{M_y}{2D'\left(\frac{m\pi}{h}\right)\sinh\left(\frac{m\pi}{h}l_r\right)}\left[l_r\frac{\cosh\left(\frac{m\pi}{h}l_r\right)}{\sinh\left(\frac{m\pi}{h}l_r\right)}\sinh\left(\frac{m\pi}{h}y\right) - y\cosh\left(\frac{m\pi}{h}y\right)\right] \tag{E.12}$$

This is the expression of the deflection of the restraining wall in the out-of-plane direction.